NASA Contractor Report 172383

Advanced Manufacturing Development of a Composite Empennage Component for L-1011 Aircraft

Phase III — Final Report
Production Readiness Verification Testing

A. Jackson, J. Sandifer, P. Sandorff,
and R. Van Cleave

LOCKHEED-CALIFORNIA COMPANY
BURBANK, CALIFORNIA 91520

CONTRACT NAS1-14000

AUGUST 1984

NASA
National Aeronautics and
Space Administration

Langley Research Center
Hampton, Virginia 23665

FOREWORD

This report was prepared by Lockheed-California Company under Contract NAS1-14000, Advanced Manufacturing Development of a Composite Empennage Component for L-1011 Aircraft. It is the final report for the Phase III - Production Readiness Verification Testing activity covering work completed between November 1, 1977 and November 30, 1983. This work is sponsored by the National Aeronautics and Space Administration (NASA) Langley Research Center. The program managers for Lockheed were Mr. Fred C. English and Mr. W. F. Priest. Mr. Herman L. Bohon was project manager for NASA Langley. The technical representatives for NASA Langley were Dr. Herbert A. Leybold and Mr. Marvin B. Dow.

Engineering Development activity (Phase I) is reported in NASA CR-144986, Design Analysis activity (Phase II) is reported in NASA CR-165634, Manufacturing Development activity (Phase IV) is reported in NASA CR-165885, and Full-Scale Ground Test activity (Phase V) is reported in NASA CR-166015.

The following Lockheed personnel were principal contributors to the program during Phase III.

A. M. James	Engineering Manager
A. C. Jackson	Engineering Manager
R. R. Van Cleave	Stress
D. C. Novelli	Materials and Processes
J. Van Hamersveld	Producibility
G. R. Brozovic	Manufacturing Research
J. F. Crocker	Nondestructive Inspection
B. Mosesian	Quality Assurance
S. W. Branton	Test Laboratory
R. S. Jusko	Test Laboratory
R. L. Lowe	Test Laboratory
W. Renslen	Test Laboratory
J. P. Sandifer	Test Laboratory
P. E. Sandorff	Test Laboratory

CONTENTS

CONTENTS (Continued)

LIST OF ILLUSTRATIONS

LIST OF ILLUSTRATIONS (Continued)

LIST OF ILLUSTRATIONS (Continued)

LIST OF ILLUSTRATIONS (Continued)

LIST OF ILLUSTRATIONS (Continued)

LIST OF TABLES

ADVANCED MANUFACTURING DEVELOPMENT OF A COMPOSITE EMPENNAGE COMPONENT FOR L-1011 AIRCRAFT

PHASE III FINAL REPORT
PRODUCTION READINESS VERIFICATION TESTING

A. C. Jackson, J. P. Sandifer, P. E. Sandorff, and R. R. Van Cleave

SUMMARY

This is the final report on the Phase III of the Advanced Composite Vertical Fin (ACVF) program.

In Phase III 22 specimens of each of two key structural elements of the ACVF were fabricated for test. One element represented the front spar at the fuselage attachment area and the other element represented the cover at the fuselage joint area. The cover elements were fabricated in the production plastics shops at Lockheed-California Company by production personnel using standard planning paper and shop line inspection and NDI. The spar elements were fabricated at Lockheed-Georgia Company by manufacturing research personnel with production shop support.

Ten specimens of each element were selected for static testing. The coefficient of variation resulting from the tests was 3.28 percent for the ten cover specimens and 6.11 percent for the ten spar specimens which compare well with metallic structures.

The remaining twelve cover and twelve spar specimens were durability tested in environmental chambers which permitted the temperature and humidity environment to be cycled as well as the applied loads. The environmental cycle consisted of temperature cycling from room temperature to -30°F then to 140°F and back to room temperature. The humidity was alternated between 0 percent and 100 percent at the 140°F peaks to represent ground soak in Las Vegas, a flight to Miami, and ground soak in Miami then return to Las Vegas. Six specimens each were tested for the equivalent of ten years of service, and of the remaining six each, four were tested for the equivalent of twenty years of service. The remaining two each of the latter six were durability tested at strain levels 1.5 times those in the basic program. For these components "limit load" was actually "design ultimate load." These were designated "high strain" specimens. The two high strain spars did not survive the full test period. These spars failed at the equivalent of 9.87 years of testing. These two spars were subjected to loads which caused buckling in the webs. The spar was designed to be unbuckled below limit load so the stiffeners were not designed to withstand the effects of repeated buckling of the web. A delamination developed between a stiffener and the web on one of the two spars and initiated failure. Because the spars were loaded as a pair failure of one caused failure of the other.

At the completion of the durability testing, all surviving specimens were shipped to NASA Langley Research Center where 6 cover and 5 spar components were tested to destruction. The results were generally above the averages of the original static tests demonstrating that such components will survive the service environment.

INTRODUCTION

The ACVF developed under this program consists of the entire main box structure of the vertical stabilizer for the L-1011 transport aircraft. The box structure extends from the fuselage production joint to the tip rib and includes the front and rear spars. It is 25 feet tall with a root box chord of 9 feet and a planform area of 150 square feet.

The master schedule for the program is shown in figure 1. The program was organized in four overlapping phases: Phase II, Design and Analysis; Phase III, Production Readiness Verification Tests (PRVT); Phase IV, Manufacturing Development; and Phase V, Ground Tests. Phase I was completed during 1976.

The Lockheed-California Company teamed with the Lockheed-Georgia Company in the development of the ACVF. Lockheed-California Company, as prime contractor, had overall program responsibility and designed and fabricated the covers and the ribs, conducted the full-scale ground tests and conducted the PRVT program. Lockheed-Georgia Company designed and fabricated the front, rear, and auxiliary spars, and assembled the composite fin at Lockheed's plant in Meridian, Mississippi, where the production L-1011 vertical fins were assembled.

Phase I, Engineering Development, reference 1; Phase II, Design and Analysis, reference 2; Phase IV, Manufacturing Development, reference 3; and Phase V, Ground Test, reference 4, were completed previously. Phase III, the only remaining phase, has been completed and is reported herein.

The PRVT investigation was conducted to answer the following questions:

1. What is the range of production qualities that can be expected for components manufactured under conditions similar to those expected in production, and how realistic and effective are proposed quality standards and quality control procedures?

2. What variability in static strength can be expected for production quality components, and are the design allowables sufficient to account for this variability?

3. Will production quality components survive laboratory fatigue tests involving both load and environment simulation of sufficient duration and severity to provide confidence in long-term durability in the service environment?

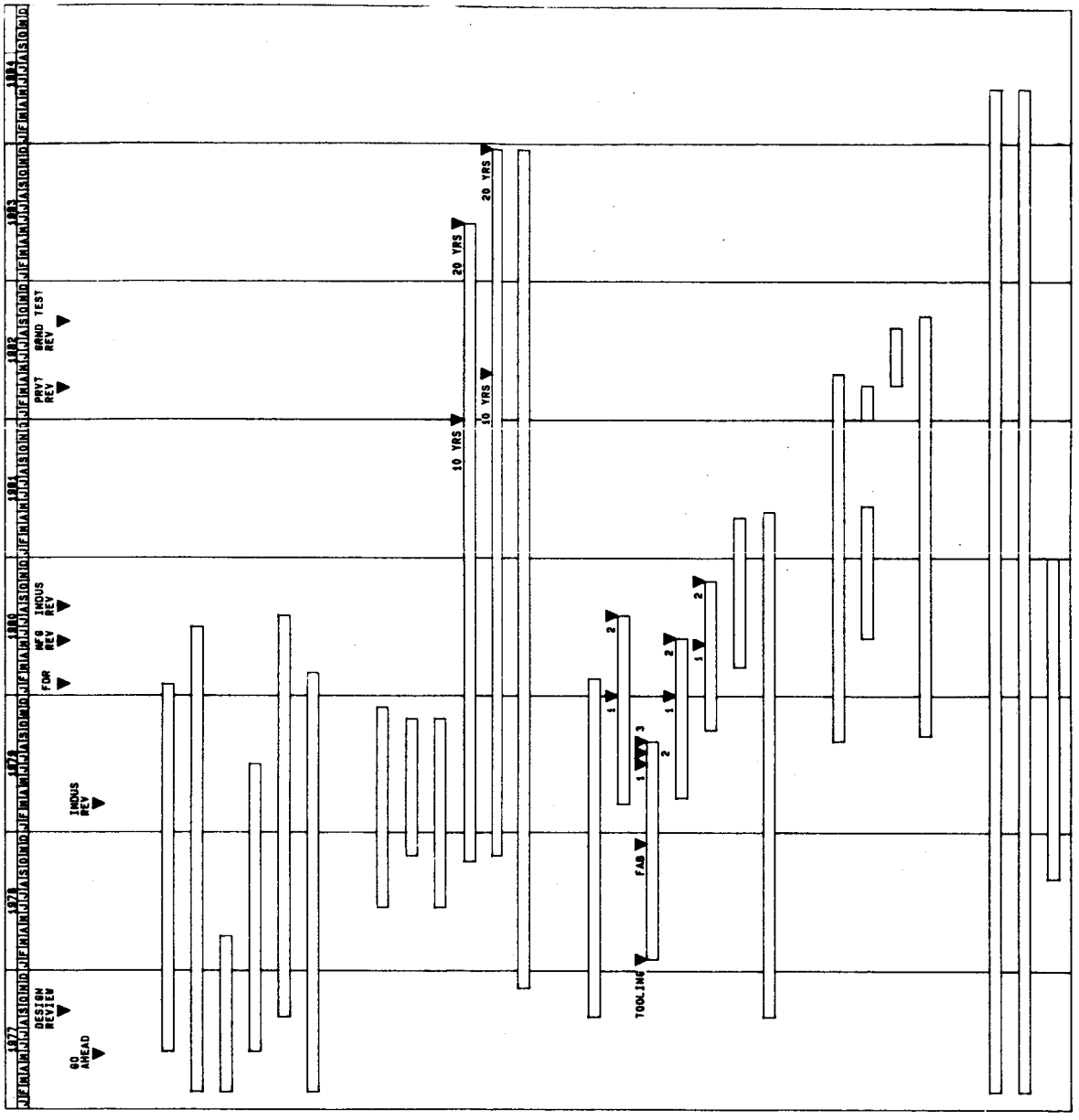

Figure 1. - ACVF program master schedule.

Use of commercial products or names of manufacturers in this report does not constitute official endorsement of such products or manufacturers, either expressed or implied, by the National Aeronautics and Space Administration.

ABBREVIATIONS AND SYMBOLS

ACEE	Aircraft Energy Efficiency
ACVF	Advanced Composite Vertical Fin
DLL	Design Limit Load
DUL	Design Ultimate Load
FAA	Federal Aviation Administration
FED STD	Federal Standard
Gr/Ep	Graphite/Epoxy
IPR	Inches per Revolution
kW	Kilowatts
LVDT	Linear Variable Differential Transducer
NASA	National Aeronautics and Space Adminstration
NDI	Nondestructive Inspection
NYC	New York City
PRVT	Production Readiness Verification Testing
QA	Quality Assurance
RC	Resin Content
SBS	Short Beam Shear
S/N	Serial Number
T/C	Thermocouple
VSS	Vertical Stabilizer Station

1. VERTICAL FIN COMPONENT DESCRIPTION

The fin box consists of two covers, two main spars, one stub spar and eleven ribs. The configuration is shown in figure 2. A brief description of the covers and spars is given below. A more detailed description is presented in reference 2. A completed fin box is shown in figure 3.

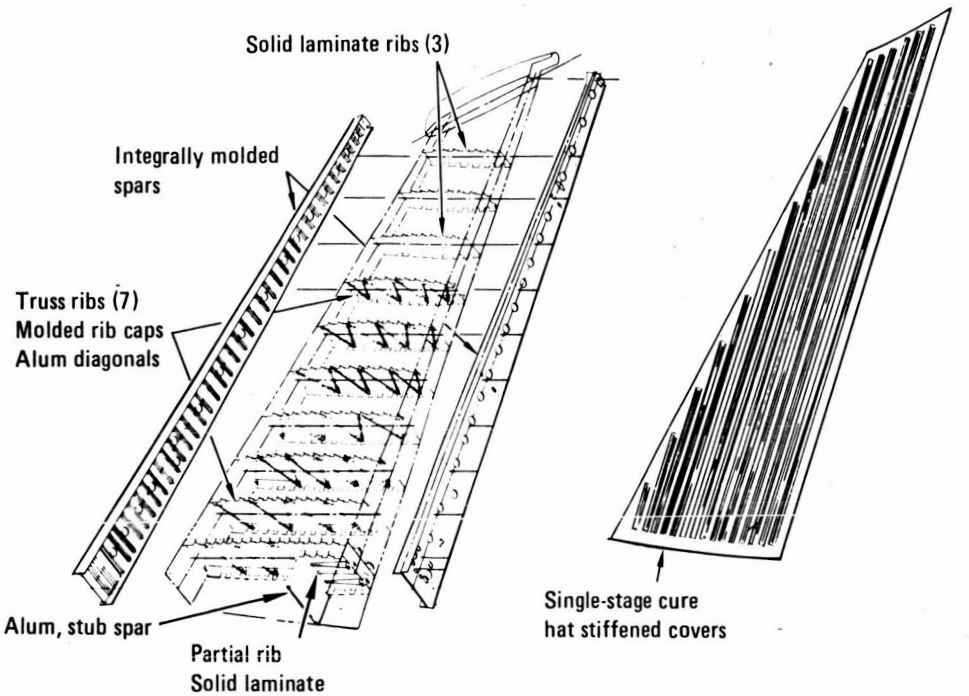

Figure 2. - ACVF design configuration.

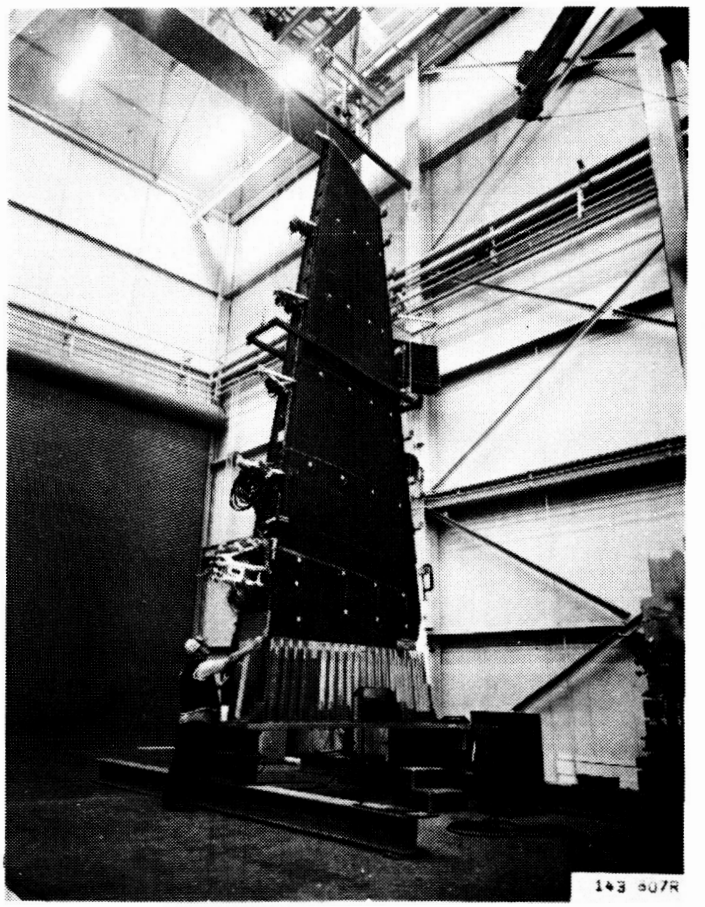

Figure 3. - Fin box.

1.1 Covers

The covers are designed primarily by stiffness. The composite fin box is designed to match the bending and torsional stiffness of the metal fin; the root end matches the existing joint to the afterbody; and all interfaces are unchanged. The (±45°, 0°) cover skin tapers in steps from 34 plies at the root end to 16, 14, then 10 plies. The edges are built up to 0.12 inches, 24 plies, to allow for countersinking holes without feather edges.

The covers are stiffened with cocured hat sections. The stiffener is built up of two five-ply segments with a ten-ply segment sandwiched between them in the crown. A short segment of eight doubler plies is added only at the root end to stiffen the side walls for shearing out the crown loads. Internal clips consisting of two plies at ±45 degrees are added for additional peeling strength.

1.2 Spars

Front and rear spars have been designed to provide at least a 20-percent weight savings over the metallic design, while maintaining production costs and ensuring structural and functional interchangeability with the baseline article.

The front and rear spars are similar in shape and size and are basically one-piece components with rib attach angles, stiffeners, caps, and webs integrally molded in a single cocured operation. The front spar cap forward flange, rear spar cap aft flange, and the fuselage joint areas have been configured to interface with the existing metallic structure.

Strength and stiffness requirements are controlled by selecting ply lay-ups with a sufficient number of ±45-degree plies in the webs to provide the required shear strength and 0-degree plies in the caps for axial loading. To facilitate fastener installation in the final assembly fixture, access holes have been provided in the spar webs. Two access holes are required in each rib bay, and this dictates that three web stiffeners are added between ribs to ensure uniform hole spacing. The access hole edges are not reinforced.

2. PRVT SPECIMEN FABRICATION AND INSPECTION

The cover and spar test specimens are shown in figure 4 and figure 5, respectively. The cover specimen is identical to the Phase II H25 test specimen and the spar specimen is identical to the H20 test specimen, both of which are described in reference 2. The fabrication process development is described in the same reference.

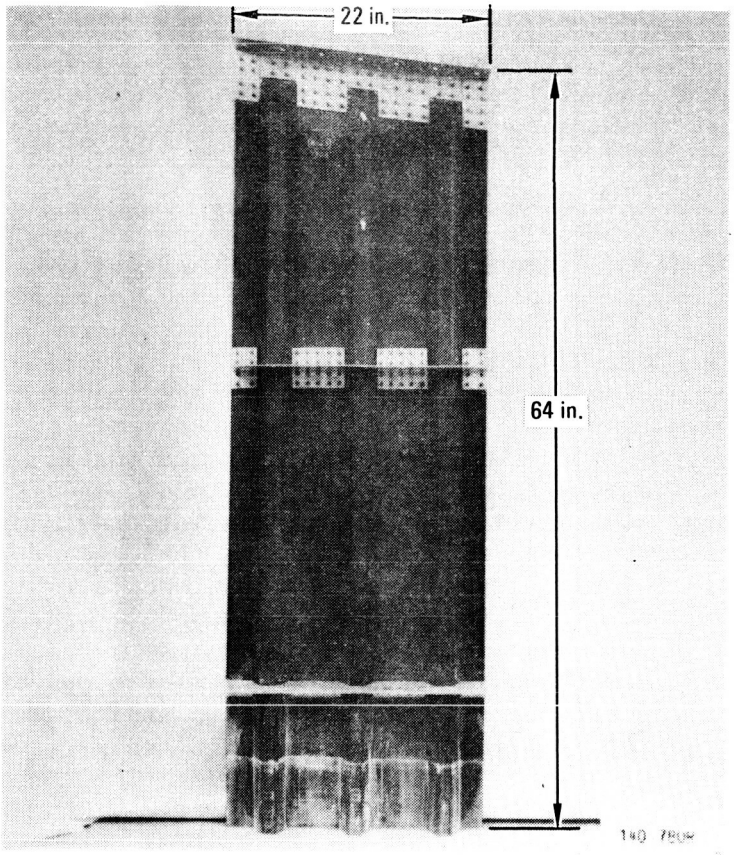

Figure 4. - PRVT cover specimen.

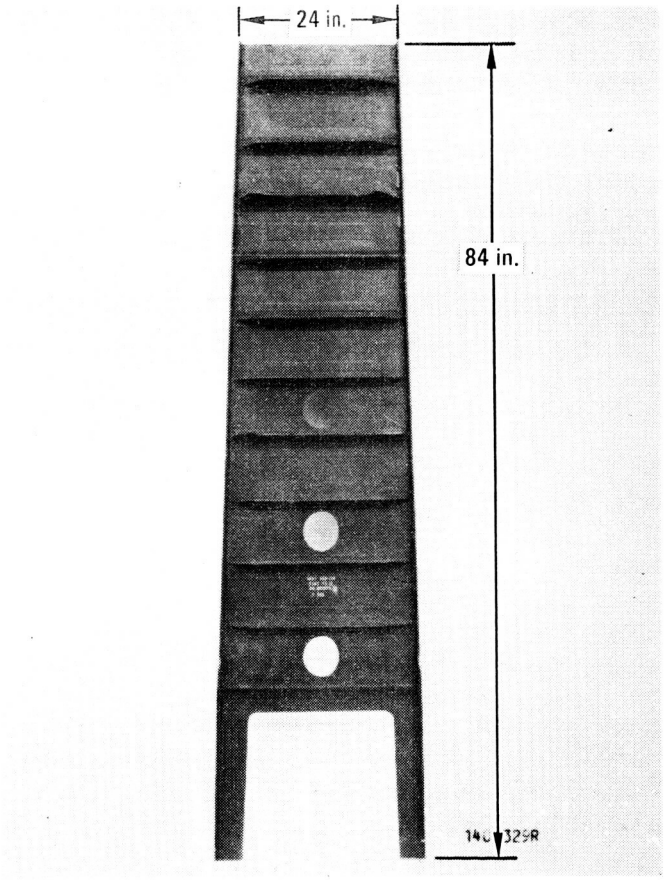

Figure 5. - PRVT spar specimen.

2.1 Fabrication and Inspection

Twenty-eight PRVT cover assemblies were produced of which twenty-two were certified for FAA conformity. Inspections were performed during the fabrication operations in accordance with inspection sign-off requirements documented in the manufacturing operation sheets. All PRVT covers were dimensionally inspected to engineering drawing requirements. All PRVT covers were nondestructively inspected using ultrasonic reflected thru-transmission or pulse-echo techniques. Tag-ends from all covers were tested by the Quality Assurance Laboratory to test requirements established in the process specification. Any deviations from the process specification or engineering drawing requirements were documented on inspection tags and dispositioned through the Material Review Board. A total of 6 PRVT covers were dispositioned scrap by the Material Review Board. A summary of inspection records is shown in table 1.

Twenty-two PRVT spars with full FAA conformity inspections were produced. Variations in materials and processes were held within the tolerances permitted by the material and process specifications. Sequential inspections during the various phases of fabrication were provided by incorporating inspection sign-off requirements into the manufacturing operation sheets. Inspection and verification of the tool and rubber details for completeness and absence of damage was accomplished by in-process inspection prior to the assembly of the broadgoods for each spar. Verification of cure cycle parameters was accomplished by real-time monitoring of recording instrumentation throughout the cure cycle. Following post-cure, visual and dimensional inspections were conducted after the removal of resin flash and process control specimens. Each spar was nondestructively inspected using pulse-echo ultrasonic techniques. Through transmission ultrasonic dual transducers were used to further assess any indications found by the NDI inspector. Dimensional plots and process control results were recorded for each spar, and a configuration documentation package was generated for each spar. The results are summarized in table 2.

2.2 Process Control Data

Process control data for covers and spars are summarized in figures 6 and 7 respectively.

The short beam shear (SBS) results exhibited high scatter because being cut from structure rather than flat panels they were not always perfectly flat. It was concluded that SBS is an unreliable indicator of quality in production components.

The compression data for the covers showed some scatter but was generally within a reasonable band. Low compression results did occur on two specimens which were scrapped but also occurred on two accepted specimens. For the spars the compression specimen used for the first four proved unacceptable because of high scatter. This specimen had ends potted into steel rings and was expensive to prepare. A small specimen was used on subsequent spars based on the FED STD 406 fixture and it proved more reliable.

TABLE 1. - SUMMARY OF COVER INSPECTION RECORDS.

Cover No.	Disposition*	Comments
1	S	Some porosity. Low compression. Trim errors
2	D	High moisture pickup .41% (allow .33%)
3	D	
4	S	Low SBS. Low resin content
5	D	Trim errors
6	D	Masking tape in hat crown. Low SBS. Chipping. Trim errors
7	S	Trim errors
8	S	Low SBS. Chipping. Trim errors
9	S	Low SBS. Scratch and scuff marks. Chipping
10	D	Some porosity. Markoff. Chipping. Trim errors
11	D	Low SBS. Scratch and scuff marks. Chipping. Trim errors
12	S	Low SBS. Markoff
13	X	Foreign matter shown by C-scan and X-Ray
14	X	Porosity and foreign matter shown by C-Scan and X-Ray
15	X	Porosity shown by C-scan and X-Ray
16	S	Some porosity. Low SBS. Chipping
17	S	Some porosity. Low SBS. Markoff. Trim errors
18	D	Some porosity. Low SBS. Markoff. Trim errors
19	X	Severe porosity. Low SBS and compression
20	X	Severe porosity. Low SBS
21	S	Low SBS. Trim errors
22	S	Markoff. Low SBS and compression. Trim errors
23	X	Trim errors
24	D	Some porosity. Low SBS. Markoff. Trim errors
25	D	Some porosity. Low SBS. Markoff. Trim errors
26	D	Low SBS. Markoff. Trim errors
27	D	Low SBS. Trim errors
28	–	Not fabricated
29	D	Excessive material out-time. Low SBS. Trim errors

* S assigned to static test
D assigned to durability test
X scrap

Resin contents varied and several coupons were below minimum or above maximum. These were generally considered to be local anomalies. High resin while increasing weight would not generally have any adverse structural effects. Low resin does reduce strengths but was accepted for test to determine if this would have a noticeable effect on ultimate strength.

TABLE 2. - SUMMARY OF SPAR INSPECTION RECORDS.

Spar No.	Disposition*	Comments
1	S	Isolated porosity. High resin content. Minor delaminations
2	D	High resin content. Stiffener delaminated and repaired
3	S	Stiffener delaminated and repaired
4	S	Isolated porosity. Low compression
5	S	High resin content
6	D	Isolated porosity. Machining damage
7	S	High resin content
8	D	–
9	D	–
10	D	Low SBS
11	D	Low resin content
12	S	Low SBS. Low resin content. Minor delaminations
13	D	Low SBS. Machining damage
14	S	–
15	S	–
16	D	Minor delaminations
17	S	Minor delaminations
18	D	Minor delaminations
19	S	Low compression
20	D	
21	Spare	
22	Trial	Low resin content prepreg
23	D	
24	D	

* S assigned to static test
D assigned to durability test

3. STATIC TESTS

Static tests were performed on ten nominally identical cover specimens and ten nominally identical spar specimens to determine the variability in static strength which can be expected for production quantities.

3.1 Cover Tests

3.1.1 Summary of results. - Table 3 summarizes the results of the ten tests and shows the coefficient of variation. The 3.28 percent coefficient of variation for ten cover specimens represents very consistent test results for compression-loaded specimens. The preodicted failure load was 78,100 lb and the design ultimate load is 57,500 lb.

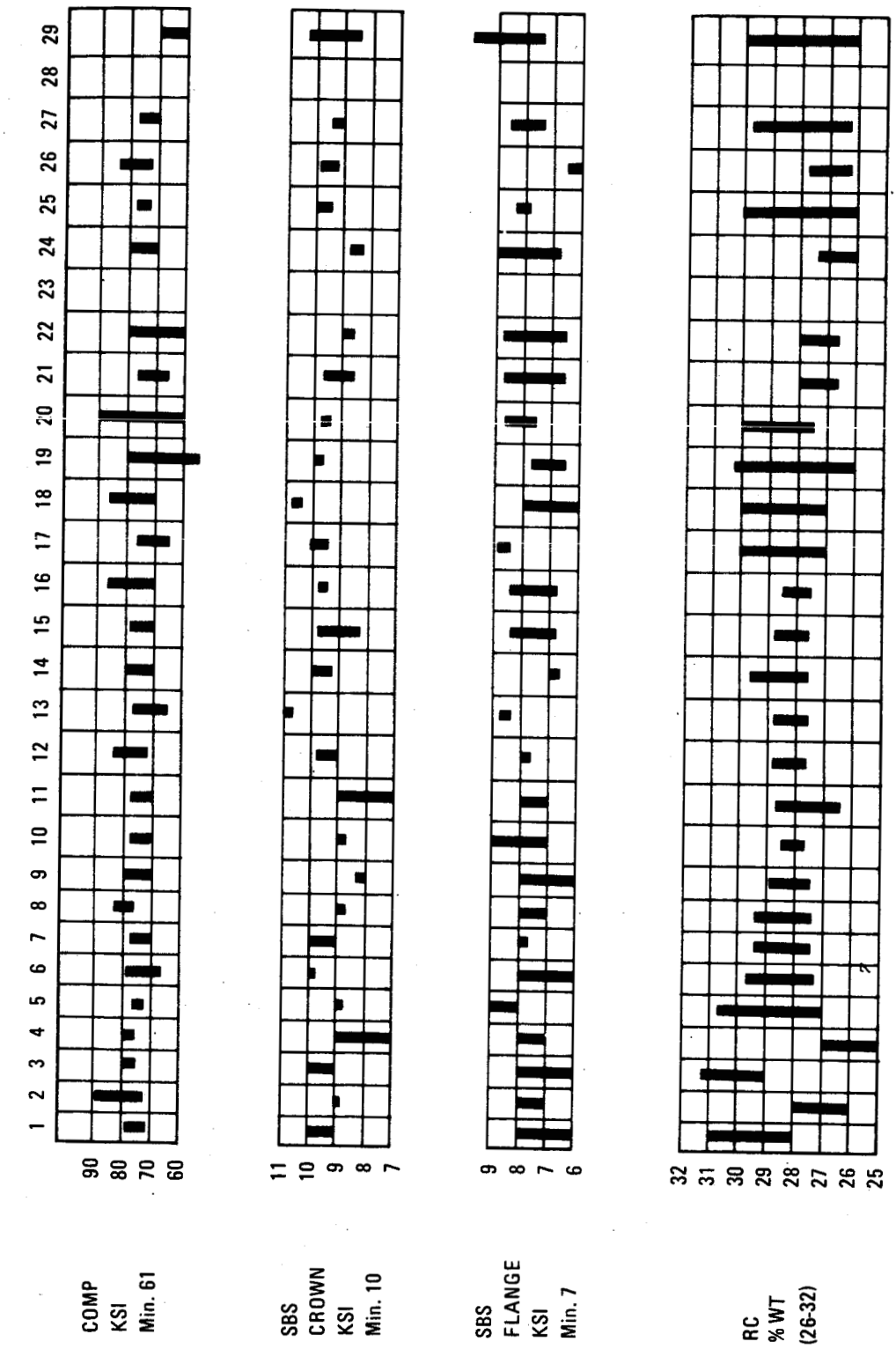

Figure 6. - Summary of cover process control data.

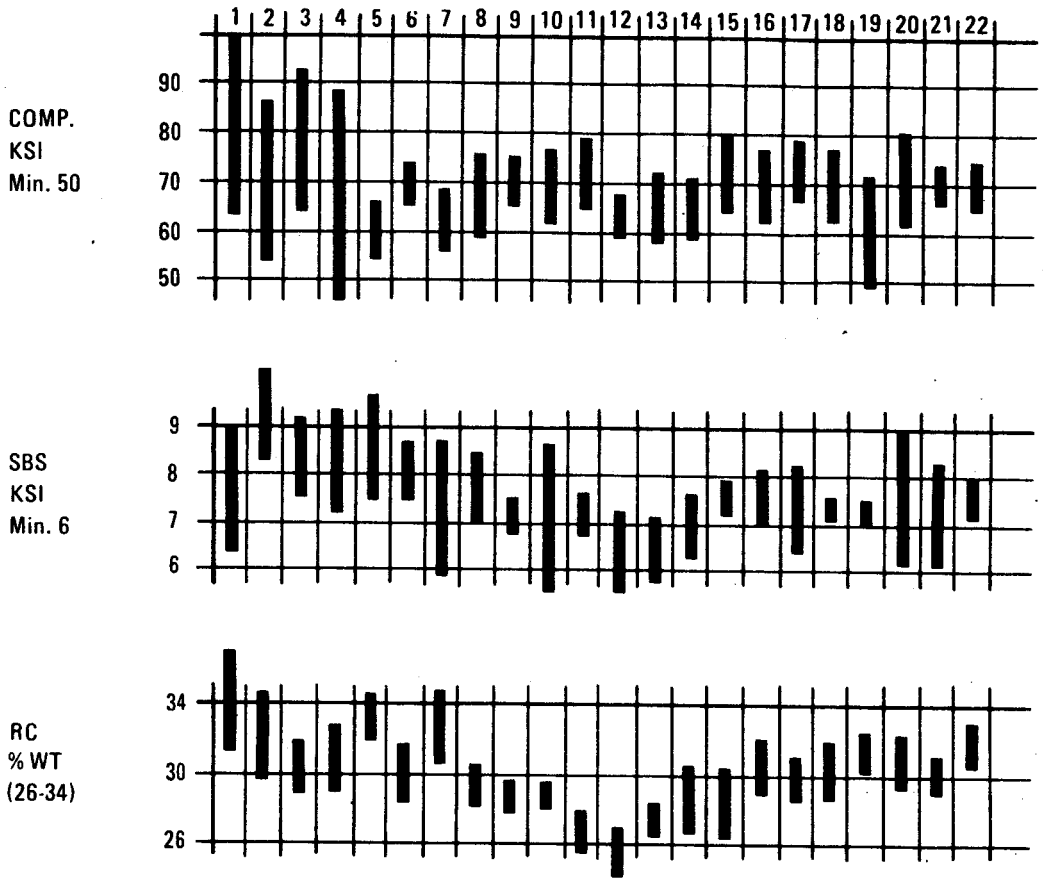

Figure 7. - Summary of spar process control data.

TABLE 3. - COVER STATIC TEST RESULTS.

Test No.	Cover No.	Failure Loads	% Design Ultimate
1	4	-88,900	154.6
2	1	-91,300	158.7
3	17	-95,400	165.9
4	7	-93,800	163.1
5	9	-96,100	167.0
6	8	-93,500	162.6
7	21	-88,500	153.9
8	12	-96,300	167.4
9	22	-89,100	154.9
10	16	-91,000	158.2
Average		-92,390	160.7
Coefficient of Variation		3.28%	

3.1.2 Test setup and installation. The first step was to assemble the graphite/epoxy cover and the aluminum details.

A special shop aid, for proper cover alignment during potting and end-milling operations, was designed and built in the Rye Canyon machine shop for the H25 test described in reference 2 and this shop aid was used in the PRVT test program also.

The second step was to pot the free end of the cover. This was done by clamping the cover to the shop aid with the stringers facing up and the root end located away from the potting box. When clamped, the centroid of the test cover was automatically located on the centerline of symmetry of the potting box. The cover, together with the shop aid, was positioned on-end for the pottting operation.

Unfortified densite, used as the potting agent, was allowed to set up overnight. The next day the assembly was laid flat and heat lamps applied to the open end of the potting box in order to expedite the removal of excess moisture from the densite. A temperature of 120 - 130°F was maintained across the end of the box for 24 hours after which the cover ends were machined flat, square and parallel, using a horizontal milling machine. With the help of the shop aid, parallelism (over the surfaces of the two ends) was controlled to ±0.0003 inch. The assembled specimen is shown in figure 8.

A rigid, steel reaction frame was used to stabilize the test cover during compression loading. The cover was prevented from buckling at the two rib supports and at the root end tee through the use of three 27 inch long aluminum alloy flexure plates. These plates were designed to provide a restraint coefficient of approximately 1.0 at the test panel. Kick loads were reacted through four solid steel links attached to the ends of the cover assembly (at the centroids) and to the reaction frame (figure 9).

Finally, the test cover was installed, in an upside-down position, in the 400 kip Universal static test machine. It was centered between the lower compression plate (resting on the movable base of the machine) and a rigid compression head attached to the fixed upper end of the machine. The reaction frame rested on the movable base of the test machine and was free to move upward along with the loading head.

In the installation procedure, the upper compression head was adjusted (through shimming) until its lower surface was parallel to the upper surface of the lower compression plate. This parallelism was later demonstrated by loading the test cover to 30 kips then observing the head deflections measured at four symmetrically located points near the upper compression head. The two edges of the cover were supported by split tube clamps with adjustable slots.

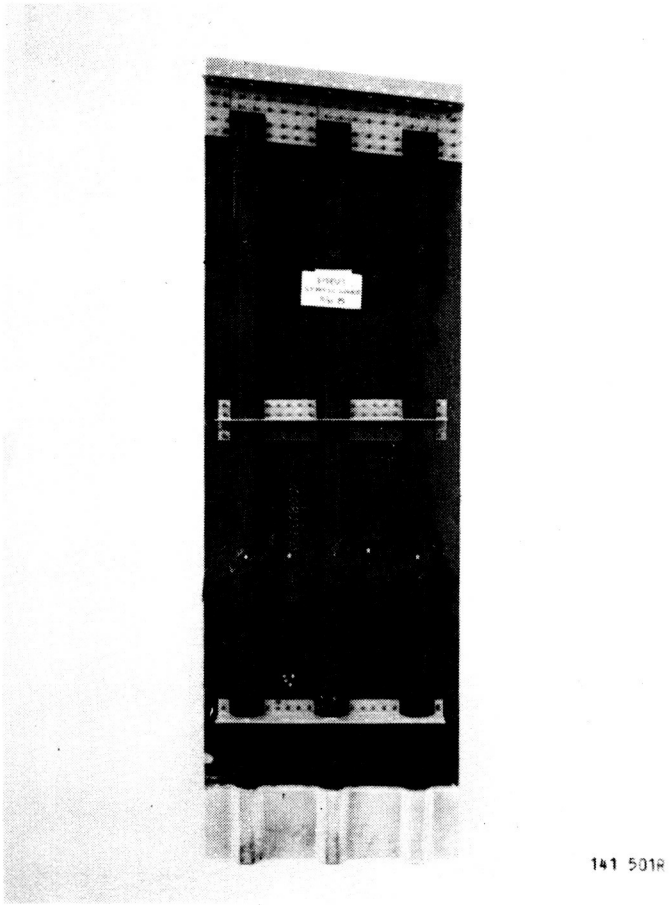

Figure 8. - Assembled cover test specimen.

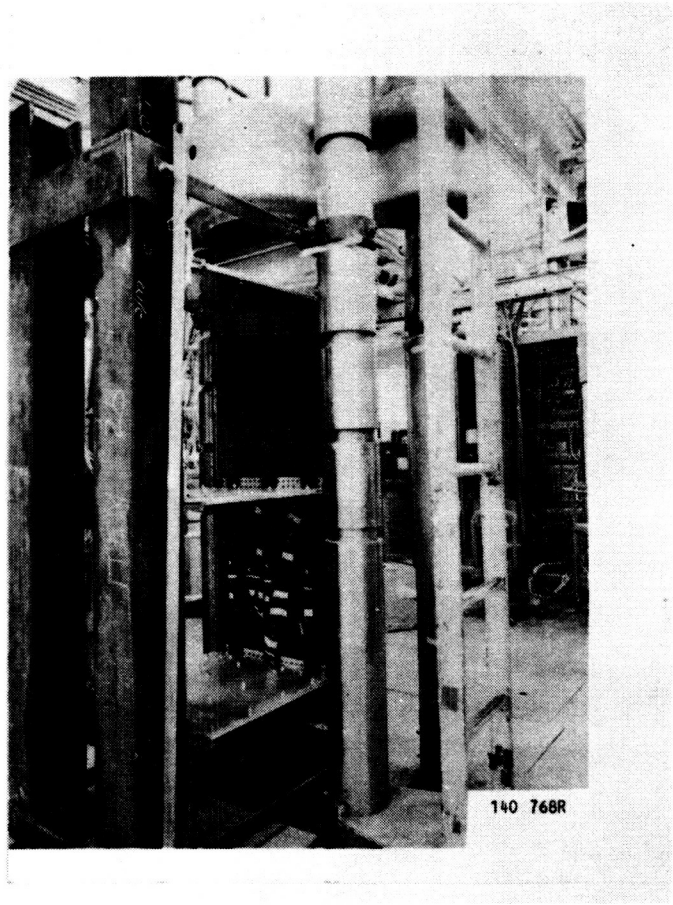

Figure 9. - Cover set-up and fixture.

3.1.3 Instrumentation. - Prior to installation in the 400 kip static test machine each cover was strain gaged. A total of eight axial gages and one shear rosette were applied to the specimens as shown in figure 10. Gages 1, 2, and 3 were located on each of the hat crowns at mid-panel to measure the uniformity of the load distribution. Gages 4 and 5 were back to back on the skin midbay between two of the stiffeners to measure buckling. Gages 6 and 7 were on the skin and hat crowns back-to-back at station 51.75 of the cover to measure bending. Gage 8 was on the hat side wall to measure shear, and gage 9 was at station 51.75 on the skin between two fasteners to measure stress concentration.

When the cover was installed in the test machine, four Linear Variable Differential Transducers (LVDT) were placed symmetrically at the four corners of the head to measure deflection and alignment.

High speed movie cameras were placed to film the final runs to failure.

3.1.4 Test loads. - Each cover was loaded three or four times prior to final test. The first loading was from 0 to -30 kips and back to 0. The gage polarity, LVDT operation, and cover alignment were checked. If any adjustment was necessary or if any data needed rechecking this loading was repeated.

The next loading was from 0 to -57.5 kips and down to -10 kips. The strain gage and LVDT data were evaluated and the loading cycle to -57.5 kips and back to -10 kips was then repeated. The data from the two runs were then compared to check that no permanent deformations had occurred. The loading was then increased continuously to failure.

3.1.5 Test results. - The covers all behaved in a similar manner up to failure. All but one cover failed in the same manner. Figure 11 shows a typical failure from the skin side and figure 12 shows another typical failure from the stiffener side. The failures were initiated by the skin buckling between the hats and the buildup of interlaminar tension stresses that caused the skin and hats to separate. These failures occurred in the 16-ply skin between the two rib supports.

A nontypical failure occurred in test number 3 (cover No. 17). The failure occurred between the root end and the first rib support, very close to the rib in the last of the 16-ply area.

High speed movies (400 frames/second) were taken during each failure run. In most cases the failures occurred within 1/400th of a second and were consequently not picked up by the two high speed cameras. In test 4, cover No. 7, the camera did show the failure initiation at the center hat as shown in figure 13. The camera also caught the failure of cover No. 16 in test 10 as shown in figure 14. In this latter figure, the failure is too far advanced to be certain of the actual origin.

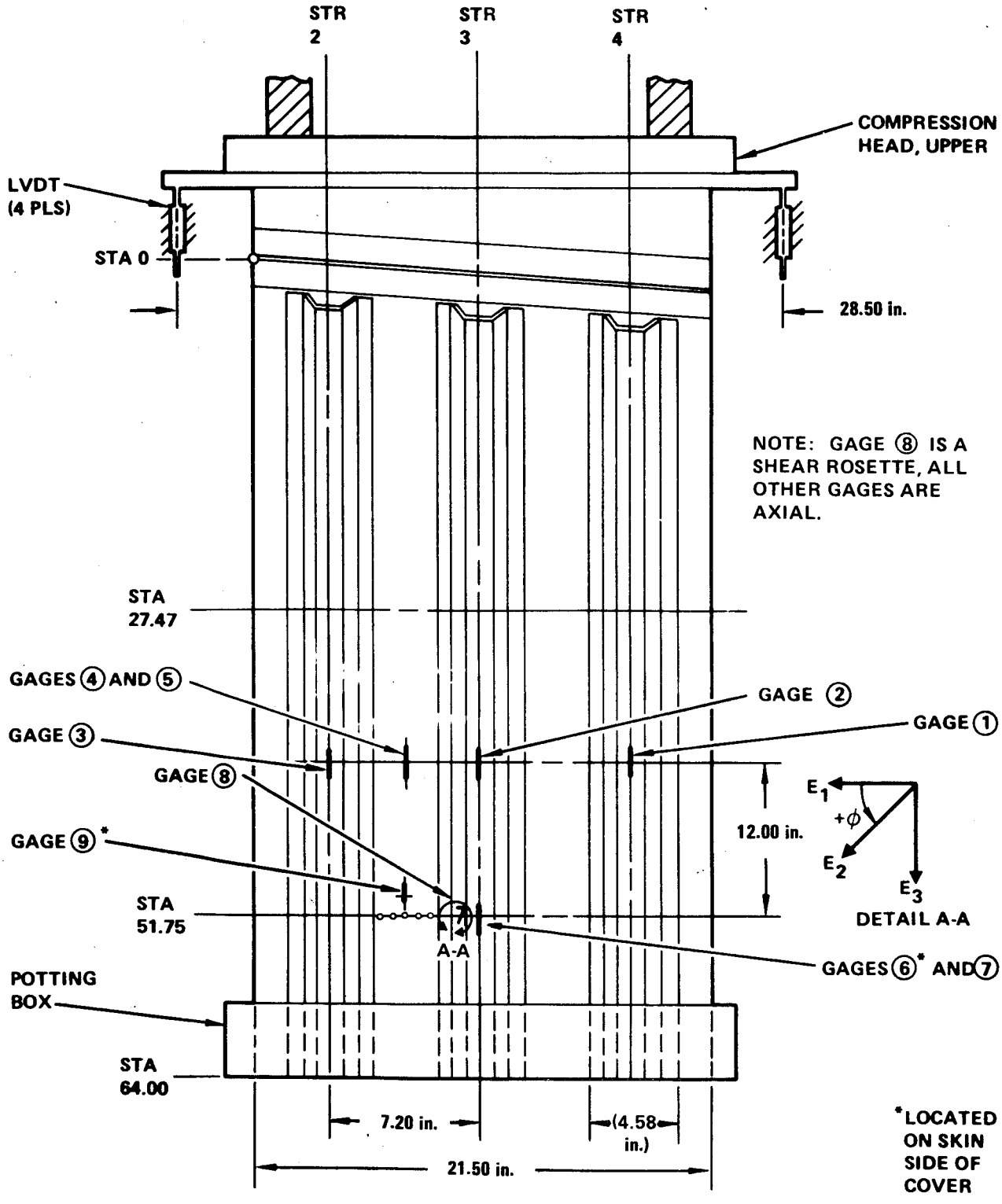

Figure 10. - Strain gage locations.

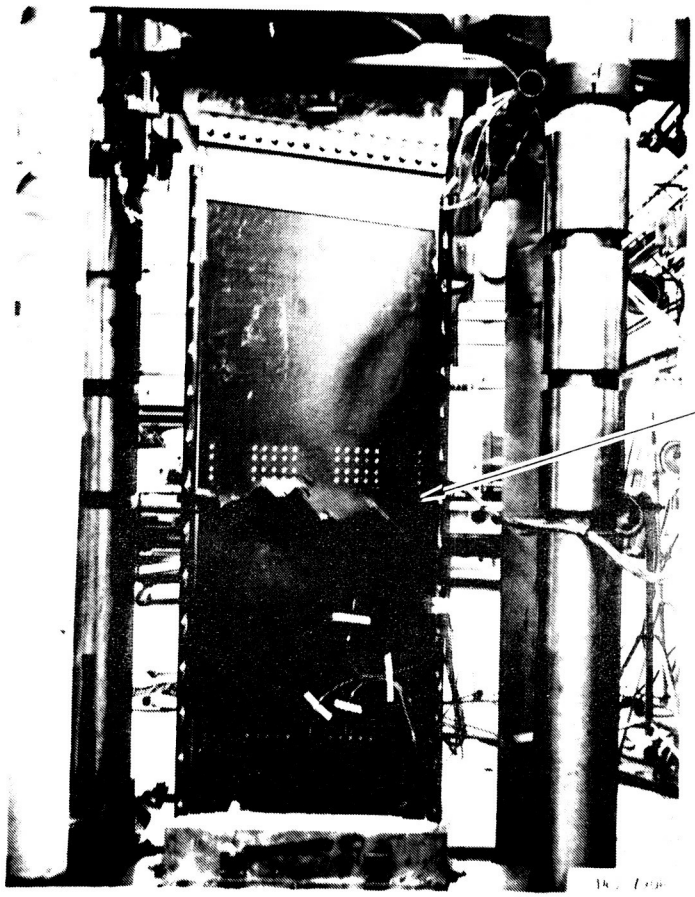

Figure 11. - Typical failure from skin side.

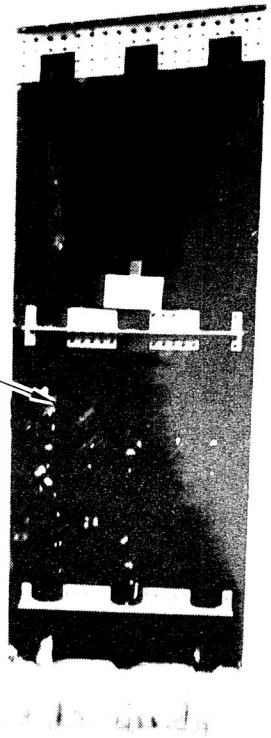

Figure 12. - Typical failure from stiffener side.

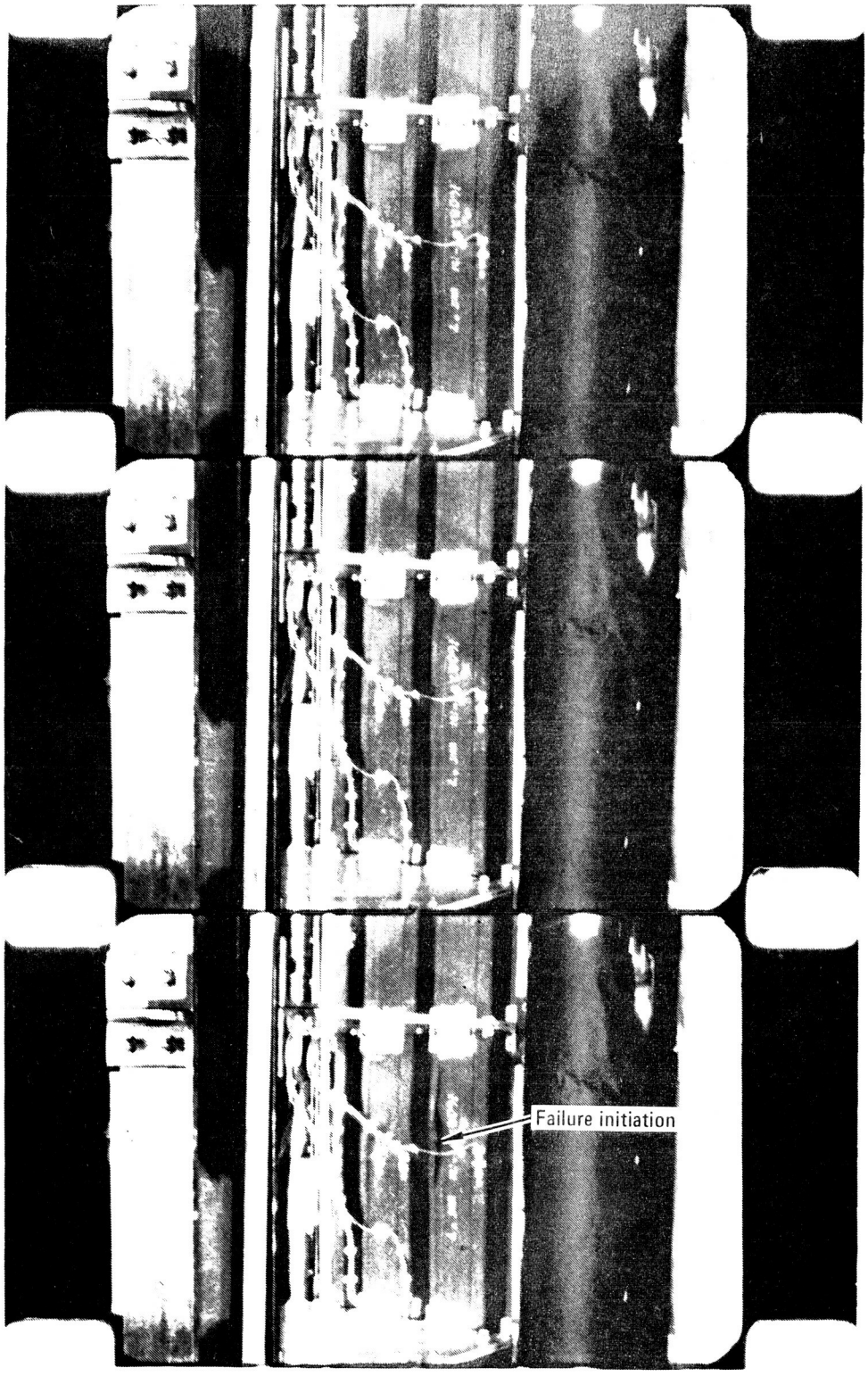

Figure 13. - Failure initiation, cover no. 7, test number 4.

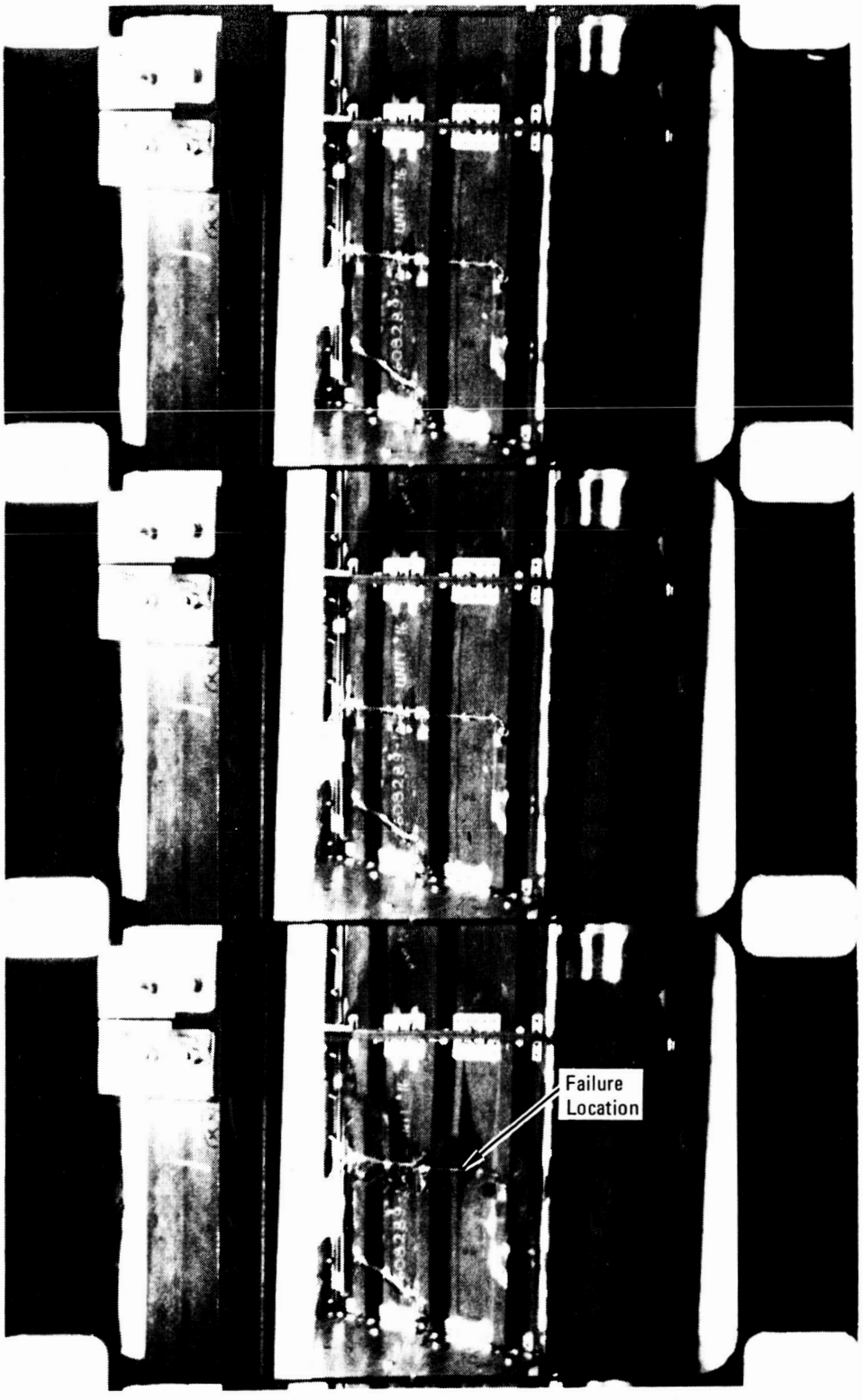

Figure 14. - Failure initiation, cover no. 16, test number 10.

Table 4 summarizes the strain data in the critical area at design ultimate load and at failure in the hats, and at initial buckling and at filure in the skin. The large variation in skin maximum strain at failure is due to the gage location relative to the buckle. The high strains occurred when the strain gage was at or close to the crest of the buckle half wave and the lower strains occurred when the strain gage was away from the crest. The failure loads are summarized in table 3.

3.1.6 Physical tests. - After completion of the static testing, coupons were cut from several covers to determine moisture content. Cover No. 12 was selected because it has the longest interval between cure and test, 223 days and cover No. 21 was selected because it had the shortest time between cure and test, 119 days. Coupons were removed from the 16-ply areas near the points of failure but far enough away from any delamination to preclude getting damaged specimens.

The moisture content tests were conducted from September 28, 1979 through February 18, 1980 using a small 200°F vacuum oven and an analytical balance. Coupons were weighed at the beginning and at intervals over the five months. Coupons from cover No. 16 and cover No. 22 were also introduced during the test span. Results for cover No. 21 are shown in figure 15, and are typical.

The results show that the skin picked up a little more moisture than the hat crown, as expected, because it was only 0.08 inch thick compared to 0.10 inc for the crown. The older cover picked up a little more moisture than the newer cover. Covers No. 16 and No. 22 showed the same trend. From these results it would appear that the moisture contents of all the covers were essentially the same at test and were representative of the anticipated levels of moisture content in service of between 1/2 and 1 percent.

3.2 Spar Tests

3.2.1 Summary of results. - Table 5 summarizes the results of the ten tests and shows the coefficient of variation the 6.11 percent coefficient of variation obtained for the ten spare is similar to test results achieved on numerous other composite and metallic test specimens. The predicted upper jack load of failure was 24,900 pounds. The upper jack load corresponding to design ultimate load is 20,715 pounds. A typical specimen is shown in figure 16.

3.2.2 Test setup and installation. - Aluminum plates were bolted to the caps to simulate the covers. The covers locally have a modulus roughly equivalent to aluminum. The plates provided the correct balance of axial load in the spar caps and shear in the spar webs. A typical test setup is shown on figure 17. The metallic structure shown at the top of the spar is test structure to help introduce the loads.

TABLE 4. - COVER STRAINS.

Test No.	Max head deflection	Critical Section Strains (μ in/in)			
		Max hat crown		Skin	
		DUL	Failure	At buckling (% DUL)	At failure*
1	.267	-2400	-3150	-2800 (99)	-4770
2	.261	-2500	-3500	-3300 (108)	-6620
3	.299	-2500	-3400	-2900 (92)	-7280
4	.298	-2400	-2900	-3000 (98)	-6230
5	.298	-2300	-2750	-2900 (96)	-5850
6	.290	-2400	-2930	-2900 (96)	-7660
7	.279	-2450	-2930	-2600 (83)	-6380
8	.293	-2300	-3100	-3000 (99)	-7000
9	.287	-2300	-2800	-2700 (78)	-6880
10	.281	-2300	-2800	-2800 (87)	-7800

*Max strain at or close to the buckle

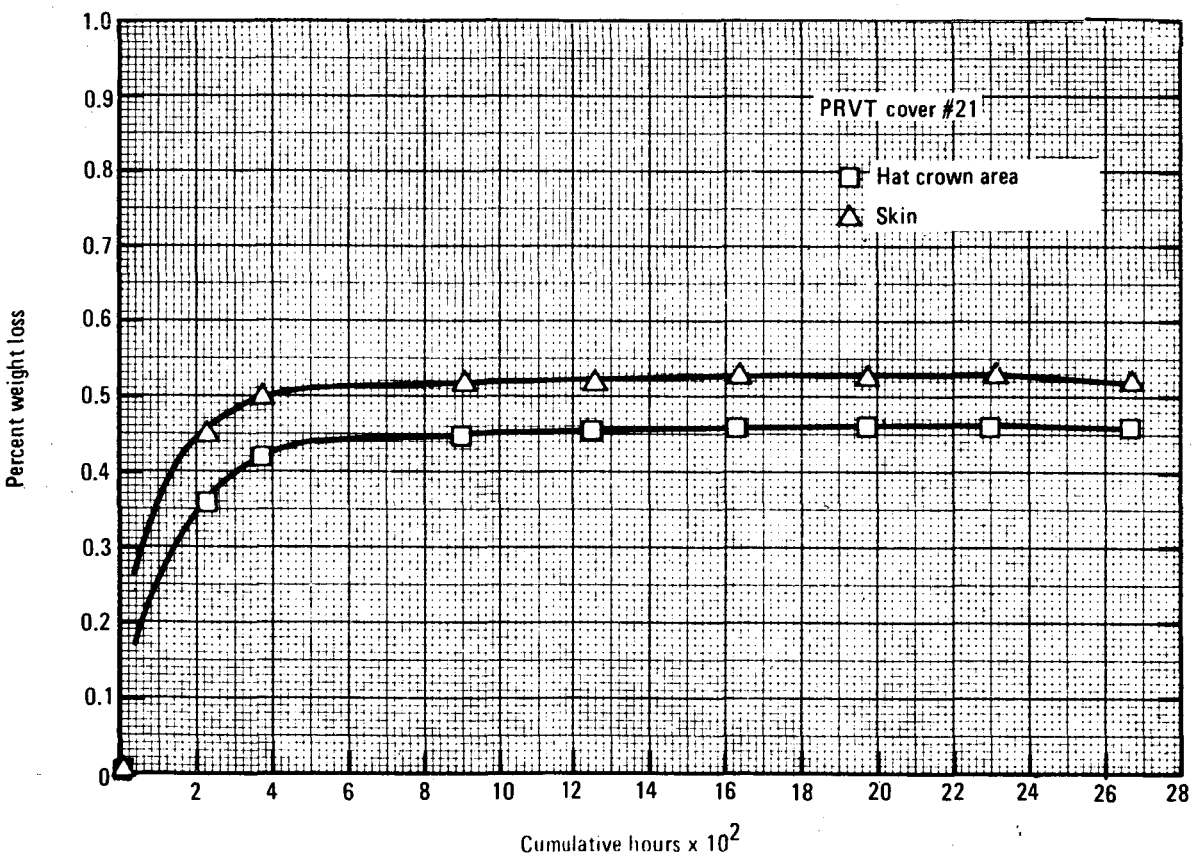

Figure 15. - Residual cover moisture ∿ soak hours vs wt loss %.

TABLE 5. - STATIC SPAR TEST RESULTS.

Test No.	Spar No.	Upper Jack Load at Failure	% Design Ultimate
1	14	25,850	124.8
2	15	26,390	127.4
3	4	27,380	132.2
4	19	27,280	131.7
5	3	28,280	136.5
6	17	27,410	132.6
7	7	28,730	138.7
8	5	30,540	147.4
9	12	26,580	128.2
10	1	30,950	149.4
Average		27,940	134.9
Coefficient of Variation		6.11%	

Each spar was loaded in bending by two hydraulic jacks, one at the tip, and one at the lower rib intersection with the spar. The spar was stabilized at the loading points by steel rods.

The spar was mounted vertically and cantilevered off a rigid I-beam attached to the floor. The loading jacks were attached to a vertical I-beam which was part of a larger general purpose test reaction frame.

3.2.3 Instrumentation. - Prior to installation in the test machine, the specimens were strain gaged. The initial plan called for five shear rosettes and four axial gages as shown in figure 18. After testing the first two specimen2s, rosette gage no. 9 was removed and two axial gages, gages nos. 13 and 14, were added in the hole on the web thickness for the remaining eight specimens. A total of five linear variable deflection transducers (LVDTs) were located as shown in figure 20 to measure deflections.

High speed movie cameras were placed to film the final runs to failure.

3.2.4 Test loads. - The design ultimate loads and the applied test loads are shown in figure 19. The stress analysis showed that the failure would initiate in the web in the bay between VSS 97.199 and VSS 121.45 (the test bay) and that the caps had a considerably higher margin of safety. The spar cap reinforcement was designed to give the best match of web shear and cap axial loading in the test bay in the durability tests which have a single loading jack at the top of the specimen.

A single loading jack in the static test set up would cause overloading and failure in the bay above VSS 121.45, so a two-jack loading arrangement was used as shown in figure 20. This gave a good match of shear loading but gave

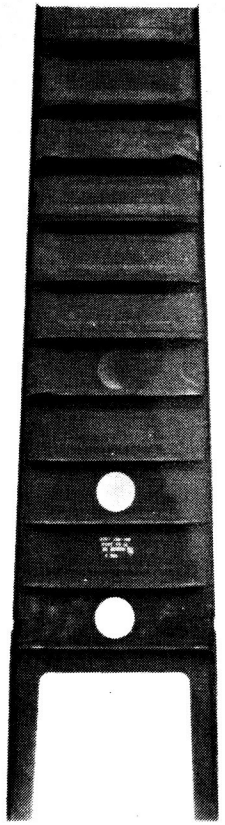

Figure 16. - Typical spar specimen from the stiffener (aft) side.

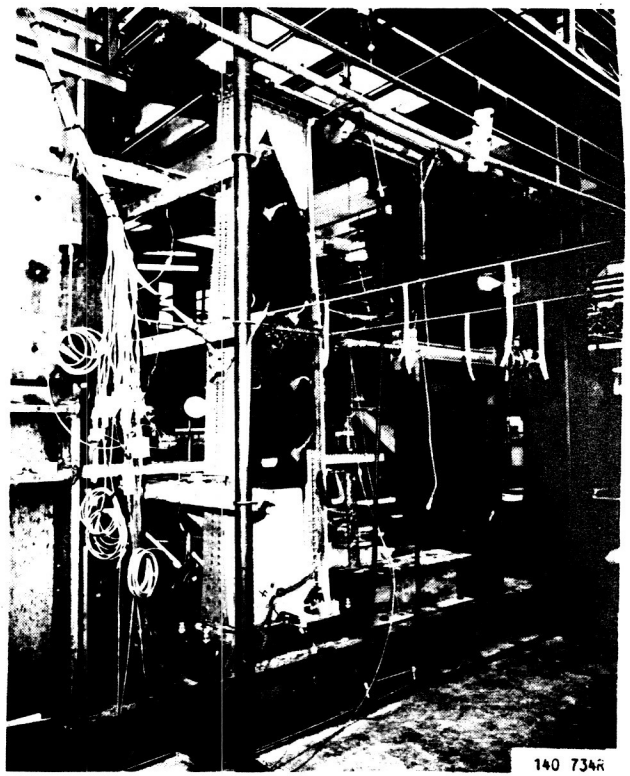

Figure 17. - Static spar test set-up.

1. Axial gages 13 and 14 bonded to web thickness
2. Rosette gage 12 is back-to-back with Rosette 6

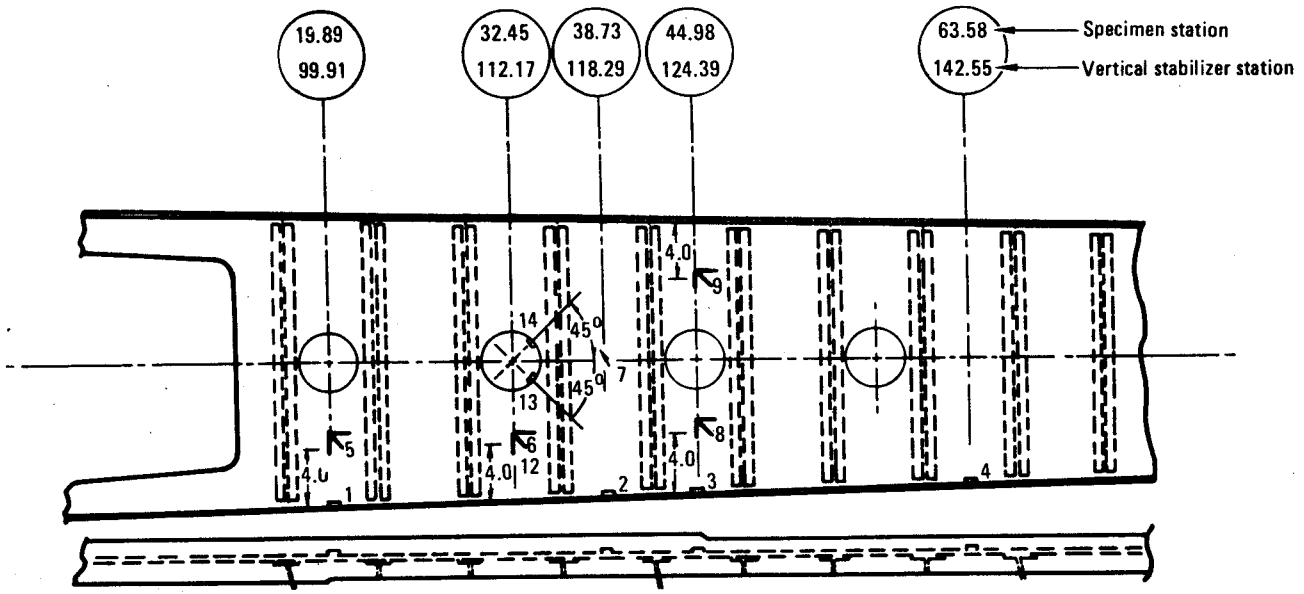

Figure 18. - Strain gage locations for spar test specimens.

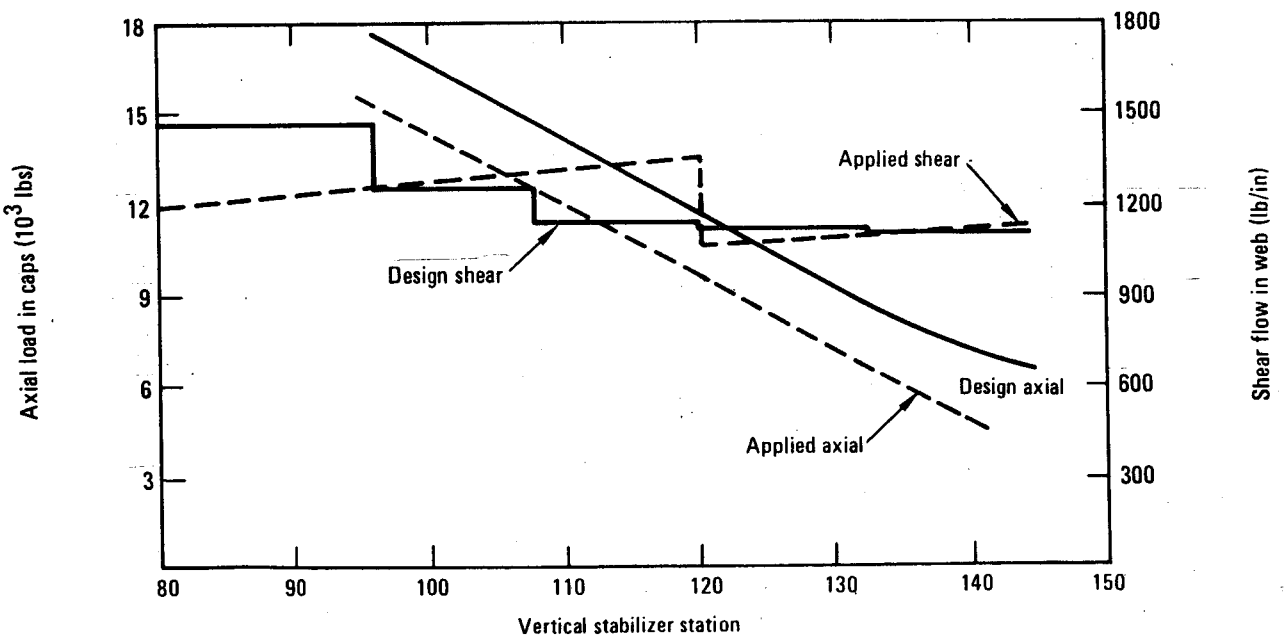

Figure 19. - Spar design ultimate loads.

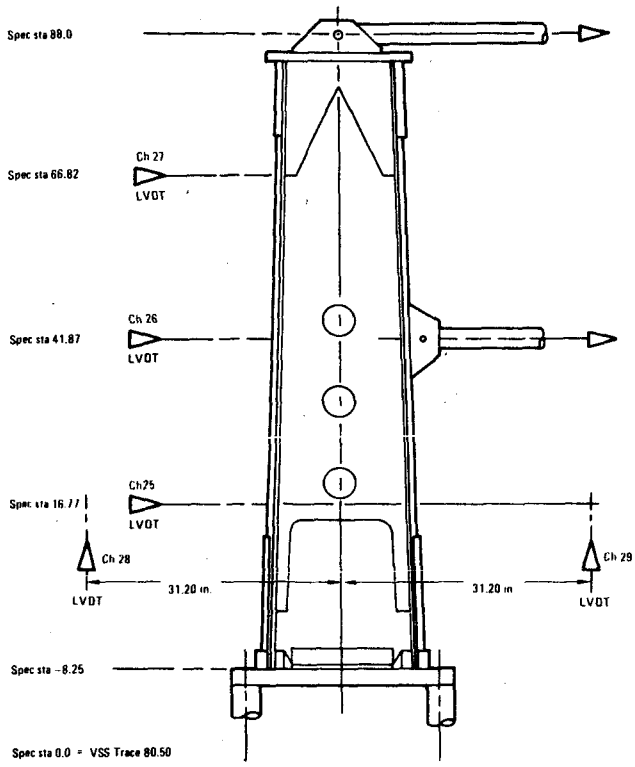

Figure 20. - Deflection measurement locations.

a lower cap axial load. Design ultimate loading in the spar was achieved when the hydraulic jack load at specimen Sta 41.87 was 5,310 pounds and at specimen Sta 88 was 20,715 pounds.

Each spar was cycled from 0 to design ultimate load, which was held for a minimum of 30 seconds, and back to 0 twice to verify repeatability. The specimen was then loaded continuously to failure.

3.2.5 Test results. - The spars all behaved in a similar manner up to failure. All failures, except one, were in the bay through the access hole, at specimen Sta 32.45, and were similar in appearance. Figure 21 shows a typical failure from the forward side of the spar and figure 22 shows a typical failure from the aft side of the spar. It can be seen in figure 22 that the stiffener just above the access hole at which failure occurred popped off. The failure shown near the top of the specimen in figure 21 was a secondary failure caused by the high deflection after the primary failure.

Spar no. 1 experienced the nontypical failure. Figure 23 shows a large buckle which occurred at the lower access hole at specimen station 19.89 just prior to failure. Failure occurred at the lower access hole as shown in figure 24.

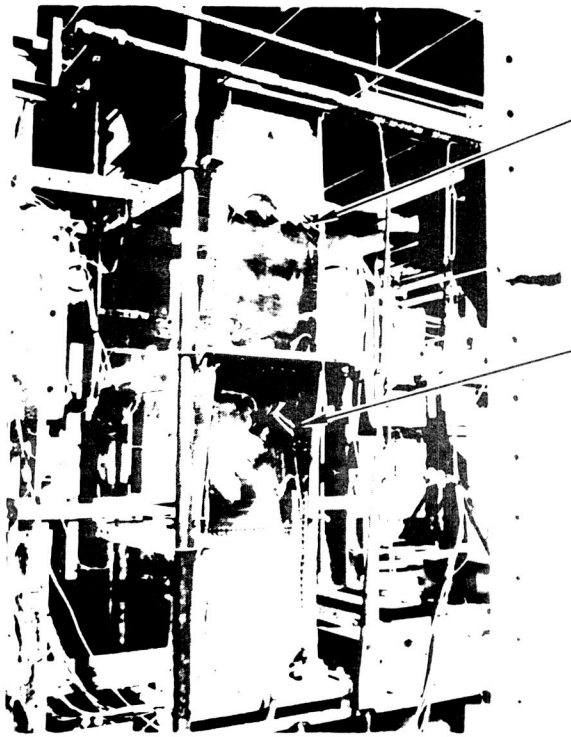

Figure 21. - Typical failure from forward side of spar.

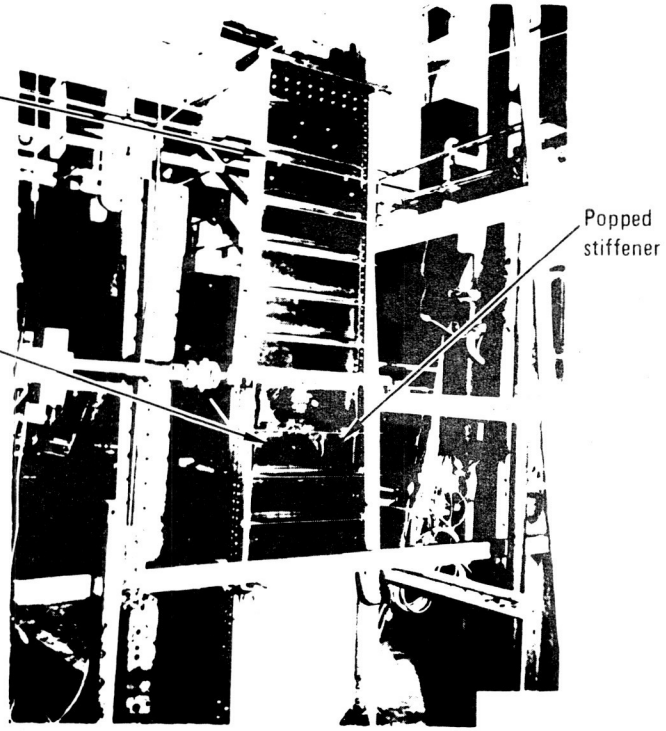

Figure 22. - Typical failure from aft side of spar.

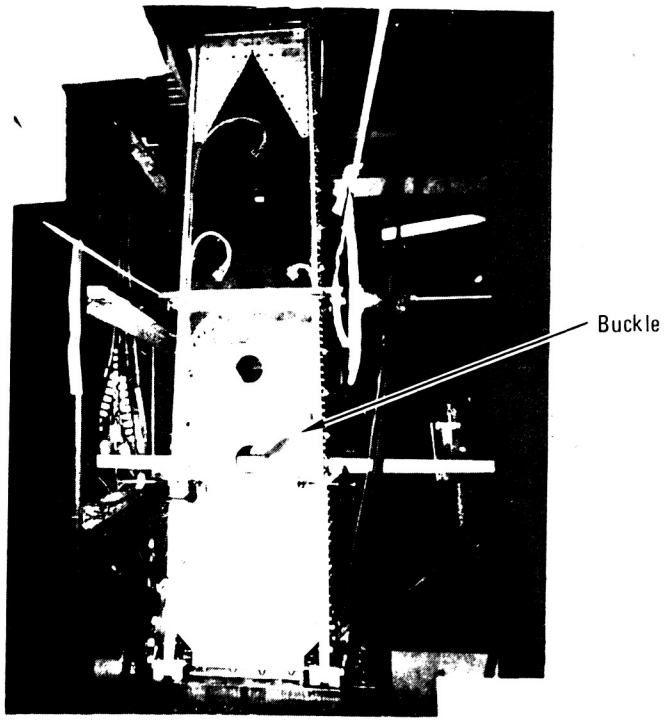

Figure 23. - Photograph of spar no. 1 taken just prior to failure showing buckle at lower access hole at specimen station 19.89.

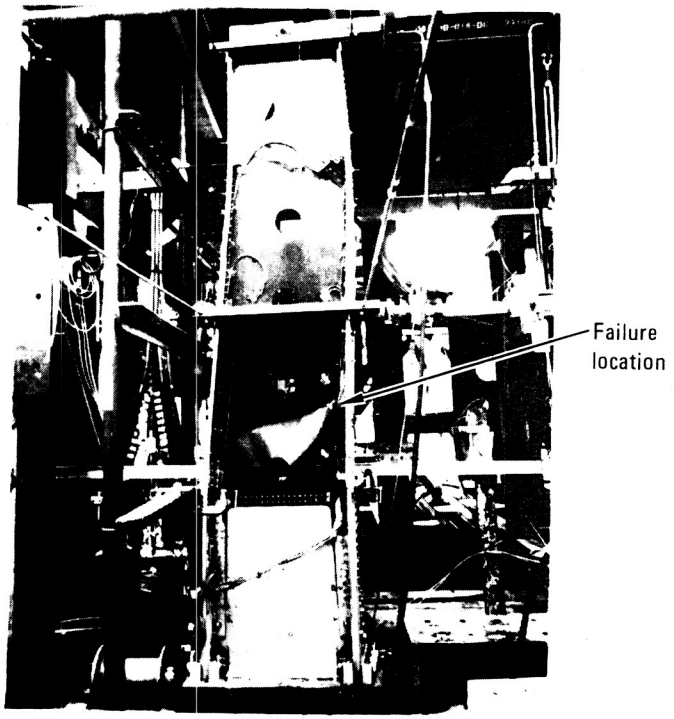

Figure 24. - Failure of spar no. 1 through lower access hole.

An anomaly occurred during the first test, spar no. 14. Two test runs to design ultimate were made with satisfactory results. The failure run was terminated at 123 percent of design ultimate when it was noted that delamination of the web had occurred. This delamination was at the second access hole at specimen station 32.45. The delamination was not visible when the load was removed. The spar was then reloaded to design limit, held for 30 seconds and then unloaded. After a review of the data, it was decided to retest the spar to determine the maximum load capability after the initial failure (or delamination of the spar web). The spar was reloaded to failure, which occurred at 125.0 percent of design ultimate.

Table 6 summarizes the strains at key locations in each test (gage locations are shown in figure 18). The results were somewhat scattered, but in general, the results were within about ±10 percent at design ultimate load. Gage 2 in test number 9 appeared to be defective as it read consistently low. The higher than normal shear strains in tests number 1 and number 10 as shown by gage 6 were due to the delamination and the buckling respectively, as reported above.

TABLE 6. - SPAR STRAINS AT MEASURED LOCATIONS

Gage*	2		6		7		13		14	
Test No.	DUL	FAIL	DUL	FAIL	DUL	FAIL	DUL	FAIL	DUL	FAIL
	ϵ	ϵ	γ_{xy}	γ_{xy}	γ_{xy}	γ_{xy}	ϵ	ϵ	ϵ	ϵ
1	-1320	-1840	4300	5510	4550	6160	–	–	–	–
2	-1160	-1580	3400	4040	4050	5690	–	–	–	–
3	-1130	-1560	3400	4780	3950	6030	-4500	-5520	4000	5500
4	-1150	-1610	3450	4460	4250	6100	-5200	-6670	4600	6350
5	-1070	-1580	3250	4170	4000	6150	-4800	-5470	4000	5600
6	-1200	-1670	3450	4270	4150	6150	-4500	-5580	4500	5900
7	-1080	-1610	3450	4680	4100	6490	-4400	-6120	4400	6130
8	-1050	-1700	3550	4880	4100	6740	-4100	-5300	4000	6140
9	-730	-1000	3150	3610	4050	5860	-4600	-5640	4200	5640
10	-1010	-1590	3400	5290	4000	6340	-4600	-5640	4200	5640

*See Figure 17.

The strain gages in the access hole exhibited more scatter than the other gages. This was expected because of the rapid changes due to the initiation of shear buckling at the edges of the cutouts.

3.2.6 Physical tests.- At the completion of static testing, coupons were cut from the webs of several spars to determine moisture content. The last three specimens were the only ones available and they represented the beginning and middle of the fabrication run. Specimens were cut from areas near the failure but away from any delaminated areas to preclude getting damaged specimens.

The moisture content tests were conducted over a period from October 23, 1979 through February 18, 1980 using a small 200°F vacuum oven and an analytical balance. Coupons were weighed at the beginning and at intervals over the five-month period. Results of these tests are shown in figure 25.

The results show that the older two spars had picked up more moisture than the newer spar. Spar no. 5 had a higher moisture content than spar no. 1 but was within a normal scatter band. The spars would appear to have had between one-half and one percent moisture at test and were thus representative of the levels of moisture content to be expected in long-term service.

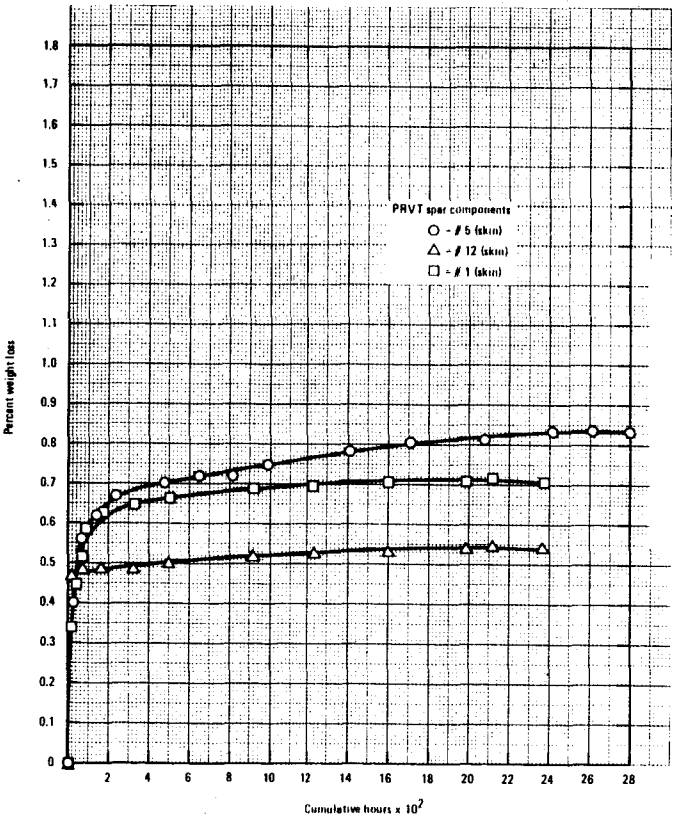

Figure 25. - Residual spar moisture ~ soak hours vs wt loss %.

4. DURABILITY TESTING SET-UP

The durability testing was designed to give quasi-real-time results and to bridge effectively the gap between accelerated coupon testing which is completed in a matter of a few weeks and the real-time exposure of structural components in flight service.

The normal ground/air/ground environment causes both absorption and desorption of moisture by the epoxy matrix. This causes a laminate to swell and shrink in thickness. This effect would be most detrimental in joint areas. The continuous swelling and shrinking may loosen the joint over a period of time or cause other detrimental effects. This would not only be an undue maintenance burden but might lead to structural failures.

4.1 Test Criteria

4.1.1 Environmental spectrum.- The upper bound of temperature was selected on the following basis. The thermal cycles being used in the test represent about 20 percent of the total cycles expected in the fin life-time. The ambient temperature, then, was assumed to be that exceeded on the average 20 percent of the time, or an ambient of 80-85°F, based on the temperature exceedance data contained in figure 26. This ambient temperature range converts to a skin temperature of about 140°F if a painted fin is assumed with the darker color of paint predominating.

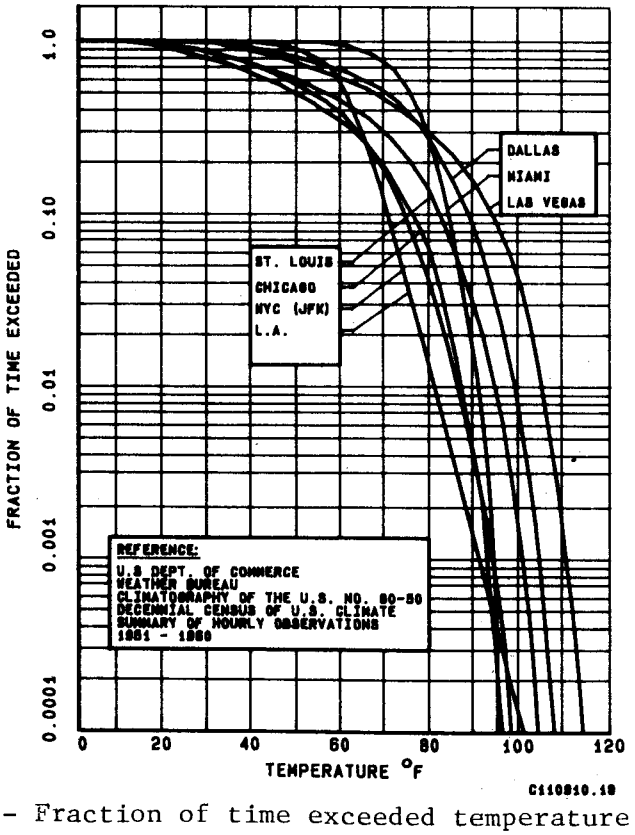

Figure 26. - Fraction of time exceeded temperature of selected U.S. cities.

The lower bound of temperatures, -30°F, was selected to be certain that the moisture in the laminate will be fully frozen prior to beginning the heating cycle. This would ensure the maximum volumetric expansion of the laminate, working against the metal fasteners.

The relative humidities were selected at 0 percent and 95 percent. This represents fairly typical conditions found in Las Vegas and Miami, respectively, in summer months. The flight cycle is thus typical of continuous operation between the two cities and would exercise the moisture gradients between layers of the laminate to a maximum.

In addition to the environmental spectrum, at dispersed times during the test the temperature was allowed to reach 160° (40 times), and 180° (10 times). These latter conditions simulated the infrequent maxima expected in service.

This environmental spectrum was intended to accomplish two primary objectives, namely to provide large changes in moisture content through the plies of the laminate and to produce some acceleration of the testing program, simulating a higher number of equivalent cycles than the actual 5800.

Temperature was measured at selected locations on the exposed surface and substructure of the test specimen. Humidity was measured in the air surrounding the test article.

4.1.2 Load spectrum.- Figure 29 depicts the loading spectrum used in the test. The spectrum is presented in cycles of load/reference load, or normalized to a reference load. One lifetime represents 36,000 flights, the equivalent of 20 years of service. Thus one thermal cycle represents approximately 6.2 flights. Figure 27 also shows the loading spectrum used for the metal fin in the full-scale L-1011 fatigue test.

Loading cycles were applied in the climb, cruise, and descent phases of a flight. In developing the block loading, the climb, cruise, and descent phases were examined separately. Figure 28 shows the segments of the thermal cycle during which loads are applied. In the climb segment loads were applied while the skin temperature ranges from 80°F down to 40°F, approximately 37 percent of the total number of the load cycles are applied in this segment. In the cruise segment, loads were applied while the temperature ranges from 0°F to -30°F, approximately 9 percent of the total number of load cycles were applied during this segment. The remaining 54 percent of the load cycles were applied during the descent segment while the temperature ranges from 40°F up to 80°F. The block loading for the three flight phases for 36,000 flights compressed into 5800 thermal cycles is shown in table 7.

The limit loads for the durability testing were somewhat different from those used for the static testing. In the case of the spars the loads were applied by one jack at the tip in the durability testing rather than by two as discussed in Section 3.2.4. For durability testing limit load applied at the tip was 17,350 lb/spar. For the covers, a mean load for the panel above the lower rib was used rather than the maximum load. For durability testing 36,400 lb/cover.

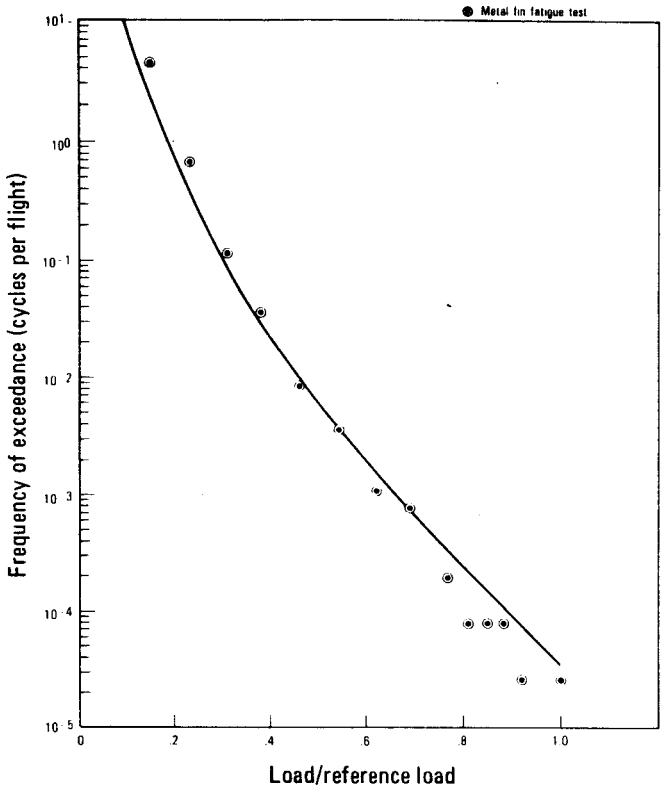

Figure 27. - Vertical tail normalized load fatigue spectrum.

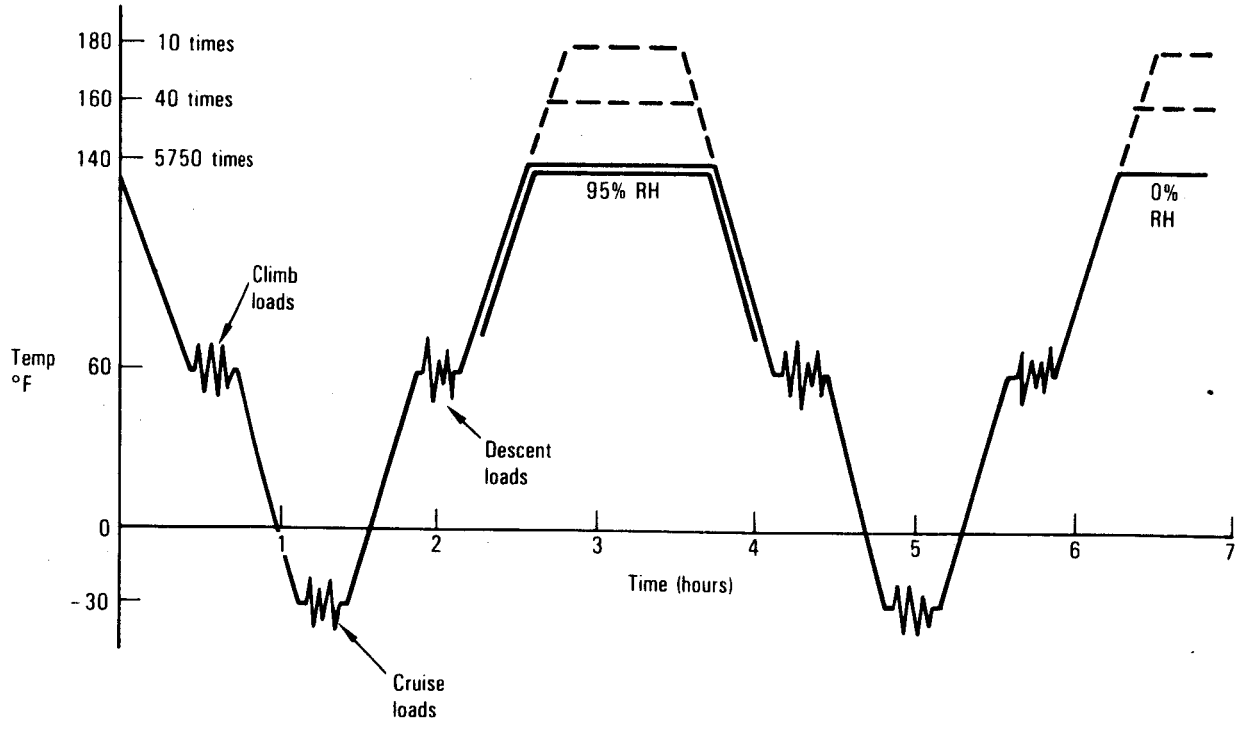

Figure 28. - Load/thermal cycle sequence.

TABLE 7. - FATIGUE TEST BLOCK LOADING

% Limit Load	N	ΣN	Flight Phase	Thermal Cycle 1	6	58	290	1450	2900	5800
15	168,184	198,218	CI	9	9					
			Cr	2	2					
			D	14	13					
23	24,044	30,034	CI		7	2	1			
			Cr		3	1				
			D		14	5	2			
31	4,192	5,990	CI		1	1		1		
			Cr		1					
			D		2	2	1	1		
38	1,245	1,798	CI			1	1	1		
			Cr				1	1		
			D		1	1	1	2	1	1
46	328	533	CI			1		1		
			Cr			1				
			D			1	1	1		
54	134	225	CI					1		
			Cr					1		
			D			1	1	1	1	
62	43	91	CI				1			
			Cr							
			D				1		1	1
69	28	48	CI					1		
			Cr							
			D				1	1		
77	9	20	CI					1		
			Cr							
			D					1		1
81	3	11	D						1	1
85	3	8	D						1	1
88	3	5	D						1	1
92	1	2	D							1
100	1	1	D							1
Count				25	53	17	12	15	6	8
Multiplier				5800	966	100	20	4	2	1

Spar Limit Load = 17,350 lb (10 Spec) Spar Limit Load = 26,025 lb (2 Spec) "High Strain" Components
Cover Limit Load = 36,400 lb (10 Spec) Cover Limit Load = 54,600 lb (2 Spec)

The magnitude, total number of cycles at each magnitude and which phase of flight the loads were to be applied were input to the computer for randomization and application to each flight. This randomized flight spectrum was applied to all four chambers with each occurring at the same flight number on each chamber. For example, if a 46 percent limit load cycle occurred at flight 3451 on Chamber 1, it would also occur at that same flight number on Chambers 2, 3, and 4.

The computer maintained a count of which loads had been applied to each chamber so that the desired number of cycles at each load were applied over the test life.

4.2 Environmental Chambers and Test Setup

Based on the number of test components, size, thermal mass, loads, time restraints, available floor space, etc., an analysis of all pertinent factors determined that the optimum test facility would require two chambers with 90 inches long by 52.5 inches high by 32 inches wide internal working dimensions for the ten durability cover specimens, and two chambers 105 inches wide by 120 inches high by 40 inches deep for the ten durability spar specimens. A schematic of the cover chamber is shown in figure 29, and one of the spar chamber in figure 30.

The chambers were constructed of a continuously heliarc welded series 304 stainless steel inner liner and an angle frame reinforced 16-gage cold rolled steel outer case insulated with Upjohn Company Trymer CPR 9945 modified isocyanurate cellular plastic. The cover chamber had double doors on the front and back sides permitting easy access for inspection of the specimens. The spar chamber had one large door on the front exposing the entire working volume. The doors were designed with both an inner and outer gasket to minimize water buildup in the gasket space and reduce thermal losses through the door breakers. The floor had drains for condensed moisture.

Air circulation within the workspace was accomplished by a blower system drawing air from the workspace, blowing it through heating and cooling coils, and returning it to the workspace.

System low temperature was achieved by a two-stage cascade water-cooled semihermetic mechanical refrigeration system. The system included:

- Two 75 CFM Carlyle semihermetic mechanical refrigeration compressors. R502 for the high stage and R503 for the low stage.
- Dual pressure refrigerant suction and discharge safety switches.
- An automatic hot gas bypass proportioning valve.
- An automatic suction cooling and suction pressure limiting thermal expansion valve to limit the suction temperature to a safe level for the compressor.

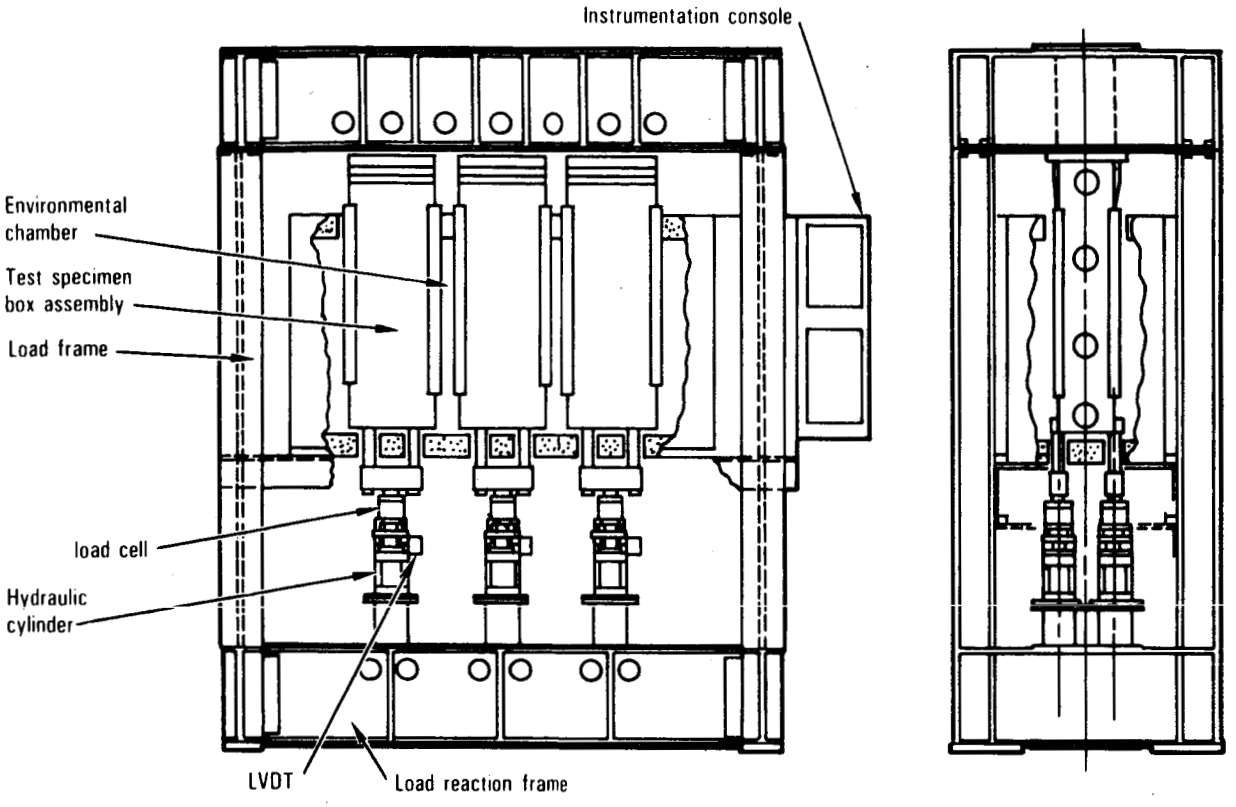

Figure 29. - PRVT cover durability test setup.

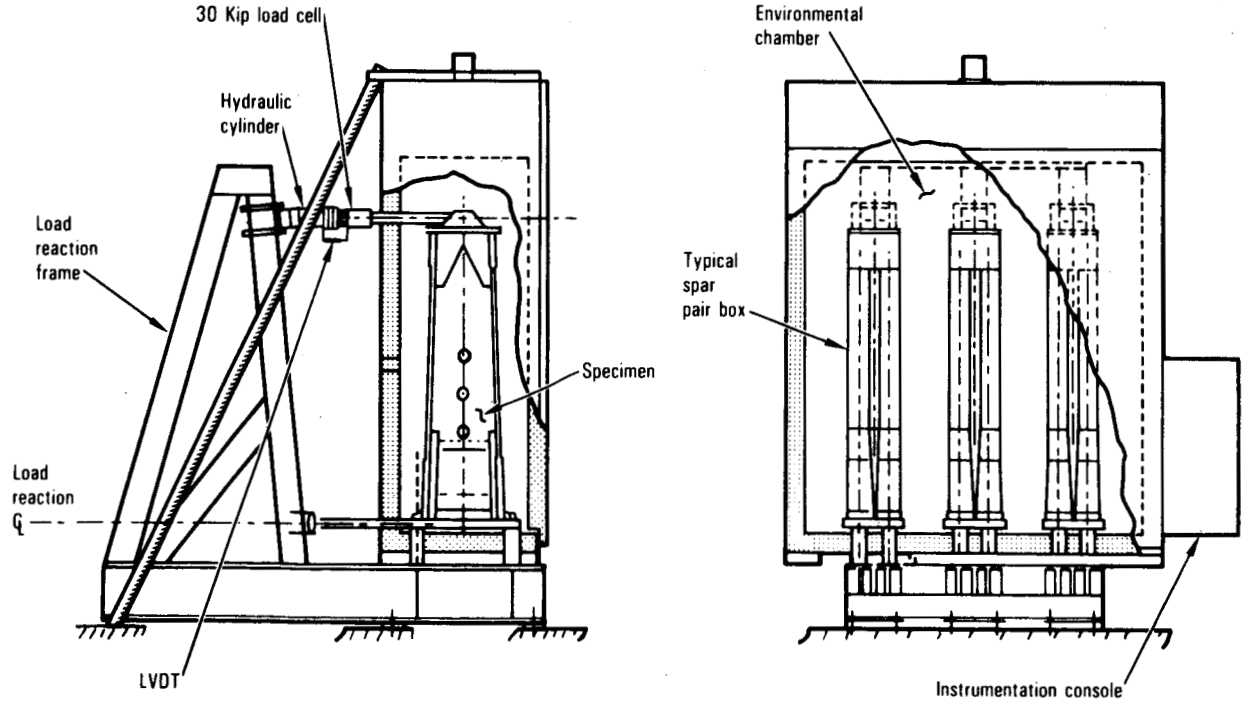

Figure 30. - PRVT spar durability test setup.

- Thermal expansion valves with automatic suction pressure limiting, adjustable superheat and external pressure compensation to modulate refrigerant flow to the cooling coils in the various chambers.

- Modulating valves to proportion fluid flow of refrigerant versus thermal load controlled by the temperature controlled in the various chambers.

This refrigeration system package is shown in figure 31.

One refrigeration system cooled all four chambers; thus, the cooling cycle was staggered into one-thirds so that only one spar or two cover chambers are cooling at any one time to minimize refrigeration capacity requirements. Should one chamber experience a down condition, it had to remain off until it could come in at the proper temperature cycle sequence. This sequence is shown in figure 32.

A central steam generator was also contained in the refrigeration system machinery console to increase vapor content in the various chambers. The steam generator included: a sight glass; an automatic low water cut-out; an automatic water level control; and a pressure control relief valve. Steam was proportioned by the humidity controllers via a solenoid valve to each chamber. Just downstream of the inlet air orifice a one-inch pipe ran perpendicular to the air stream the full width of the air orifice and sprayed steam into the air steam through six 3/32-inch holes.

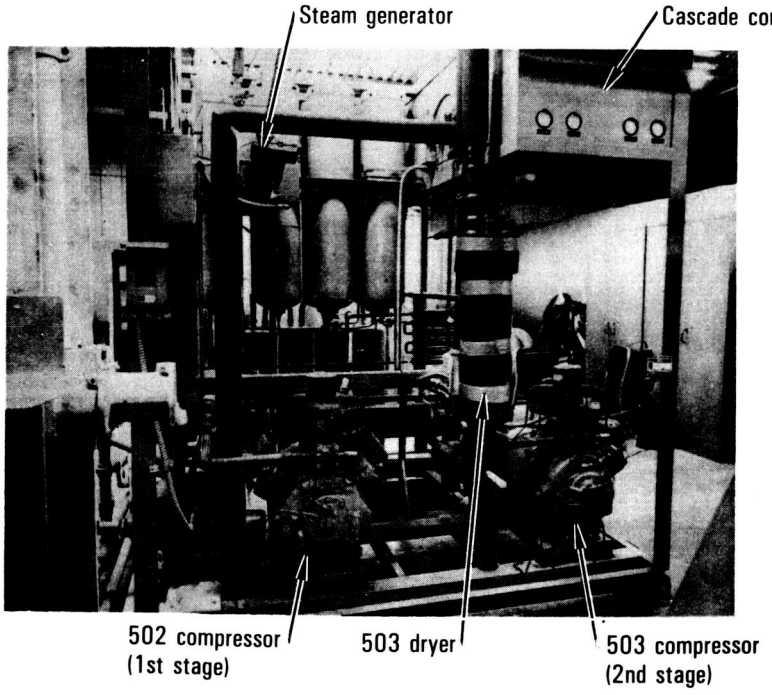

Figure 31. - Refrigeration/steam generator unit.

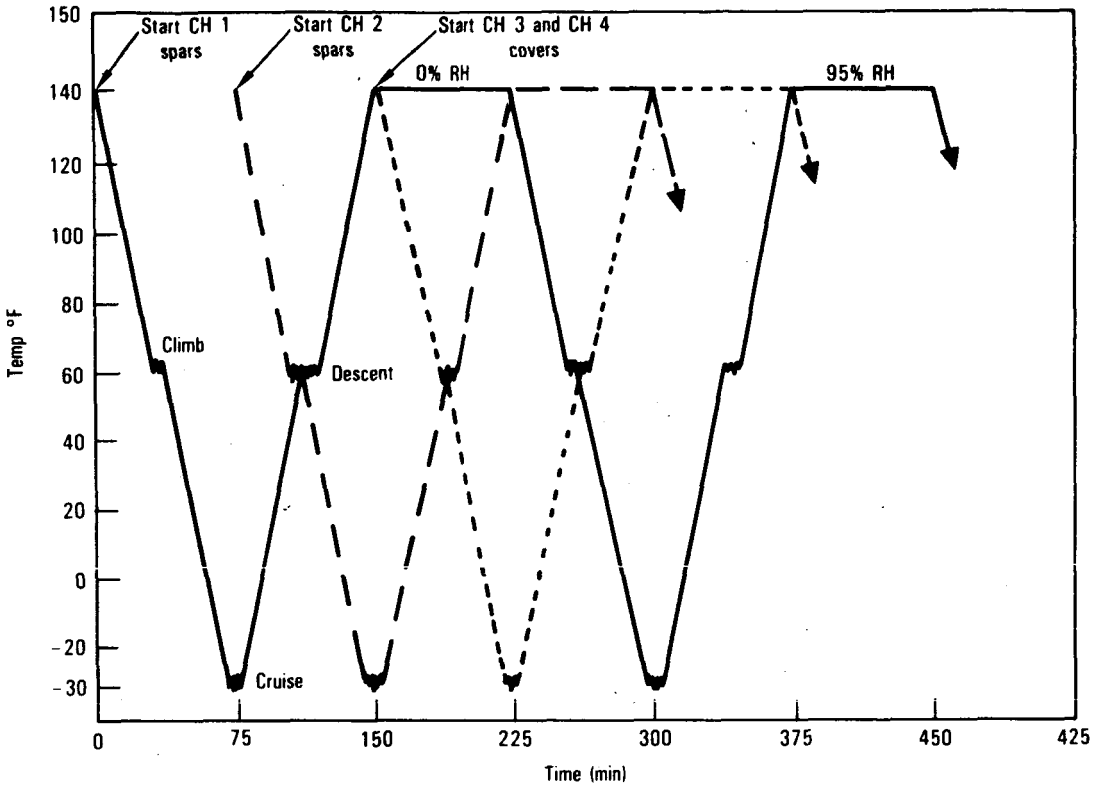

Figure 32. - Thermal cycle schematic for all four chambers showing staggered sequence and load application points.

Chamber high temperature was achieved by using Nichrome element heaters controlled by heavy duty mercury relays integrated with a dry bulb temperature controller. The heaters were protected by a separate power controller interlocked with a high temperature safety thermostat and a solid state electronic high-low temperature safety control interlocked with the setup relay and visual and audible alarm, as well as the central computer monitoring system.

An electronic suppression system was included to reduce transients. This system included five three-phase, three-leg, zero-crossover solid state SCR power controls for the chamber heaters and steam generator. Solid state zero crossovers were on all solenoids and relays.

Control instrumentation specifically for each chamber was contained in a rack mount on the right side of each chamber. All central control systems were mounted in a separate console with the minicomputer and data acquisition system.

As seen in figure 29, the cover specimens protruded out the top of the chamber. This was done to get the potted ends out of the high humidity and temperature environment since the potting materials would be severely degraded by the environment over the four-year test time span.

The lower end of the specimen were gripped by a built-up metal structure and the load transmitted through the chamber bottom by four two-inch diameter hollow stainless tubes per specimen. These tubes were selected to minimize heat transfer through the chamber wall. Similar tubes were used at the base of the spar beams.

Penetration of the spar chamber for the hydraulic jack rods, which were solid stainless rods insulated for minimum thermal excursion, were placed on the back side. All penetrations through the chamber were lined and welded. Rubber boot seals were attached to the rods and chamber inner liner to prevent leakage yet permit motion transfer. Closed-cell polyurethane foam gaskets four inches thick were also placed in all penetrations for added insulation and to block air flow caused by the high capacity circulating fans.

4.3 Control and Data Acquisition System

Application of the load and environmental spectrum and sequencing between chambers plus all safety systems were provided by a Hewlett-Packard 21MX-E computer. A schematic of the overall system is shown in figure 33, and a detailed schematic of control and data acquisition system in figure 34. The computer supplied a direct digital signal to the servovalves in each jack group, compared the response to command and corrected any discrepancy.

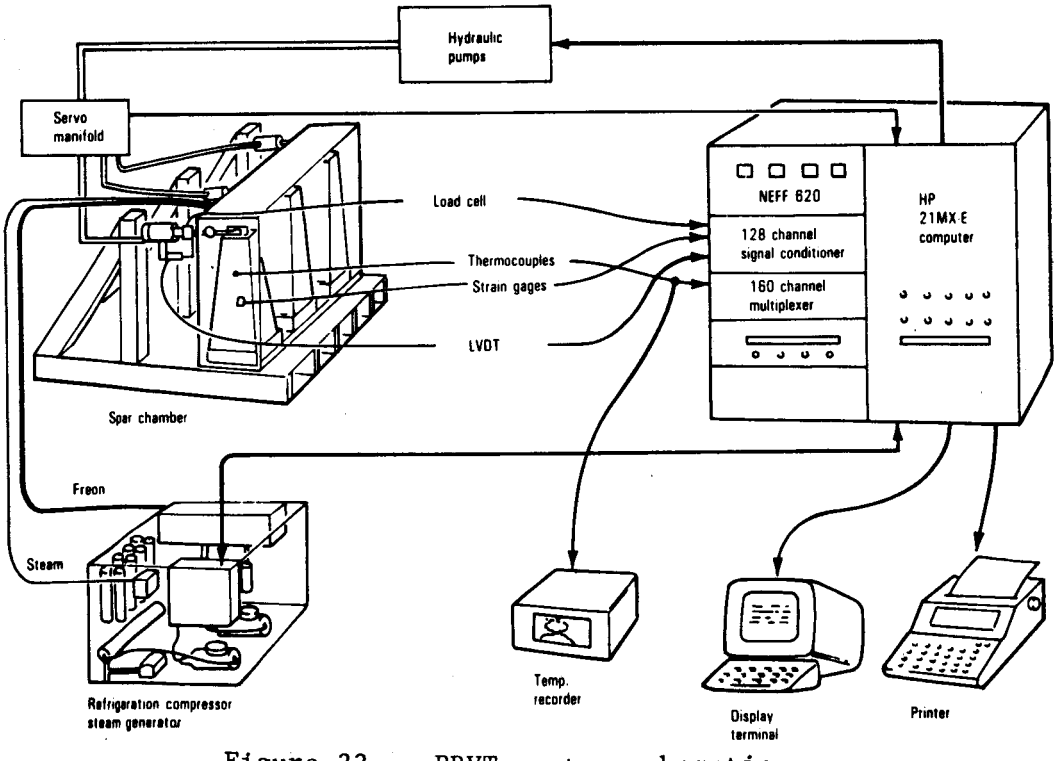

Figure 33. - PRVT system schematic.

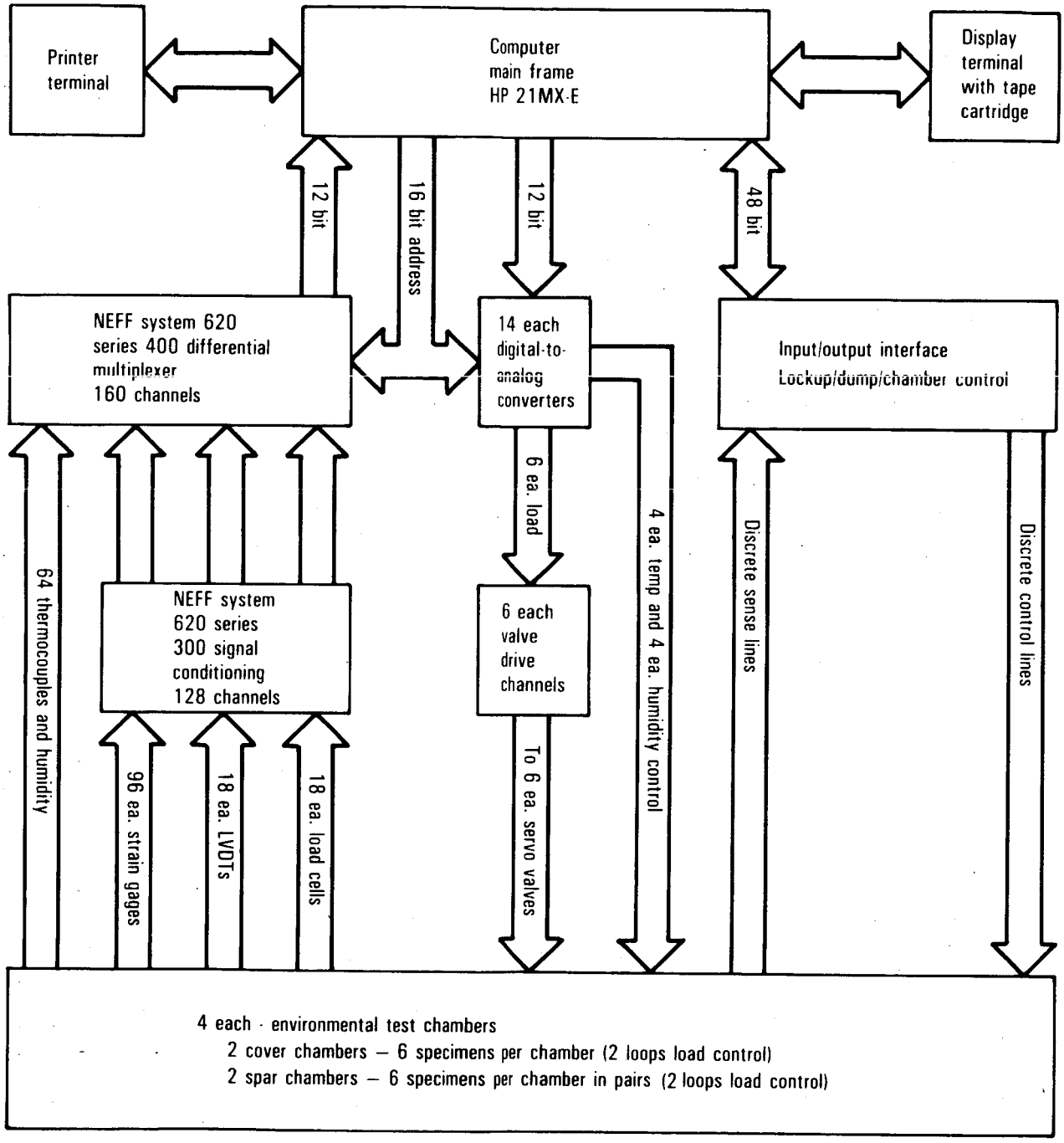

Figure 34. - PRVT chamber control and data acquisition system.

Two 64-channel NEFF signal conditioners were used to interface load cell, strain gage, and LVDT signals to the computer. One 160-channel NEFF low level MUX/ADC interfaced thermocouples to the computer.

Software requirements for data acquisition were modified during the course of the program to provide more usable data. At first, the system capability would only allow the test operator to request a printout of the next block of load cycles, (e.g., climb, cruise, or descent) to be applied to a specific chamber. During that time until printout no other data could be taken. Modifications finally permitted automatic printout of all load cycles on all chambers of loads above a preselected level which was set at ±38 percent limit. This printout included most strain gages, load cells, and LVDTs. A strip chart temperature recorder connected to all four chambers ran continuously throughout most of the program. The charts were manually indexed at least weekly to calendar date/time to supplement the intermittent printer temperature data.

Figure 35 shows the data acquisition system in operational condition. Cover Chamber 3 is in the background and Cover Chamber 4 immediately behind the instrumentation console. Cables going to each chamber were carried in overhead trays visible in this figure. The darker lines above the cable tray are insulated freon supply and return for Chambers 3 and 4. Figure 36 shows the facility area from the opposite side with Spar Chamber 2 opened. High on the side of the chamber is the water tank and platinum resistance wet bulb humidity measuring system.

4.4 Durability Test Specimens

The specimen configuration for the cover durability test is shown in figure 3. It consisted of a 22-inch wide by 64-inch long three hat-stiffened root end panel. The specimens were mounted in pairs as shown in figure 37.

The specimen configuration for the spar durability test is shown in figure 4. This consisted of the first 84 inches of the spar as measured from the fuselage attachment end. In order to obtain as close a match as possible with the required cap and web loads, a box configuration with one jack loading two spars was designed. The setup is shown in figure 38. Three of these double spar boxes were mounted in one environmental chamber and two regular strain boxes and one high-strain box in the other chamber. A plan view of the test area showing chamber and specimen identification is shown in figure 39.

4.4.1 Loading configuration.- Each cover specimen was loaded by individual 100 kep dual bridge transducer load cells. Specimens were mounted in pairs as shown in figure 37, with three cover pairs in one environmental chamber and two pairs of regular strain covers and one pair of high-strain covers in another chamber. Buckling restraint as obtained by connecting the transverse ribs and edge restraints of each specimen to a shear box located between the specimen pairs through a flexure system. Failure of one specimen would not affect the loads or stability of the other mating specimen with this box/flexure design. As a positive safety, mechanical stops were installed on

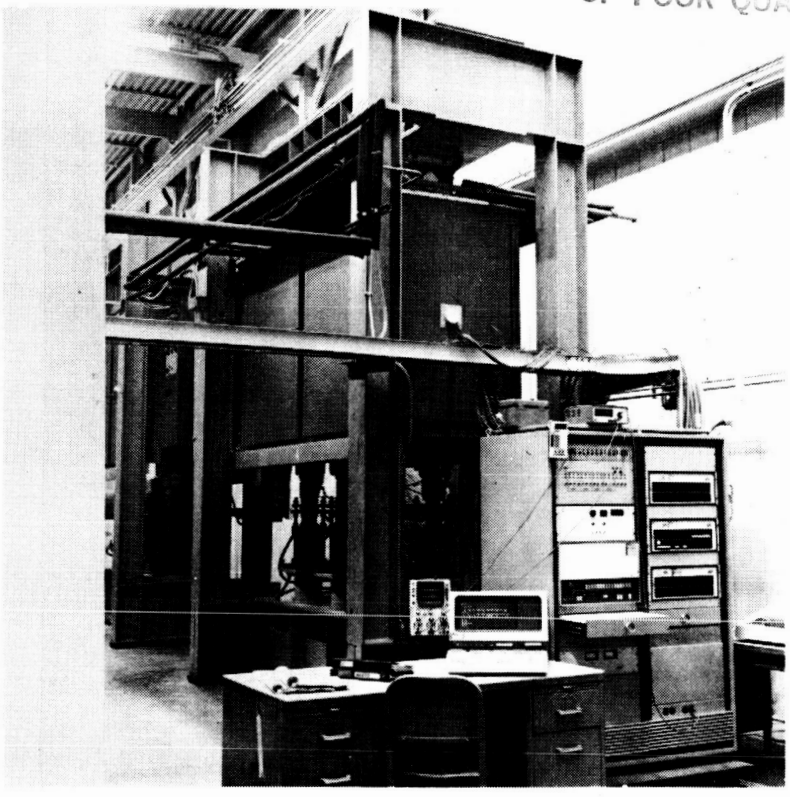

Figure 35. - Computer control console with display terminal and printer. Cover Chambers 3 and 4 are visible in the background. Insulated liner in the upper left are from supply and return.

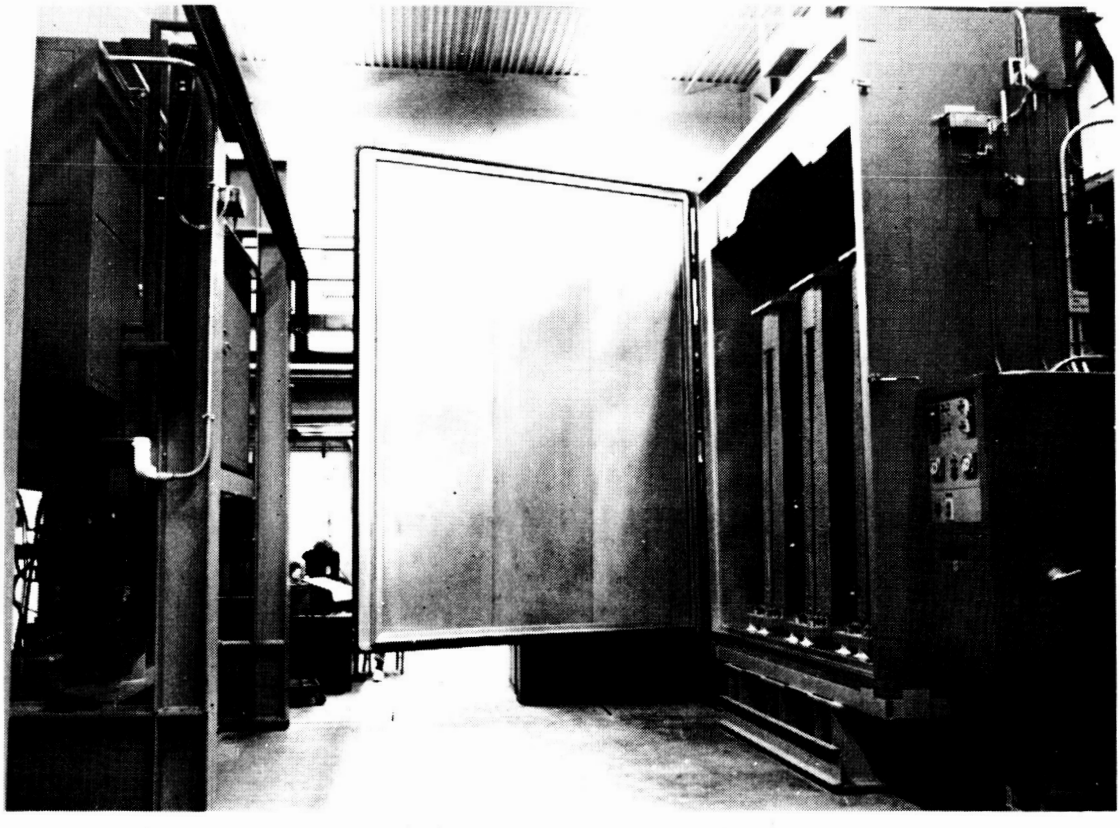

Figure 36. - Test area with door of Spar Chamber 2 open.

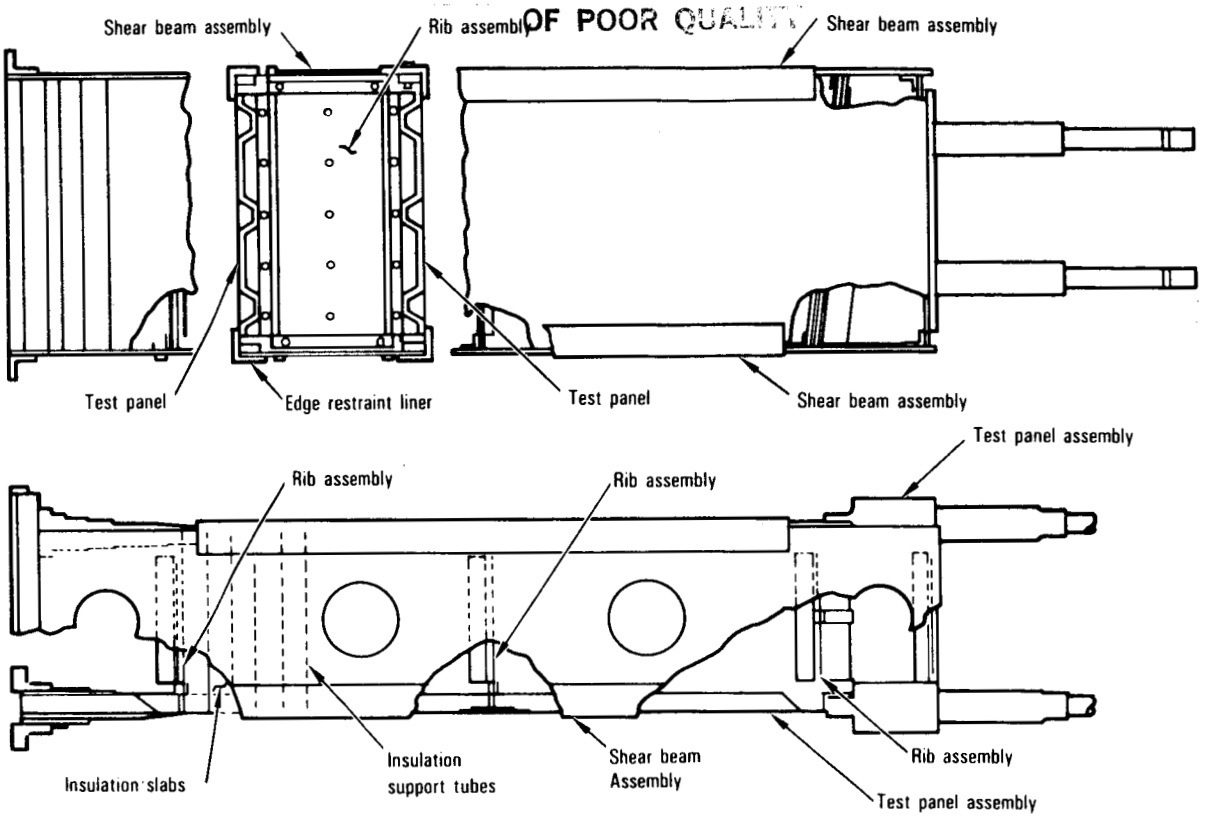

Figure 37. - Cover durability test specimen assembly.

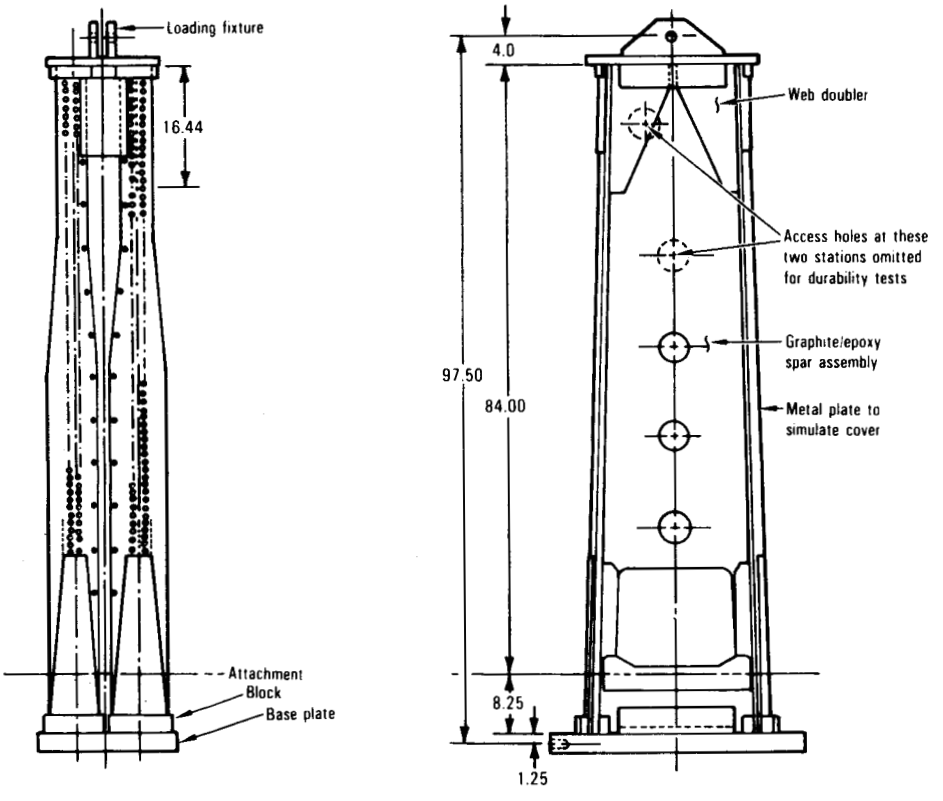

Figure 38. - Spar durability test specimen assembly.

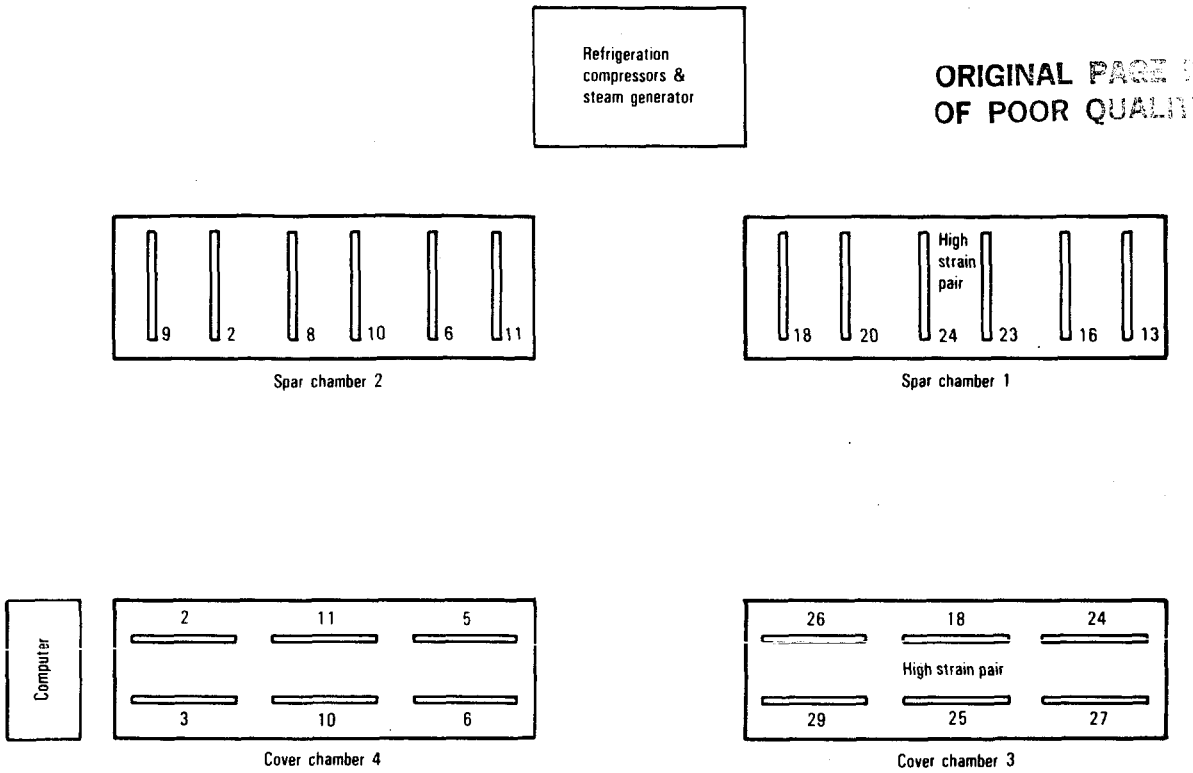

Figure 39. - PRVT facility layout and chamber/specimen location (plan view).

all hydraulic jacks to limit jack stroke. Should one specimen fail, mechanical stops would prevent damage to the other mating cover specimen. All 100 kip jacks were matched equal areas, and operate in phase.

All six jacks on each cover chamber operated from one servovalve. Problems were encountered at low load and deflection levels due to stick-slip of the jack piston and variations in seal friction so that all six jacks did not track to precisely the same load. As loads were increased this error became quite small. Various methods were tried, such as reducing the jack body tie bolt torque and adjusting seals, to minimize this drag error. Moderate success was achieved.

As an added safety, hydraulic pressure relief valves were installed on each chamber frame and adjusted to vent at a pressure slightly above the limit load pressure. Since this pressure varied between spars and covers, separate relief valves were necessary. Additionally, the normal 3000 psi laboratory hydraulic system, containing five pumps, dedicated one pump to this test program and operated it at 2150 psi which was just above the maximum required by the highest loop at limit load. As a result no overloads were experienced during the program.

Spar specimen pairs were loaded by a single 30 kip jack at the outboard end through a spherical ended joint and pin arrangement. Each spar jack train contained a dual bridge transducer load cell for load monitoring each, though all 3 jacks in each chamber are plumbed to a common hydraulic source and all

jacks were matched equal areas. The friction and stick-slip problem encountered with the cover jacks did not occur with the spar jacks because of the larger deflections at the low loads as compared to the very small deflections in the covers. Each spar jack was monitored by an LVDT for deflection.

4.4.2 Durability covers.- The covers were to be loaded axially in fully reversed tension-compression fatigue. One end had hats tapered down to the skin and attachment was made through a bolted joint to a fuselage-type aluminum structure. A series of aluminum sheet fingers were bolted to the skin. On the opposite end the hats ran to the end of the specimen. To attach this end to the reaction frame a built-up assembly of fiberglass, wood and aluminum doublers was used. The cover pairs were supported by three flexures each which would have permitted one to fail without damaging its mate. Also each cover was loaded by a separate hydraulic jack through individual load cells. The flexure system can be seen in the views of figure 40. This figure shows, in the center view, the pair assembly without the side plate; the left view shows the flexure near the outboard built-up end; and the right view shows the center flexure. Figure 43 shows the final cover pair assembled and ready for installation in the chambers.

The cover load reaction frame had a bolted-on top which was removed during specimen installation. A cutout in the chamber top allowed the three cover pairs to be lowered vertically into place. The four load rods visible on the top of the pair in figure 41 (which is upside down from the installed position) went through holes in the chamber bottom and bolted to a cross bar shown in figure 42. This cross bar was attached to a load cell, then to the hydraulic jack. When all three pairs were in place, the top loading beam was replaced on the reaction frame structure and bolted securely. The covers were then brought up close to the upper beams by a series of 12 bolts per cover, Devcon potting material was applied to assure proper alignment, and allowed to cure before final tightening of the attachment bolts. The gap between the specimens and chamber access hole was sealed with closed-cell polyethylene foam.

4.4.3 Durability spars.- To obtain the desired web and cap loads in the spar, aluminum doublers had to be attached to the caps and a multipiece root attachment, which simulated the production fin/fuselage joint, bonded and fastened to transmit loads to a reaction baseplate. Also since the cap was off-perpendicular to the web by approximately seven degrees, bending loads caused the spar to twist. To counteract these forces, spars were mounted back-to-back in pairs. Three steps in the assembly are shown in figure 45. First the end attachment plates and doublers, as seen in the right background of figure 43 are installed. Two such spars were then placed in a specially designed alignment/assembly fixture for mating into a pair. Here the cap reinforcements were mated and temporarily attached. End blocks and plates were mated which fix the two relative to each other. The pair were then removed from the fixture and holes drilled, inspected, and fasteners installed in the cap doublers. Invar rods were attached to the spar cap doublers on the inside of the pair to stabilize the box structure under bending loads.

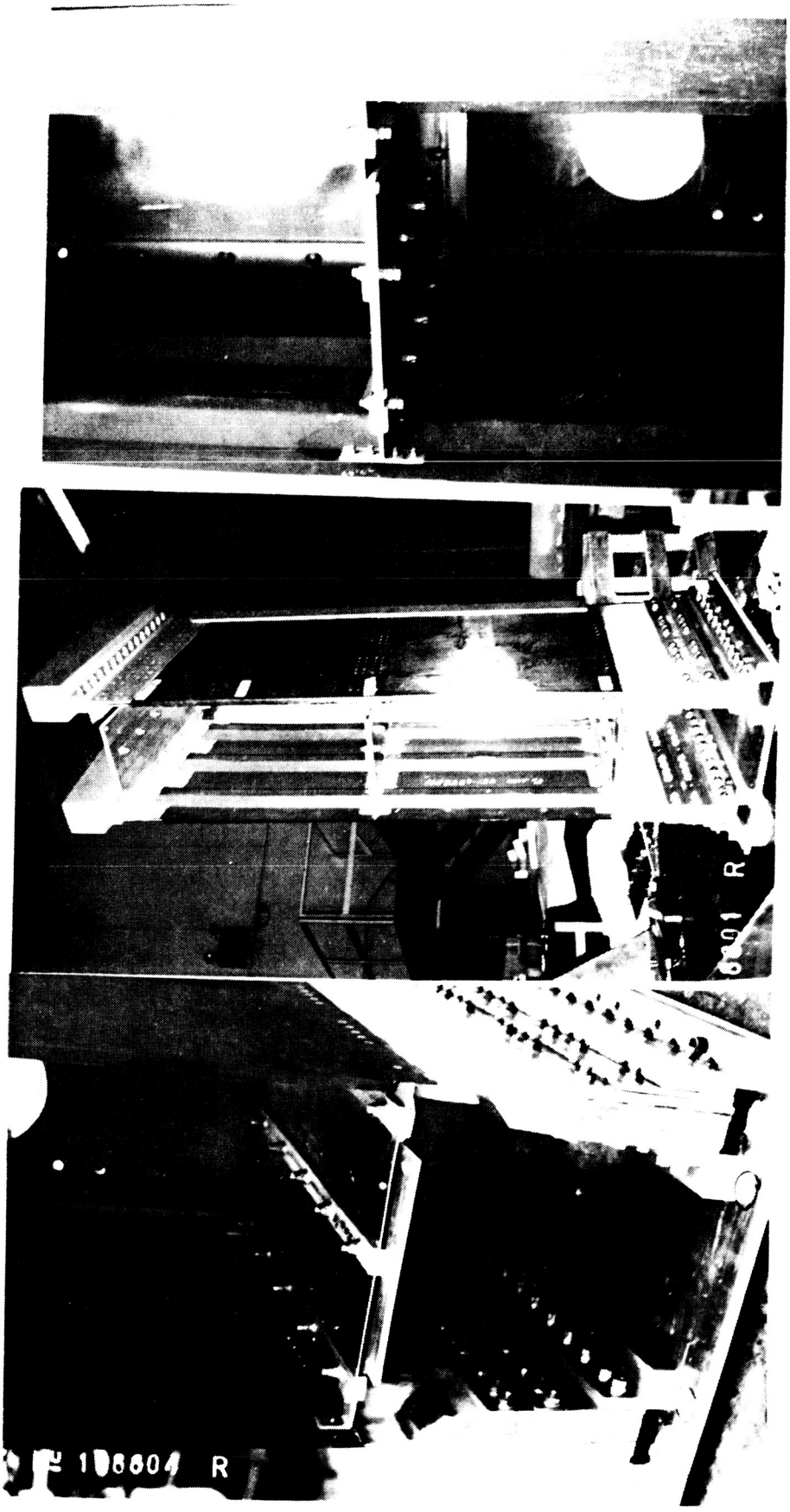

Figure 40. - Cover pair assembly showing details of flexure in outer photos.

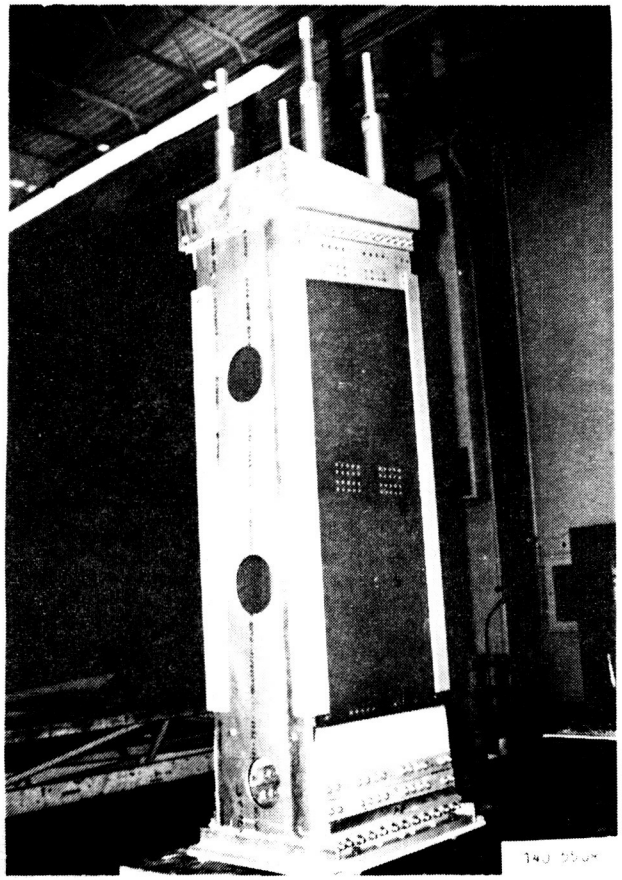

Figure 41. - Assembled cover pair ready for installation in load frame.

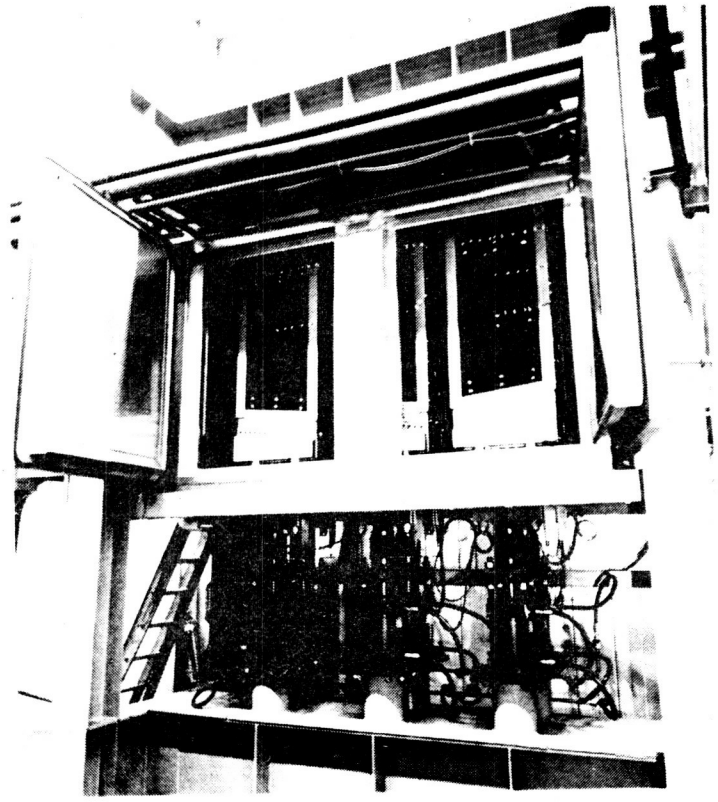

Figure 42. - Three cover pairs installed in Chamber 4 ready for test. Load train details and LVDTs are visible for all six channels. White spots on specimens are RTV rubber beads holding thermocoupler.

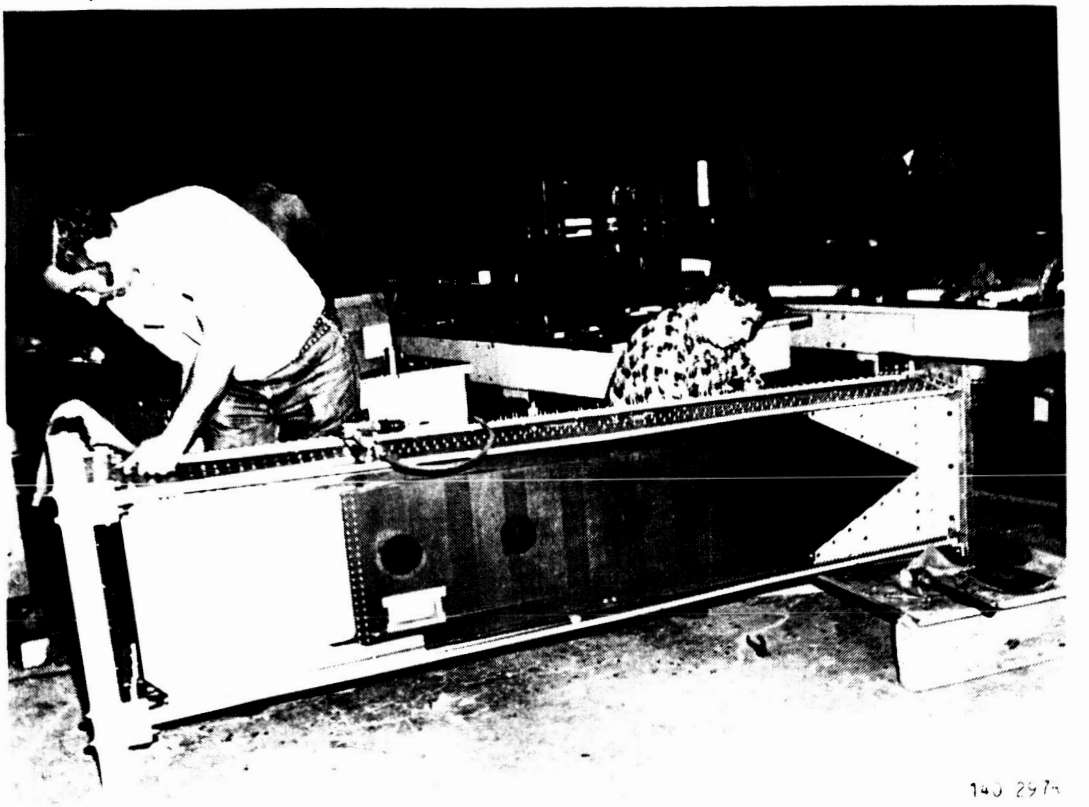

Figure 43. - Final assembly of spar pair. In the background can be seen the assembly jig and installation of root aluminum. Doublers on a single spar.

Holes in the graphite/epoxy spar were drilled with Spacematic drills with templates. Each hole was inspected for diameter, roughness and rear surface breakthrough. Backup plates were used to minimize the rear surface breakthrough problem. Some holes had to be redrilled and larger diameter fasteners installed.

Titanium Hi-Loks were used in graphite/epoxy exclusively. Fasteners were installed with sealant. Where rear surface breakthrough produced splintering at the hole, a room temperature curing epoxy was applied to prevent further delamination growth.

Once the spars were fully assembled into pairs they were transferred to the environmental chambers. Figure 46 shows Chamber 2 fully loaded with six spars. Once in place, jack trains were attached. Each spar pair was loaded by a single hydraulic jack and load cell.

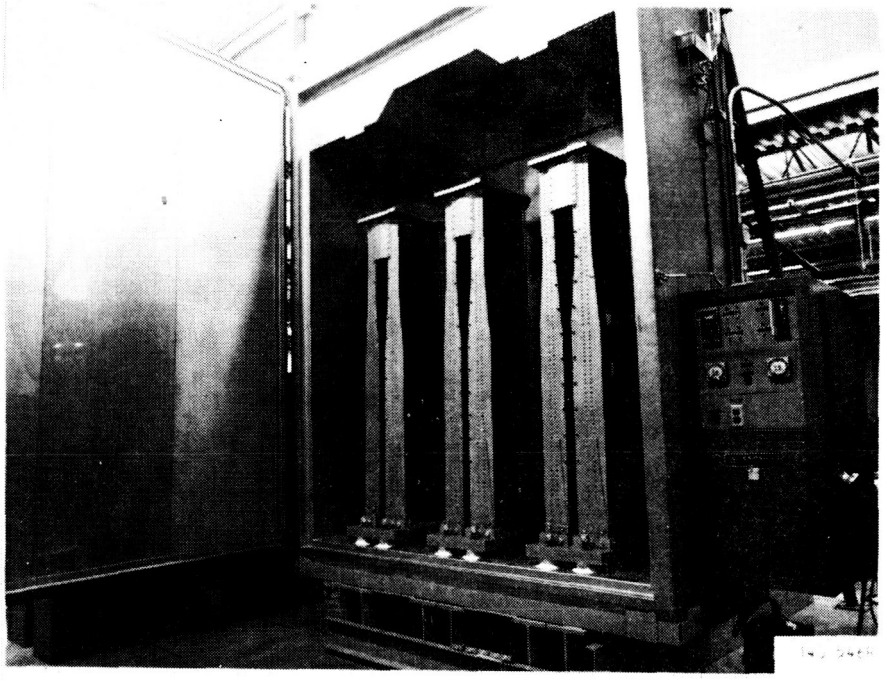

Figure 44. - Spar Chamber 2 with six spars installed ready for test.

4.5 Instrumentation

4.5.1 Strain gages.- Both axial and rosette strain gages were applied to spars and covers. Axial gages were all of the CEA-00-125-UW120 tape and rosettes were of the CEA-00-125-UR120 type. All were bonded with AE10 adhesive and cured for two hours to 125°F. Several gage/tab coating treatments were applied to various gages because of the concern for long-term moisture migration and corrosion. These coatings were M-Coat A, RTV silicon rubber, and teflon tape. Both the teflon tape and M-Coat A gave adequate protection for the gage. Teflon tape did not adhere adequately to the tabs.

Those few gages that did fail were the result of corrosion of the soldered joints. No indication of moisture migration to the underside of the gage causing debond were observed. During the first 2900 thermal cycles, six gages failed out of a total of 86. Since one spar and one cover chamber were stopped at 2900 thermal cycles, only 36 gages were exposed for the remaining 2900 thermal cycles. Of the 36 left, 4 failed during the second 2900 thermal cycles giving 32 that survived the entire 5800 thermal cycles. These four failures occurred after 3526, 4423, and 4815 thermal cycles.

Some gages that failed due to solder joint corrosion were resoldered. For this reason tracking strain data throughout the test life had to be done with caution to assure that any changes were due to repair and not to a potential delamination. Some of the strain data presented herein demonstrates this problem.

Spar 13 in Chamber 1 and spar 6 in Chamber 2 were fitted with a complete complement of four axial gages and six rosettes (see figure 45). The other eight spars had only the single rosette No. 5. The two high-strain spars NC's 23 and 24 had only a single rosette each in position R6. When these were installed, rosettes 9 and 10 on spar 13 were disconnected and those channels used for spars 23 and 24.

Cover 6 in Cyamber 4 had seven axial gages and one rosette (see figure 46. The remaining covers in Chamber 4 had only one axial gage on each. All of the covers in chamber 4 had a single axial strain gage on each except for the two high strain covers (18 and 25) which had four axials on each.

4.5.2 Thermal mapping - spars.- Prior to start of the durability test program, checks were made to determine the system thermal response relative to heating and cooling rates and temperature distribution in the chambers at various specimen locations. Since Chamber 1 initially had four spars and Chamber 2 six spars, thermal mass and air flow patterns were different; thus they had to be checked individually.

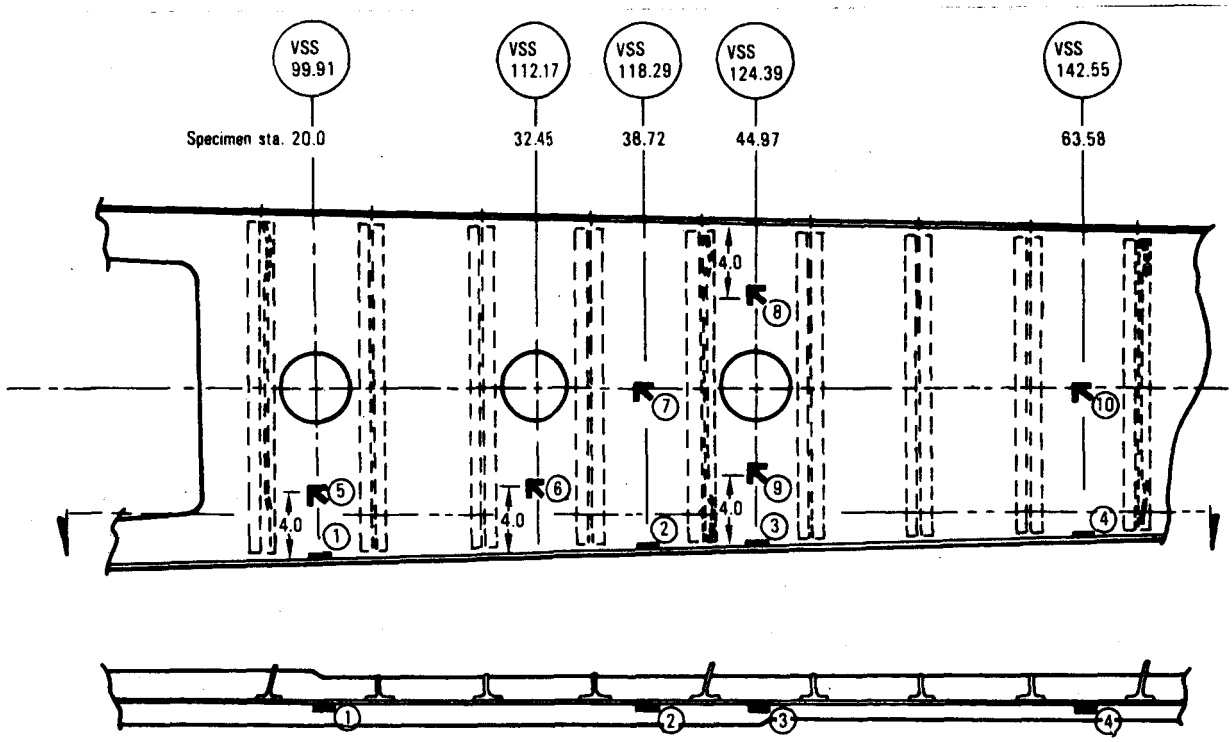

Figure 45. - Locations of strain gages on PRVT spar specimens.

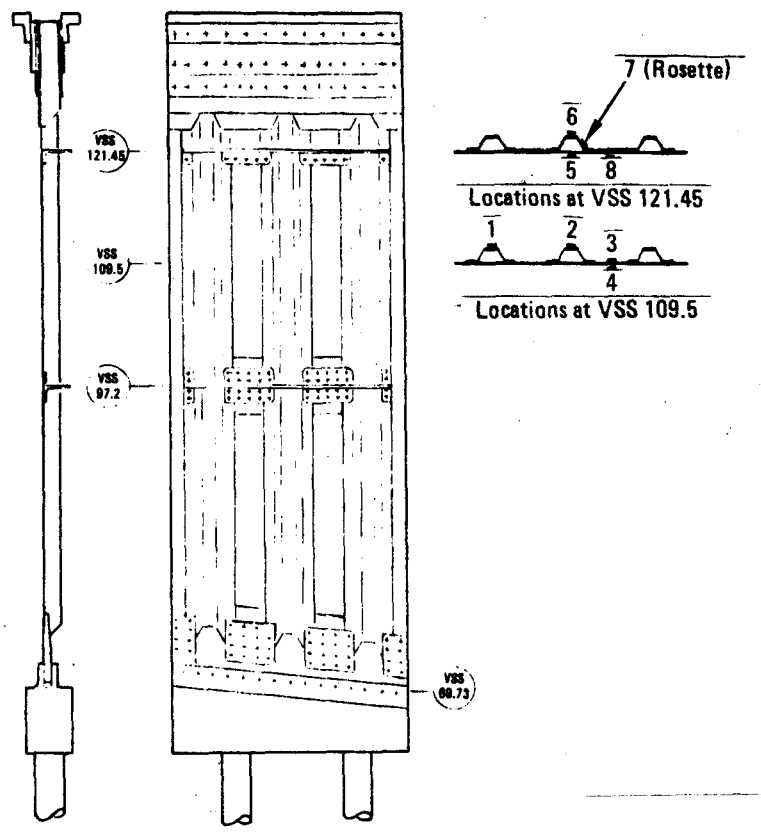

Figure 46. - Strain gage locations, cover specimens.

A total of 32 mapping thermocouples were used to supplement one permanent thermocouple attached to each specimen. Additionally, in each chamber, there were permanent thermocouples located in both inlet air ducts and one at the fan exhaust. Both inlet air ducts were monitored as a system safety and performance check to provide information in the event one heater element malfunctioned and injected heated air from only one side at a higher than normal temperature, or if one cooling coil were to ice up. This feature proved its value as each of these events occurred several times. Likewise, the control fan outlet temperature would give an indication if the fan speed dropped. Thermocouple locations on a spar specimen can be seen in figure 47. The ends of each thermocouple were held against the specimen and covered with white RTV rubber to bond it against the specimen surface and isolate it somewhat from measuring air temperature rather than the specimen temperature. Measurements were made on both outside and inside surfaces of the specimen box assemblies.

Tests were conducted with both spar chambers to evaluate temperature spreads on the specimens while going from one extreme to another. These results are shown in figure 48. The test was started with both chambers at ambient, then cooling Chamber 1 and heating Chamber 2. Chamber 1 contained only the four permanent thermocouples plus the control thermocouples, and it

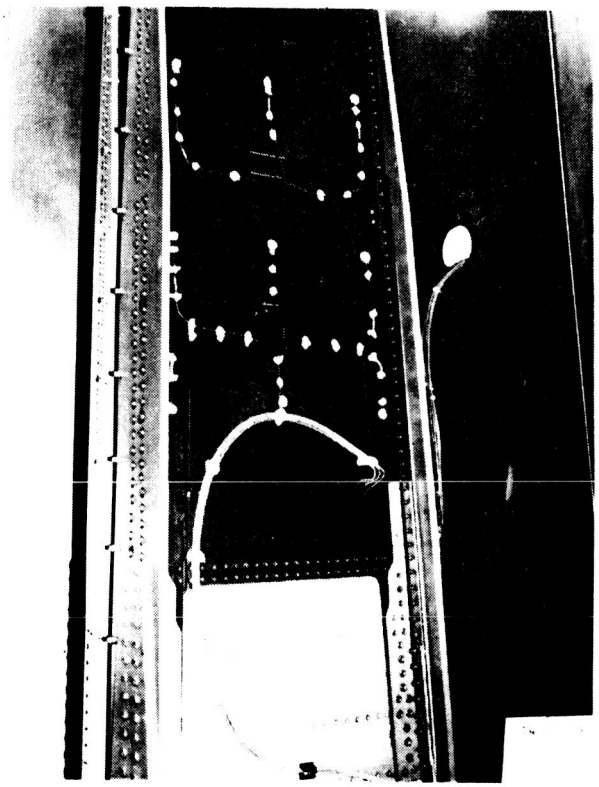

Figure 47. - Mapping thermocouple and strain gage installation location on spar 20 in Chamber 1.

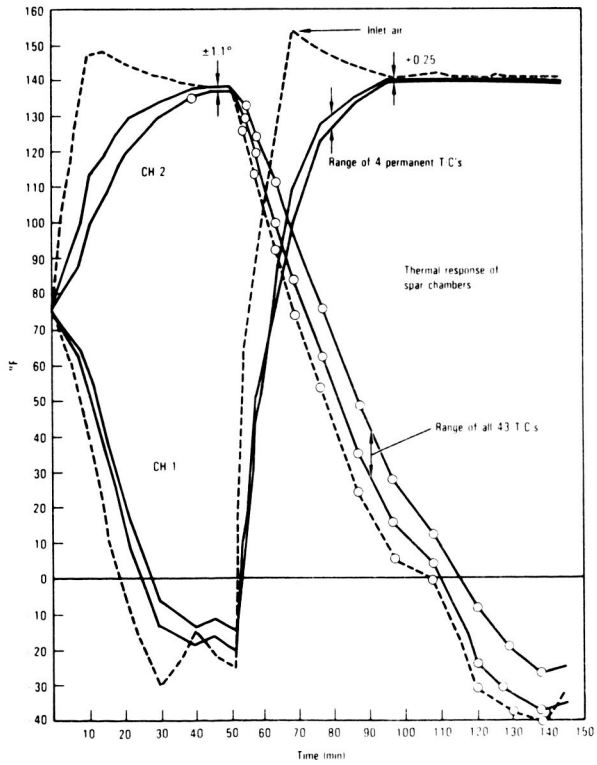

Figure 48. - Thermal response of spar chambers.

had only four spars; therefore, the rate of temperature change and range of variability was less than in Chamber 2 with six spars and forty-three thermocouples. Inlet air temperatures are included for system response comparison. A larger variation in temperature can be seen on the cold side, compared with the hot which for all the thermocouples in Chamber 2 is ±1.1°F after 50 minutes from start at 75°F, and ±0.25°F in Chamber 1 on the four thermocouples after 50 minutes from -20°F. Cooldown from 137°F to -37°F took 87 minutes. At the time this mapping was conducted, Chamber 2 as not performing at its maximum rate, the manufacturer subsequently adjusted the coolant flow rates so that it would cool from 140°F to -30°F in less than the required 75 minutes.

For evaluation of possible thermal stresses, several thermocouples were selected for detailed analysis. Figure 49 presents a comparison of two sets of back-to-back thermocouples at the critical spar-to-fuselage joint area. The range of all thirty-six thermocouples and the inlet air temperature are included. As expected, with the inlet air first striking thermocouples, 46, 4, and 21, their response was more rapid than those in the center of the chamber or inside the spar box assembly. Differentials of less than 10°F indicate that thermal induced stresses due to variations in temperature were of very minor significance.

Thermal distributions in Chambers 1 and 2 were considered satisfactory, and did not require baffeling.

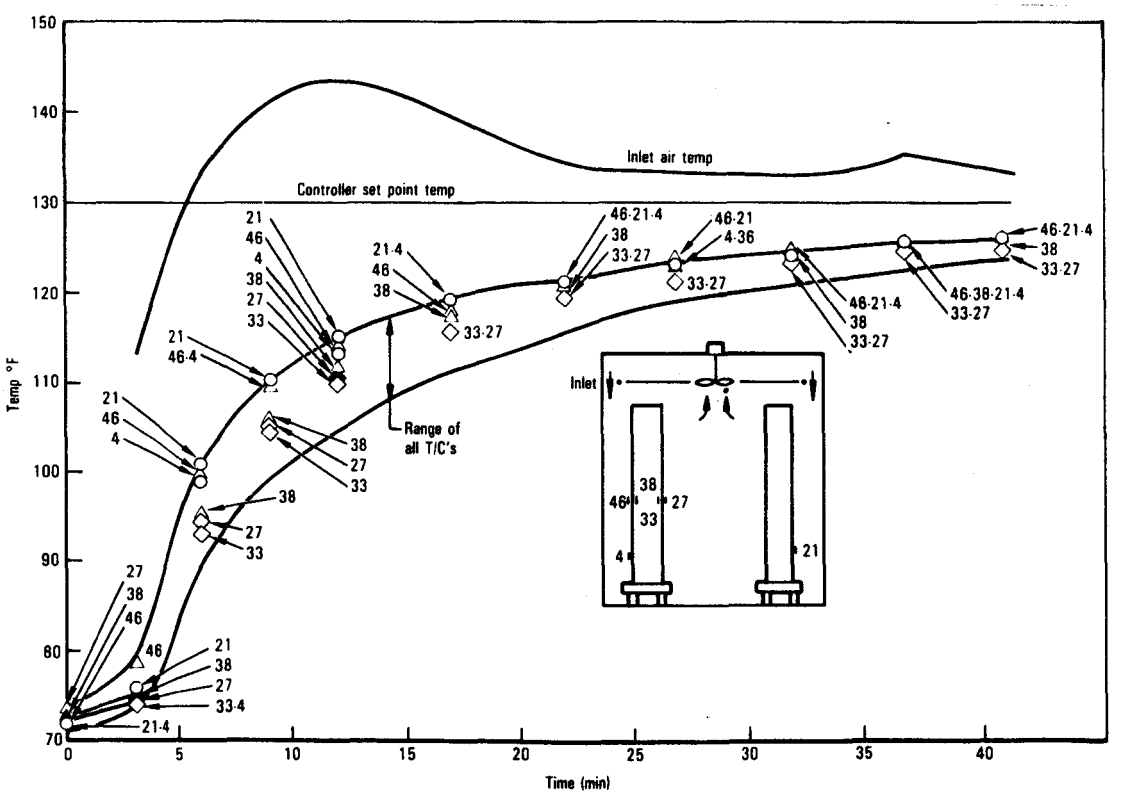

Figure 49. - Four-spar chamber thermal response.

4.5.3 Thermal mapping - covers.- After mapping the spars, the 32 thermocouples were moved to Chamber 4 and thermal cycling checks made. Thermal distributions were not within desired ranges due to the long rectangular shape of the chamber and air inlet and outlets in the same end. A baffle was fabricated from stainless steel sheet and installed to divert the inlet air across the top of the cover pairs to the far end of the chamber. Some gaps along the specimen and chamber wall were left so that the baffle was not a perfect seal to allow seepage all along the top. This design proved effective in producing a more uniform temperature distribution in the chamber. Similar baffle was installed in Chamber 3 without mapping in Chamber 3 since it is identical to Chamber 4. Figure 50 shows the location of the permanent thermocouples in Chamber 3. A temperature profile at extreme points in Chamber 3 with the baffle is shown in figure 51.

On May 27, 1982, the temperature spectrum was changed reducing the 140°F hold time from 75 minutes to 5 minutes. At this time Chamber 2 had been shut down so that the 75 minute delay for cooling it was not required. This allowed a considerable speedup in thermal cycling rate.

4.5.4 Load cells.- Spar pairs were monitored by one load cell for each pair. They were calibrated prior to installation and not removed until program completion. Cover specimens loads were measured by a load cell attached to each cover individually and calibrated in the same manner.

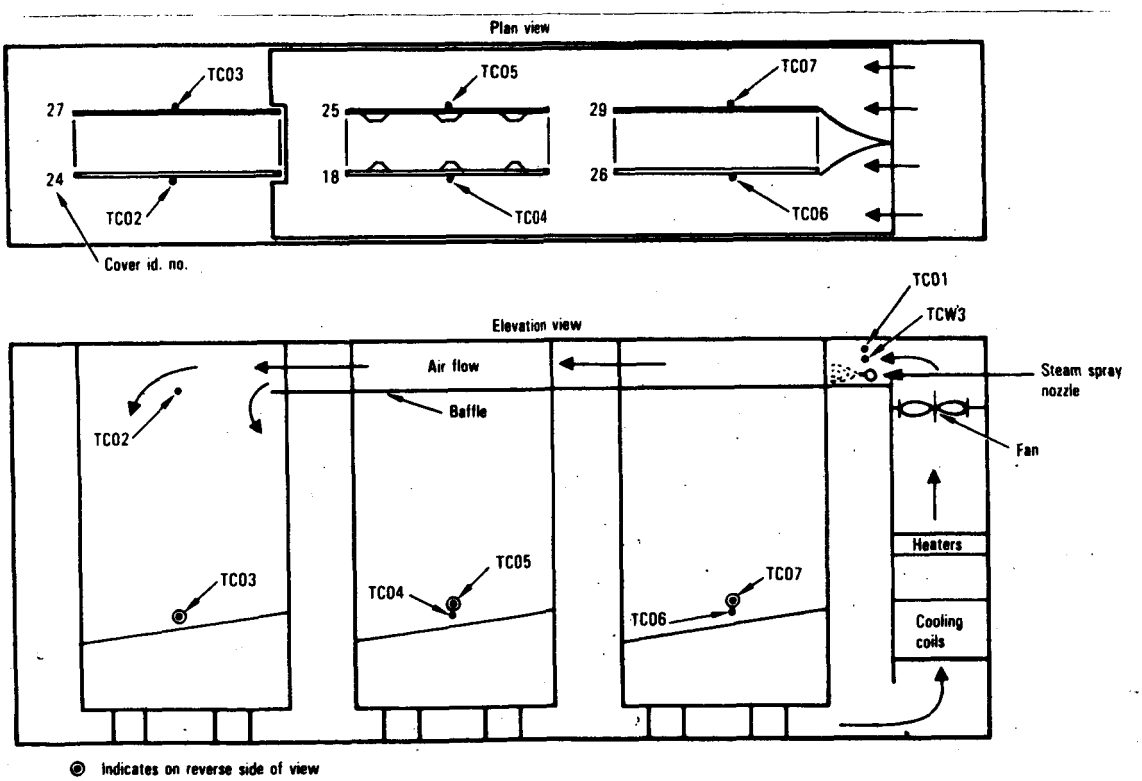

Figure 50. - Cover Chamber 3 thermocouple locations.

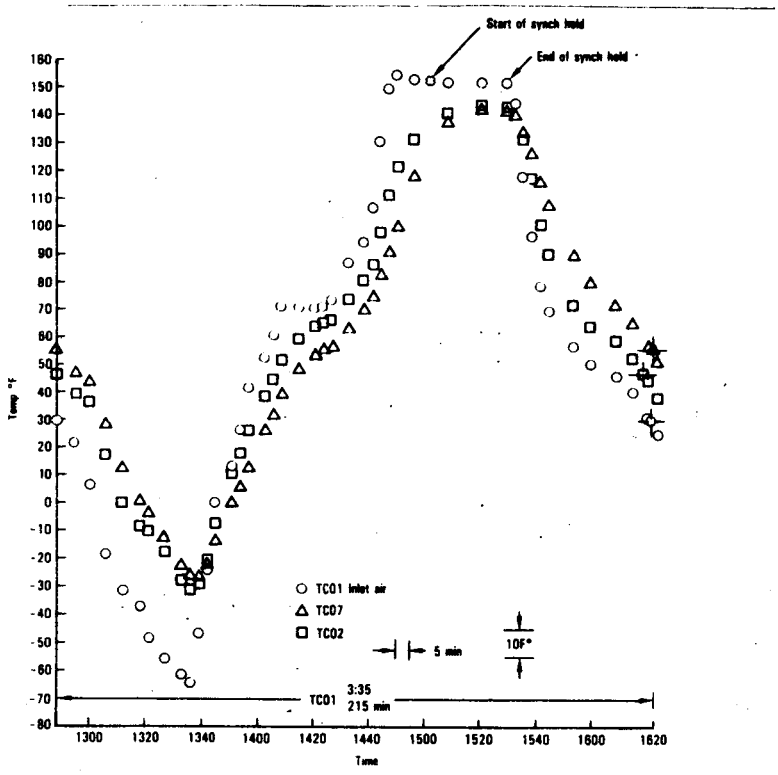

Figure 51. - Temperature vs. time PRVT Chamber 3.

The load cells for all the covers and for the high strain spars were 100 Kip Lebow Model 3156. The remaining spar load cells were 30 kip Lebow Model 3117. Although the spars were loaded to 34.6 kip in a very slow cyclic rate nine times in 36,000 flights they were assumed to be static loads. The rated capacity of the load cell is in fatigue, for static applications the rating is increased by 50 percent. These spar load cells were used because they were readily available from Calac inventory.

4.5.5 LVDTs.- Stroke of each hydraulic jack was monitored by individual LVDTs. On the spars eight-inch Collins SS-109's were used and on the covers four and one-half-inch Collins SS-107's were used. These were monitored throughout the test program for deflection. They were regularly checked for calibration and always found to be within ±0.001 inch. Two LVDTs failed during the test and had to be replaced.

4.5.6 Humidity.- A wet bulb platinum resistance thermocouple was installed with a float valve water supply tank in each chamber in the inlet air stream. The difference between the wet bulb and dry bulb located in the same area was used to control the amount of steam dumped into the chamber to achieve the 95 percent or 0 percent relative humidity. Periodic computer printouts and continuous strip chart records of both wet and dry bulb data were taken.

4.5.7 Safety systems.- In addition to the mechanical jack stops and hydraulic pressure relief valves which afford specimen overload protection only above limit load, at lower loads an error tracking feature was incorporated into the computer software which would shut the system down and dump hydraulic pressure to zero if any load deviated above or below the command load by more than ±3.0 percent.

A similar error tracking system was incorporated into the temperature control system as well as separate upper and lower limit controller built into each chamber. These individual controllers were set at 190°F and -70°F to allow some tolerance for inlet air temperature being greater than that desired on the parts. Additionally heating and cooling rate values were set to put the system in a hold if one chamber was not keeping up with its planned spectrum envelope since all four chambers had to be run sequentially so that refrigeration supply capacity was not exceeded.

Sonalerts (audible alarms) were built into each chamber to trigger when test parameters were exceeded so that an operator could correct the problem immediately.

5. LONG-TERM DURABILITY TESTS

The cyclic durability testing commenced on May 3, 1979 when Chamber 1 containing four basic spars and Chamber 2 containing six basic spars were brought on line. The two high-strain spars were added to Chamber 1 on March 4, 1980.

The six basic covers in Chamber 4 were brought on line on June 18, 1979 and the four basic covers and two high-strain covers in Chamber 3 were brought on line on February 27, 1980.

Prior to the initiation of the cyclic testing, static strain and deflection surveys were run on each spar and cover. Several other static surveys were run during the four years or so of testing.

5.1 Durability Test Results

The principal measurement of interest during the durability test program was deflection. Changes in deflection would be a good indication that the repeated load, temperature and humidity cycling was having an effect on the components.

Early in the program the deflection data were recorded for the low load level high frequency cycles. About halfway into the program the computer was reprogrammed to record automatically data for all of the load cycles above ±31 percent of limit load.

Deflection measurements recorded included fixture deflection as well as specimen deflection, as the LVDT was reading the total jack stroke. Deflection surveys performed during the program used dial gages to determine fixture deflections so that these could be subtracted to determine the specimen deflections.

Strain/deflection surveys were conducted on all of the PRVT structural assemblies as installed in the environmental chambers prior to durability testing, to establish initial reference conditions of stiffness, strain distribution, and load-deformation characteristics. Additional surveys of this type were conducted after various intervals of durability testing to provide a more detailed determination of changes, if any, than was available from the routine computer print-outs, which furnished only abbreviated coverage for monitoring purposes. The number of such tests was restricted because they introduced additional cycles of high load into the spectrum of applied loads. A listing of the surveys is given in table 8. The table shows the environmental cycle number just prior to the survey and the maximum loads applied.

The total number of environmental cycles applied to each specimen is summarized in table 9.

5.2 Spar Test Results

The internal load distribution for the durability test spars compared with the design limit load distribution is shown in figure 52. Because only one jack was used to apply load the shear flow in the upper panels was higher than the normal design load. This had no detrimental effects on the basic spars but proved to be significant for the high-strain spars wich saw loads in excess of design ultimate on several occasions and resulted in their premature failure. This is discussed in detail in Section 5.2.2.

5.2.1 Durability testing of the spars.- The durability testing commenced on May 3, 1979 when the four basic spars in Chamber 1 and the six basic spars in Chamber 2 were brought on line. The two high-strain spars were added to Chamber 1 in March of 1980 when the basic spars had completed 870 environmental cycles. Figure 53 shows plots of the load deflection data for two typical spar pairs for the entire 36,000 flights (5800 environmental cycles). These plots are typical of all the spars. A significant drop in deflection occurred during the first 6000 flights which implies an increase in stiffness. The deflection plotted is the deflection of the spar tip from peak to valley of the cycle, all fixture deflection has been subtracted.

The apparent increase in stiffness was hypothesized to be due to swelling of laminate as it absorbed moisture, which in turn caused an increase in the clamping pressure by the fasteners producing increased frictional effects. This was confirmed by a series of tests performed under separate Lockheed funding. A summary of these tests is contained in Appendix A.

TABLE 8. - STRAIN-DEFLECTION SURVEYS

Survey \ Chamber	1 4 Basic Spars	1 2 Hi-Strain Spars	2 6 Basic Spars	3 4 Basic Covers	3 2 Hi-Strain Covers	4 6 Basic Covers
1	0 ± Limit	0 ±.75 Limit	0 ± Limit	0 ± Limit	0 ± Limit	0 ± Limit
2	1727 ±.57 Limit	857 ±.51 Limit	1679 ±.54 Limit	853 ±.50 Limit	853 ±.50 Limit	1294 ±.50 Limit
3	3021 ±.50 Limit	2151 ±.50 Limit	2903 ±.50 Limit	2141 ±.50 Limit	2141 ±.50 Limit	2564 ±.50 Limit
4	3654 ± Limit	2784 ± Limit	2976 ± Limit	2765 ± Limit	2765 ± Limit	2900 ± Limit

TABLE 9. - DURABILITY TEST SUMMARY

Chamber	Contents	Flights	Equiv. Service Years
1	4 Basic Spars	36,000	20.00
	2 High-Strain Spars	17,752	9.86
2	6 Basic Spars	18,472	10.26
3	4 Basic Covers	36,000	20.00
	2 High-Strain Covers	36,000	20.00
4	6 Basic Covers	18,000	10.00

Prior to durability testing a strain-deflection survey was made on each spar pair. Deflections were measured with the LVDTs as during the durability testing. Some dial gages were used to determine the extent of the fixture deflections but insufficient data was obtained from these gages to determine the total fixture deflections. Typical dial gage locations are shown in figure 54.

Because of the marked reduction in deflection during the early durability testing a much more comprehensive survey of fixture deflection was made in a subsequent strain-deflection survey. These deflections were then subtracted from the LVDT data to determine the specimen deflections alone.

Figure 55 shows a comparison of total deflection (jack stroke) for each of the spar pairs during the first survey prior to durability testing. Hysteresis is evident in each plot. Stiffness is quite consistent from station to station for the five basic spar pairs. The reduced deflection for the high strain spars is due to the increased stiffness in the test frame at this location for the higher loads.

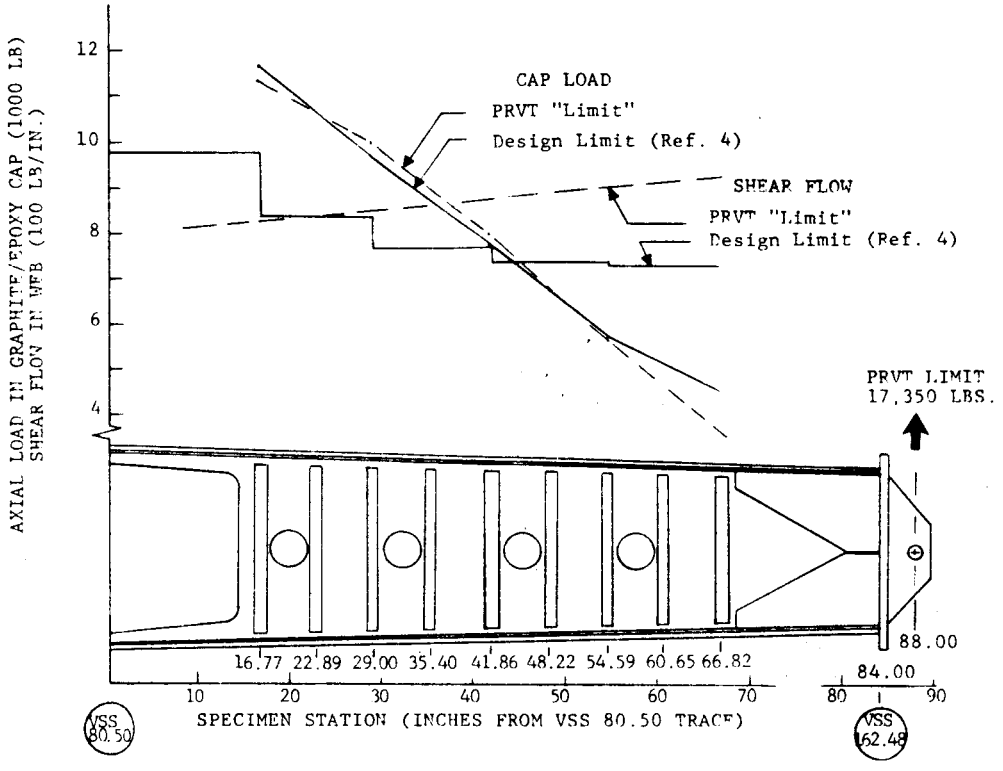

Figure 52. - Calculated limit loads on PRVT spars.

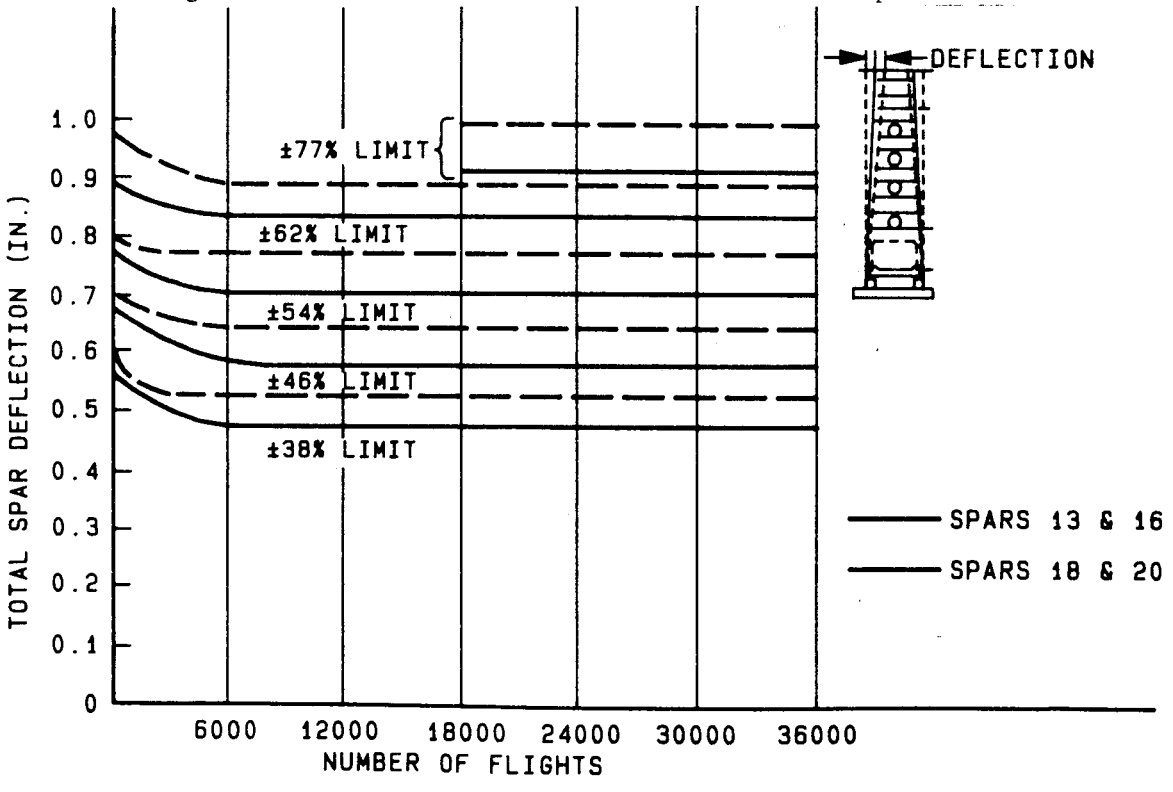

Figure 53. - Load-deflection data for Chamber 1 four basic spars.

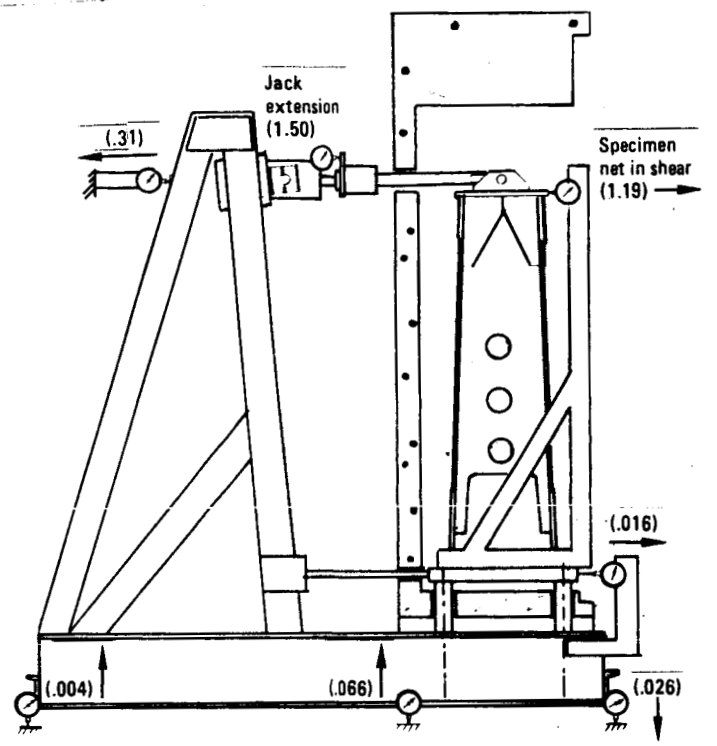

Figure 54. - Locations of dial gages in static load-deflection surveys of spars.

Figures 56 thorugh 61 show the spars total deflections and the specimen-only deflections from the survey taken at the half lifetime. It can be seen that the total fixture deflection is about equal to the specimen deflections.

A comparison was made between some of the deflection and strain data recorded in the surveys. The strain data were corrected to zero to eliminate the hysteresis effects. Figure 62 shows the deflection of Spars 13 and 16 during the three surveys and figure 63 shows the deflection of Spars 8 and 10 during the same surveys. It can be seen that no deflection changes occurred.

Similarly, figures 64 through 67 show typical strain gage data comparisons. Figure 66 compares the strains recorded by strain gage 1 on Spar 13 (see figure 45) and figure 65 shows the shear strain recorded by the rosette at location 5 on the same spar. It can be seen that no change in the strain response occurred. Figures 66 and 67 show similar typical plots for spars in Chamber 2. Again, no change in strain response occurred.

5.2.2 Hi-strain spar failures.- Failure occurred on May 21st 1982 during application of the 150 percent Design Limit Load (DLL) cycle. The full load

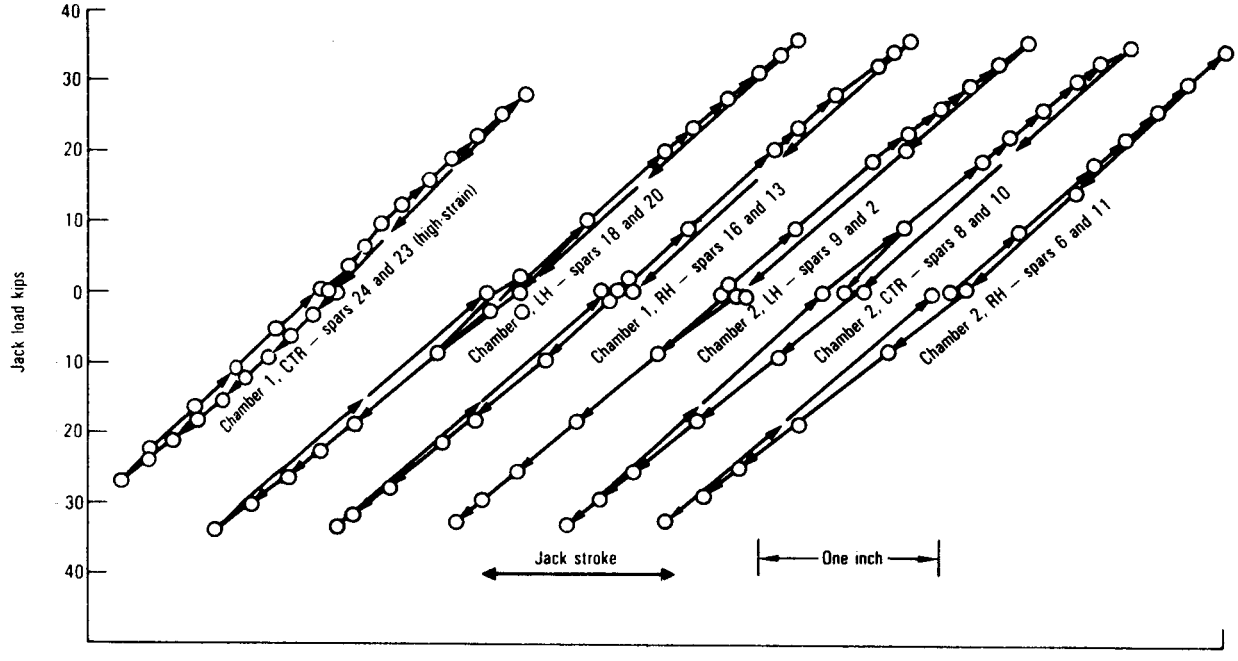

Figure 55. - Total deflections, specimen plus frame and fixtures, in static test prior to durability testing.

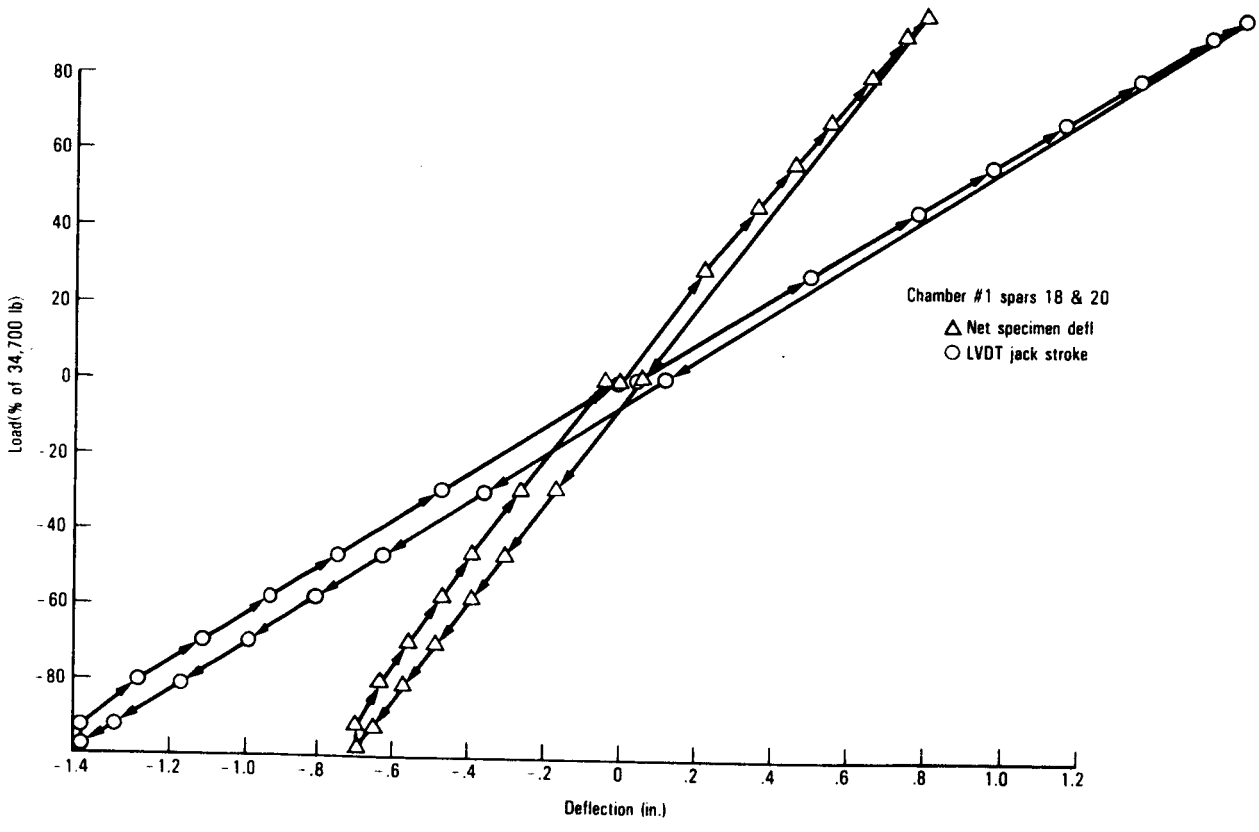

Figure 56. - Load-deflection measurements on spar assembly 1 (spars 18 and 20).

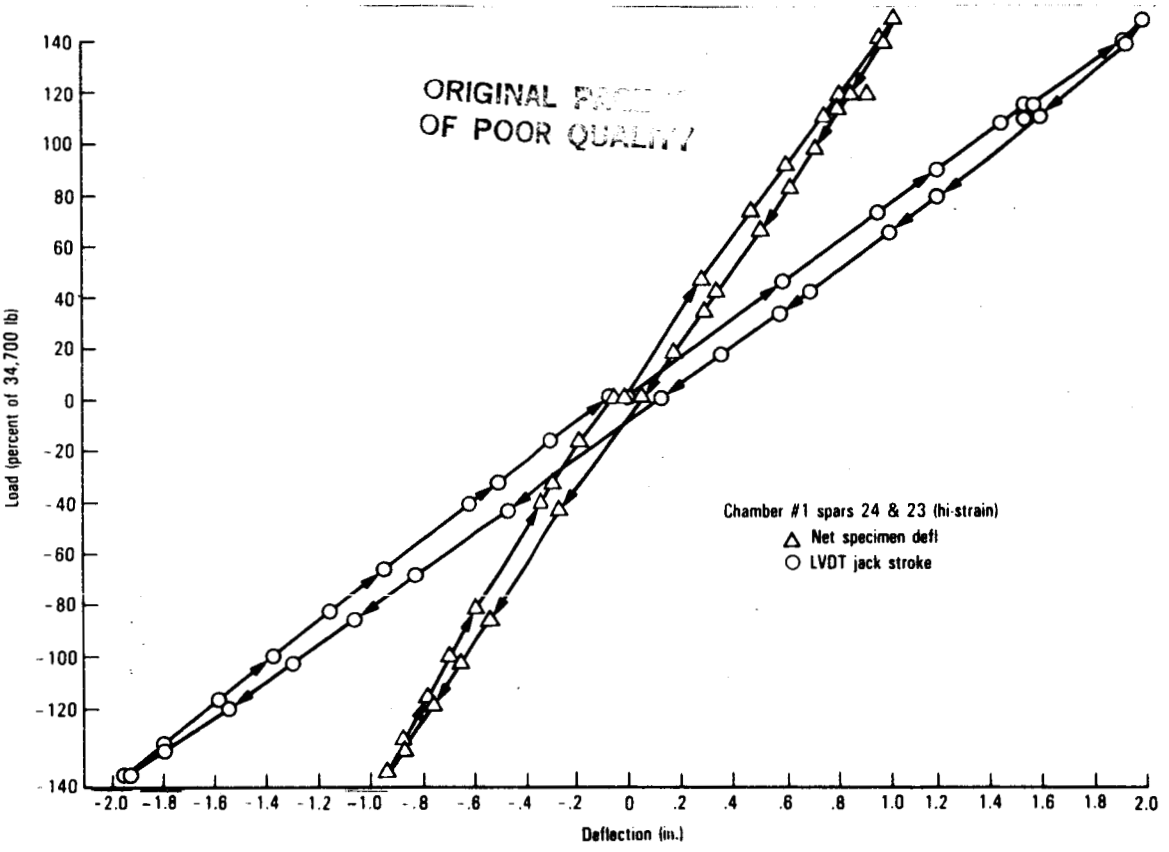

Figure 57. - Load-deflection measurements on high-strain spar assembly (spars 24 and 23).

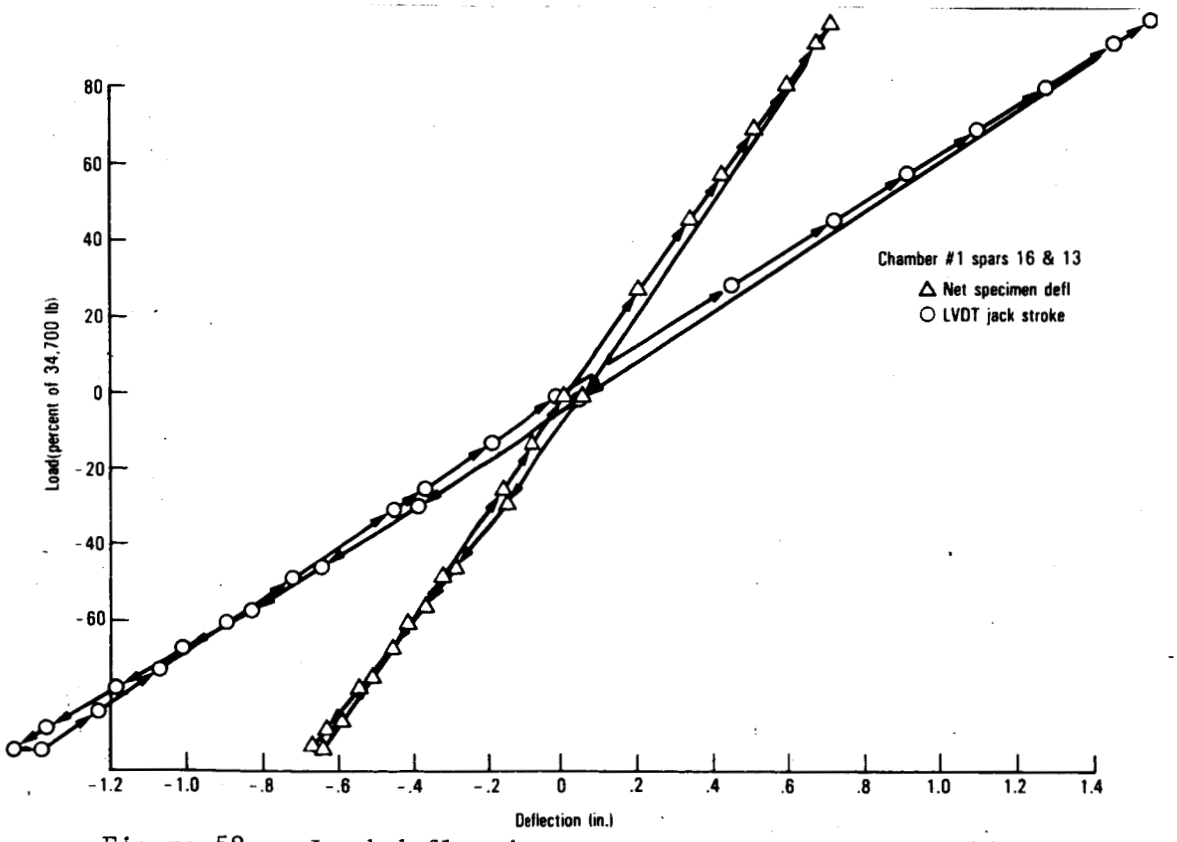

Figure 58. - Load-deflection measurement on spar assembly 2

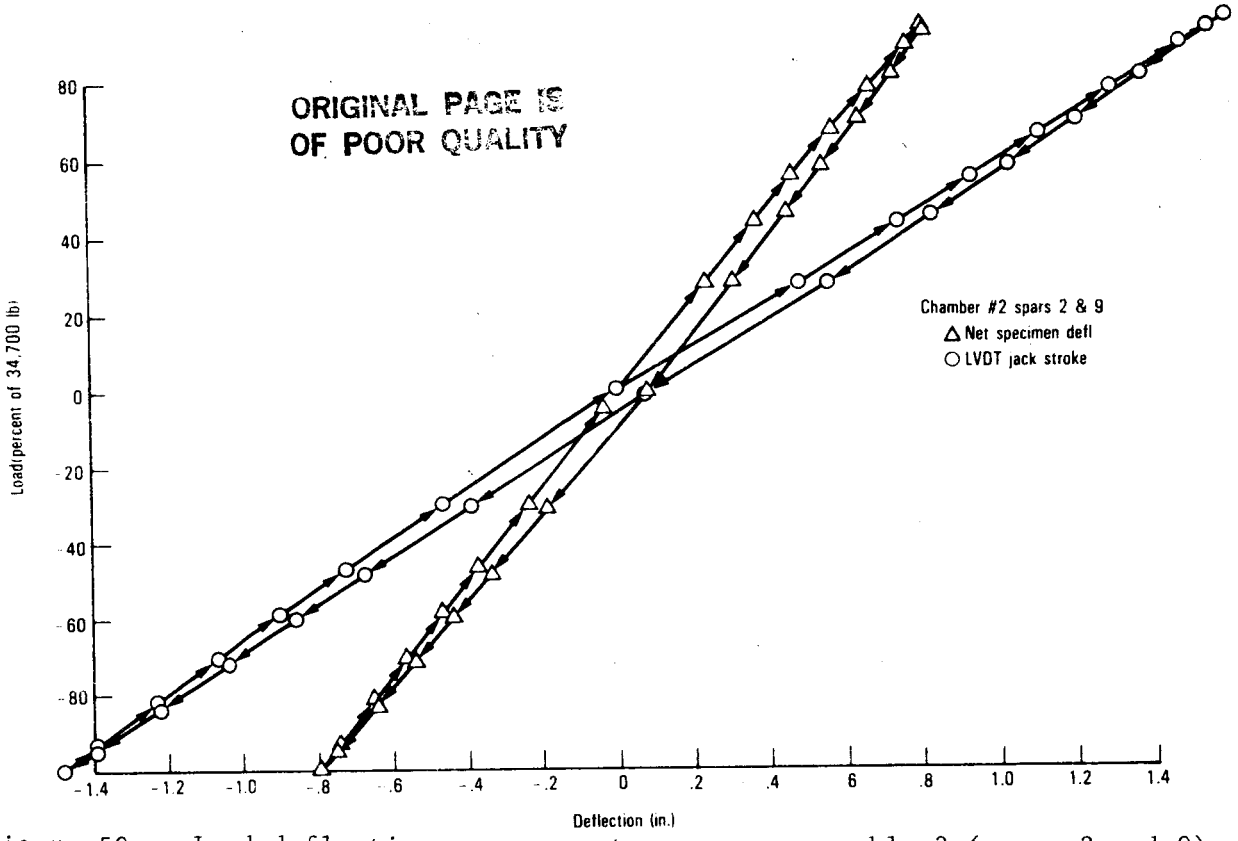

Figure 59. - Load-deflection measurements on spar assembly 3 (spars 2 and 9).

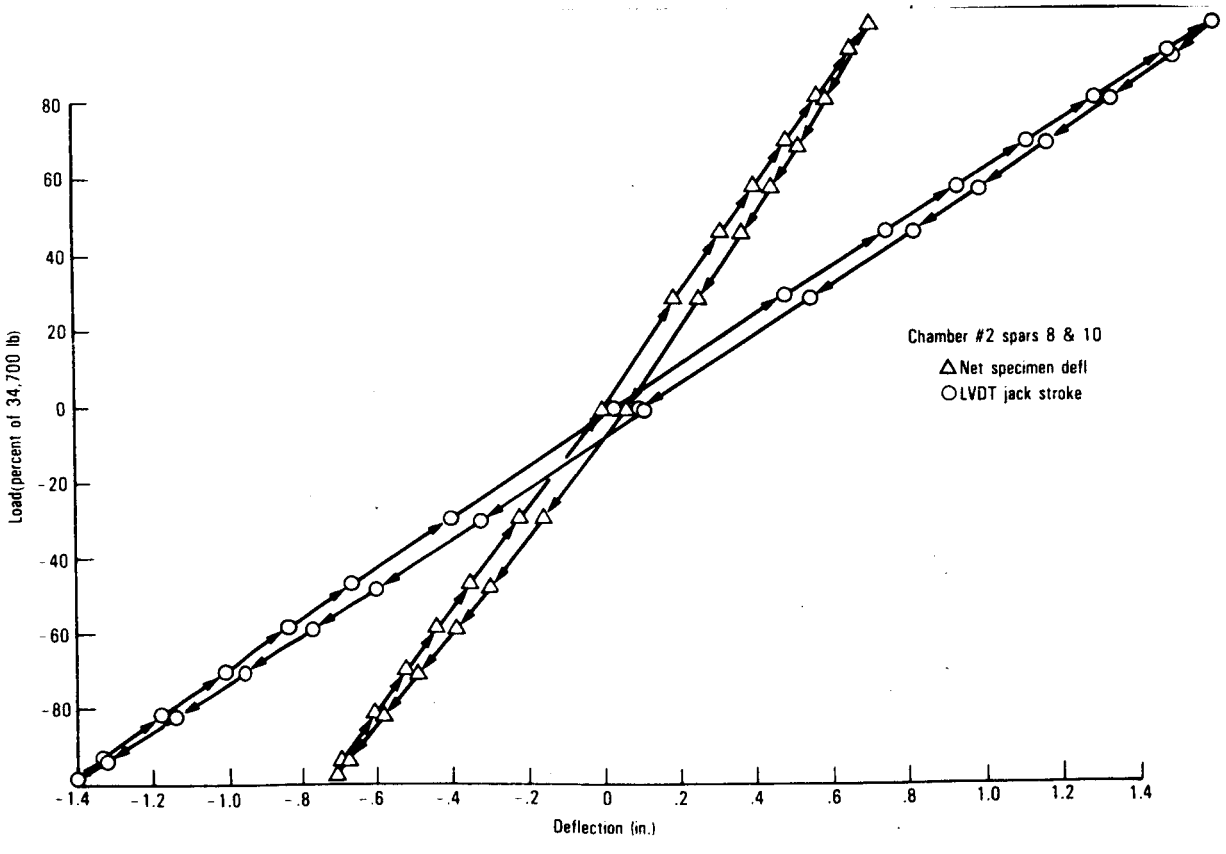

Figure 60. - Load-deflection measurements on spar assembly 4 (spars 8 and 10).

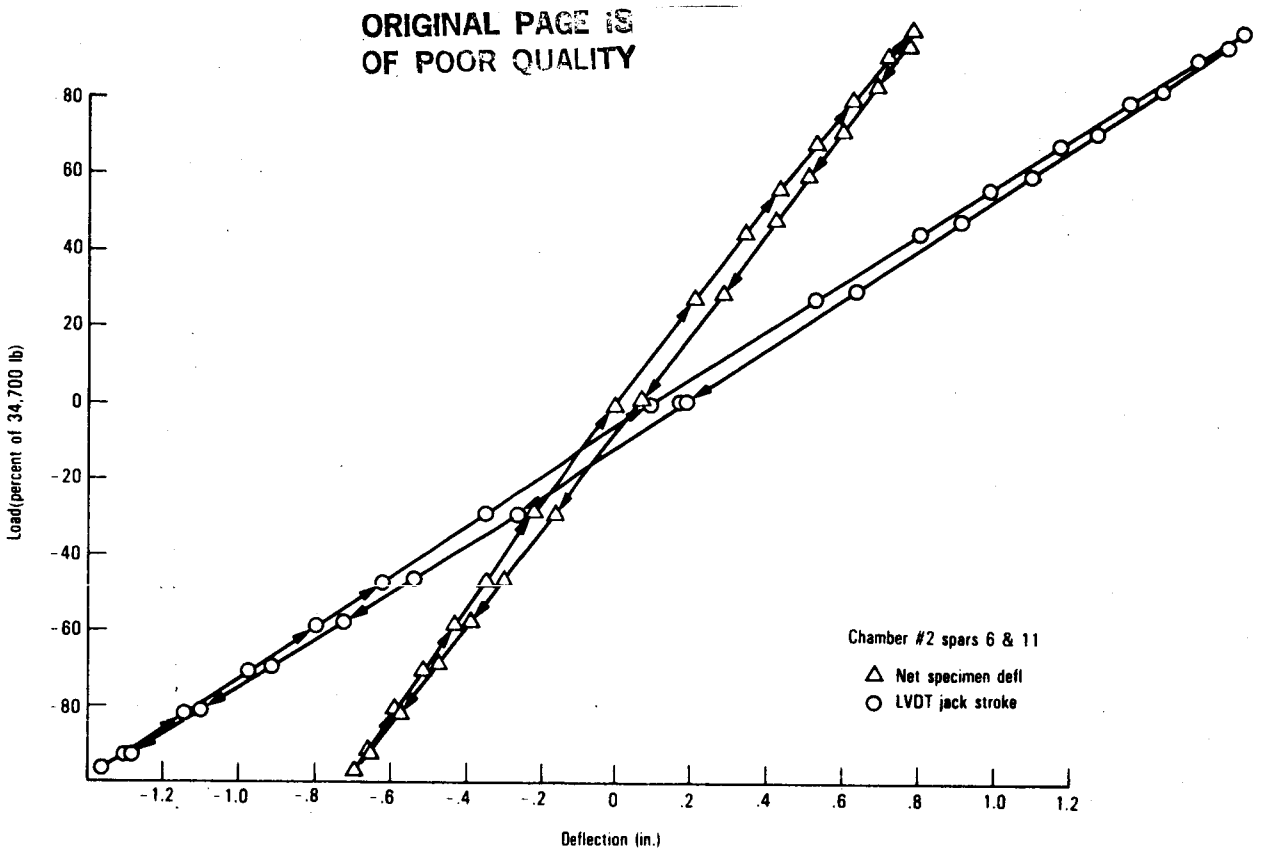

Figure 61. - Load-deflection measurements on spar assembly 5 (spars 6 and 11).

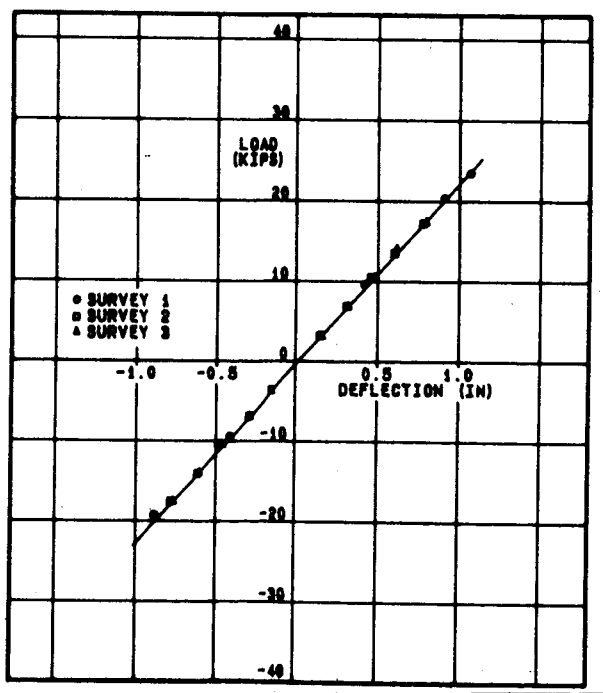

Figure 62. - Deflection comparison for spars 13 and 15 (Chamber 1)

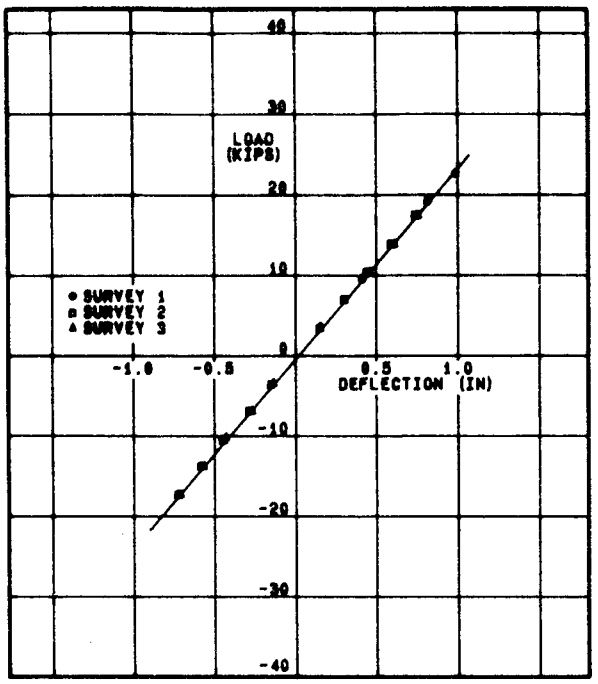

Figure 63. - Deflection comparison for spars 8 and 10 (Chamber 2).

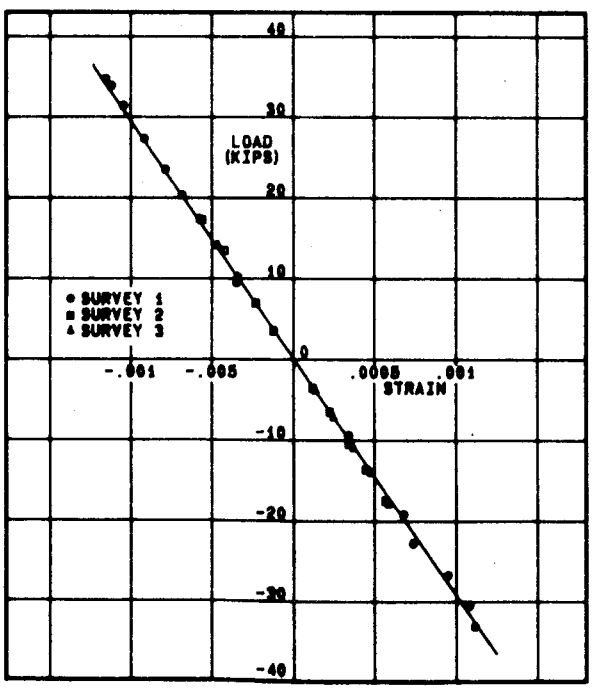

Figure 64. - Strain comparison (axial gage 1) on spar 13.

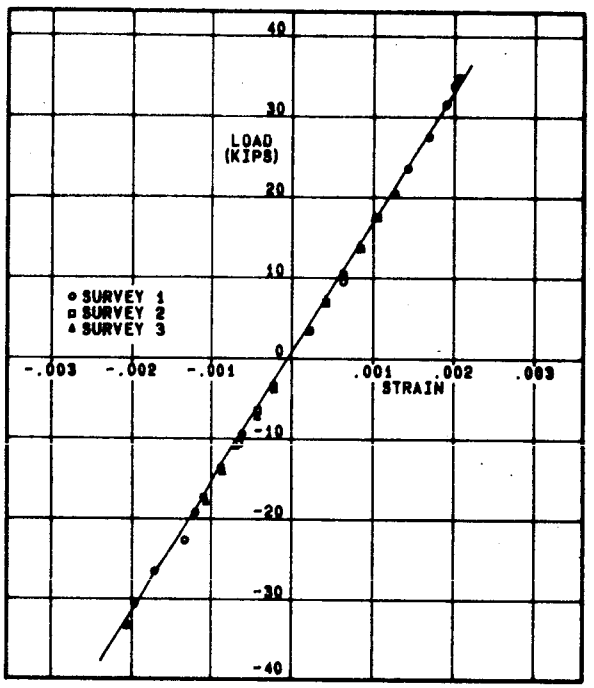

Figure 65. - Strain comparison (rosette 5) on spar 13.

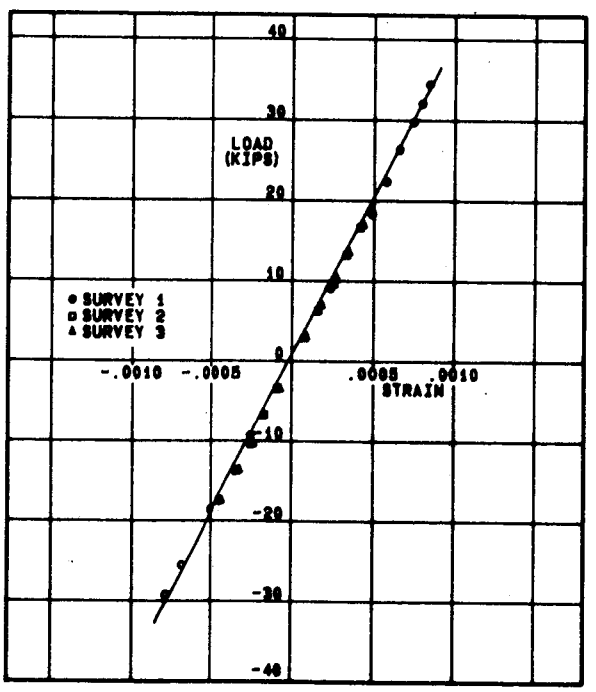

Figure 66. - Strain comparison (strain gage 1) on spar 6.

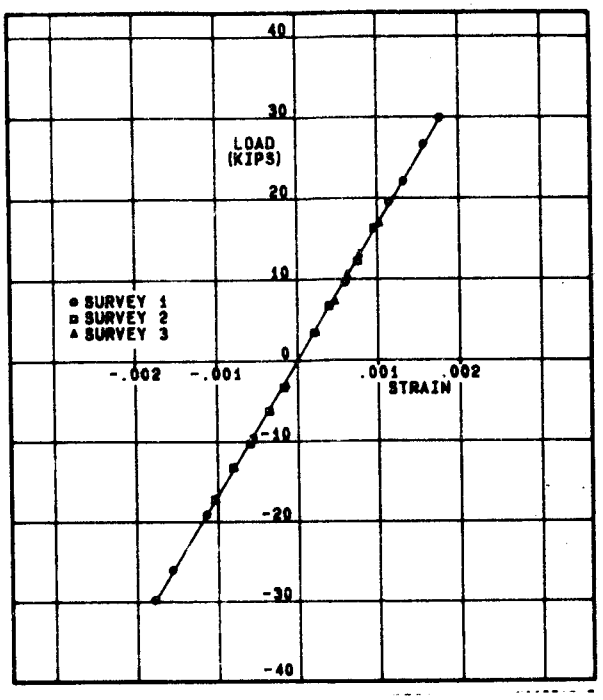

Figure 67. - Strain comparison (rosette 5) on spar 2.

had been applied with the jack in tension and the reverse load with the jack in compression was being applied when failure occurred at 140 percent DLL. Spar 24, which was the left hand spar when looking into the chamber, is shown in figure 68 and Spar 23, which was the right hand spar, is shown in figure 69.

A review of the failures and the loading linkage indicated that Spar 24 failed first and that Spar 23 failed due to the resulting displacements. The failure in Spar 24 occurred in the bay above VSS 121.45, which carried the highest shear flow of the three bays with access holes. The failure mode was relatively typical of all static test failures except for the location.

The design ultimate loads and the applied test loads are shown in figure 70 for both the static and the durability tests. The stress analyses predicted that the most critical location in the front spar due to the design loads was in the bay between VSS 97.199 and VSS 121.45, with a margin of safety at 0.05. The caps had considerably higher margins of safety. Based on the H23 test which failed at 129 percent DUL, the analysis was considered to be conservative. The lowest margin between VSS 121.45 and the VSS 145.71 was 0.16. Assuming this was equally conservative, the PRVT spars should be capable of withstanding in excess of 120 percent DUL at any location. Because the durability spars are to be static tested after completion of durability testing the cap reinforcement plates were identical for both set-ups. These

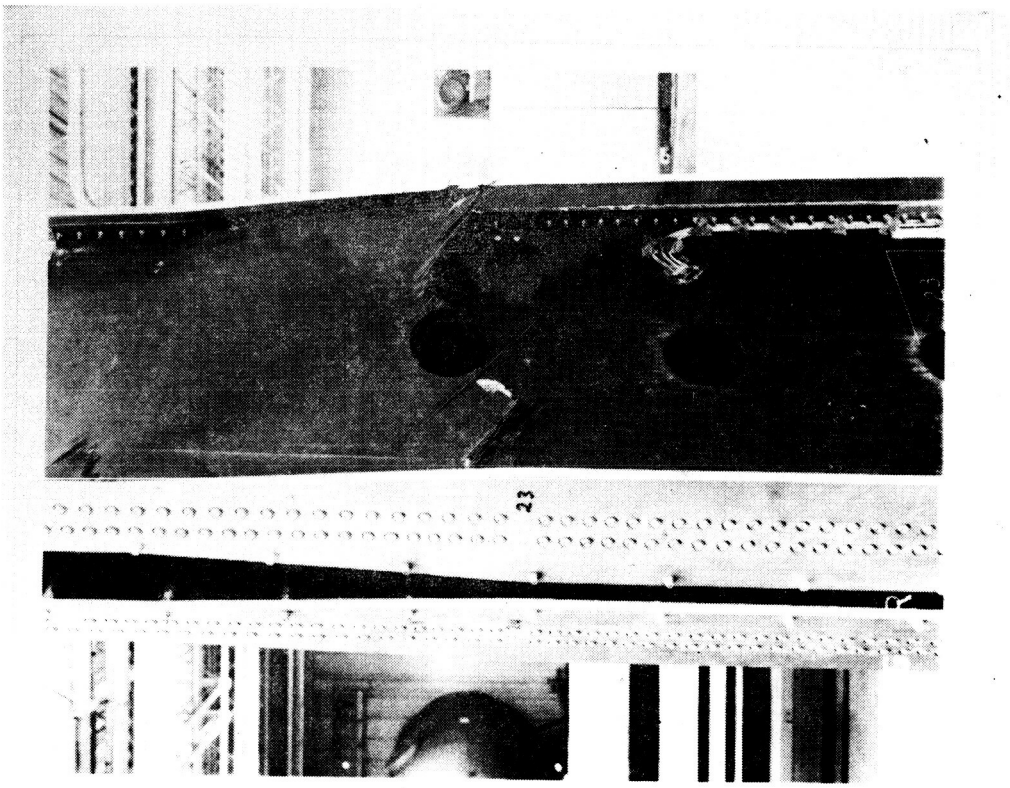

Figure 69. - Spar 23 failure.

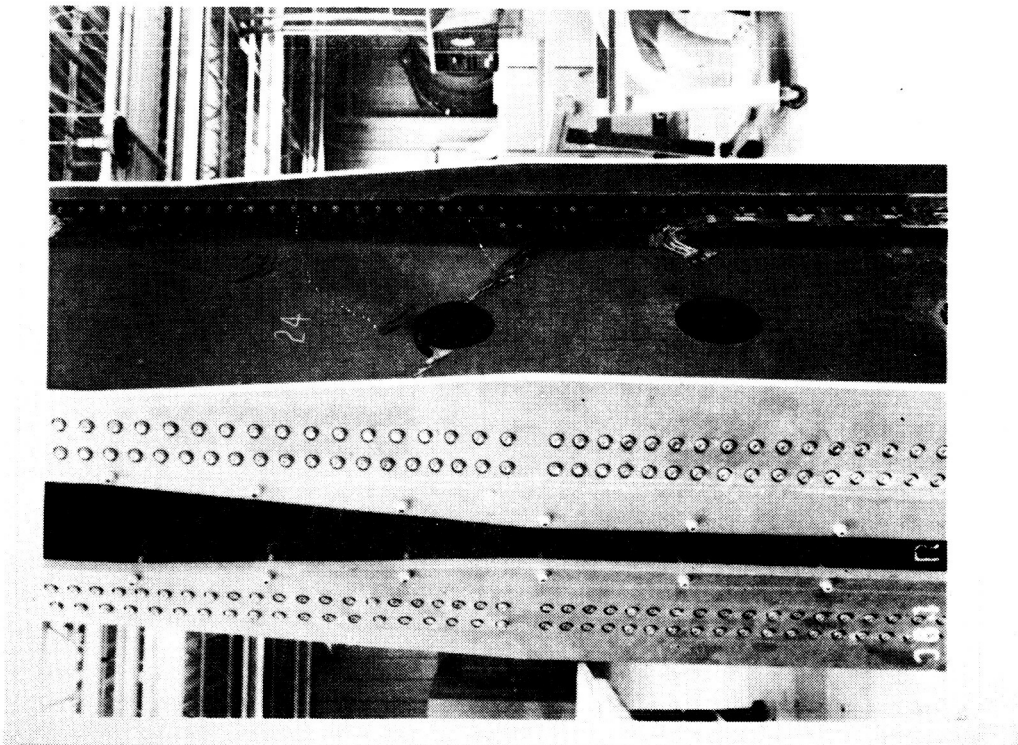

Figure 68. - Spar 24 failure (initial failure).

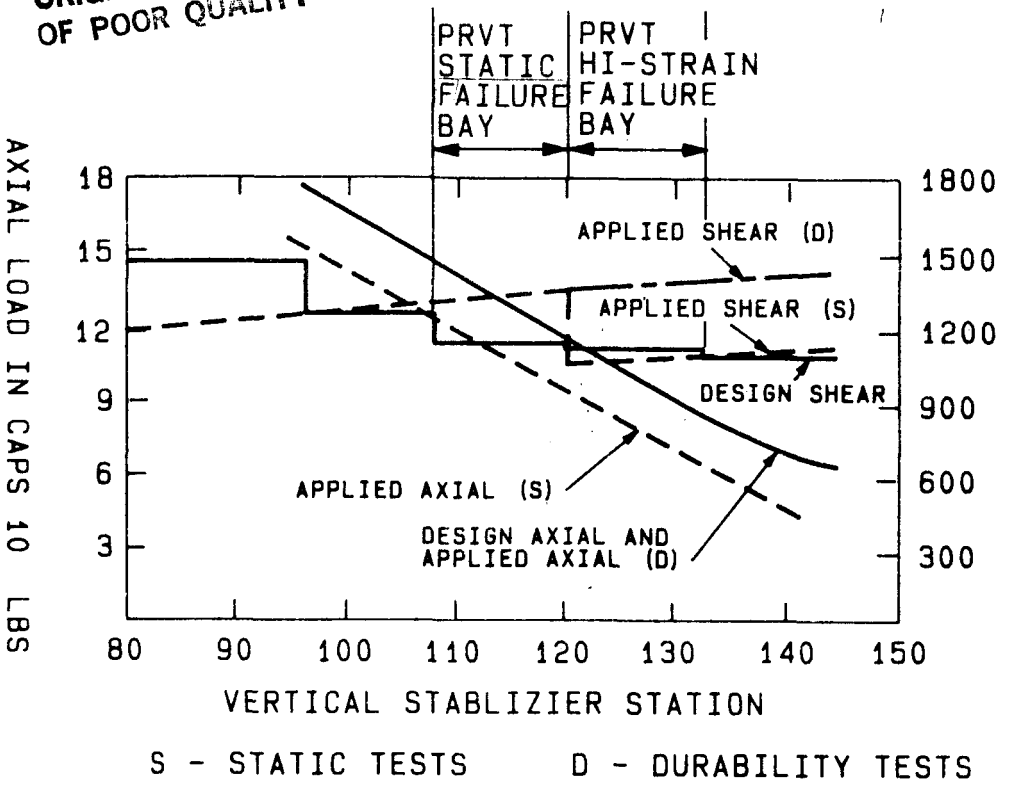

Figure 70. - PRVT spar loads.

plates were designed to give the best match of web loads and cap loads in the critical bay during durability testing. The static test set-up employs two jacks, one at the tip and one at VSS 121.45, and gives a good match of design shears for the full length of the specimen, but the cap loads are lower than the design loads. The durability test set-up could not employ two jacks because of limited number of computer control channels available. Also the long-term control of two jacks operating together in fully reversed load cycling presented an overload hazard.

The single load point setup for durability testing, while matching loadings well below VSS 121.45, caused a 20 percent higher shear to be applied above VSS 121.45. The upper access hole was not included in any of the PRVT spars as a precaution against failure due to uneven load introduction across the spar web. The access hole just above VSS 121.45 was not considered to be a problem for the basic spars where the highest load in that bay would be 80.4 percent DUL. However, in the high strain spars this bay would see 120 percent DUL. Based on the static test results, where failures occurred between 124.8 percent and 149.4 percent, the cycle at 120 percent was not anticipated to cause a problem.

Several strain and deflection surveys were performed. The load history of the high strain spars during these surveys is shown in table 10.

The April 23, 1982, survey was performed to ascertain fixture deflections so that the true spar deflections could be determined from the LVDT data recorded during cycling. A review of dial gage and LVDT data showed obviously erroneous results at one location and thus questioned the accuracy of all dial gage data. A different set-up was then used to mount the dial gages and the surveys were repeated on May 6, 1982 and May 7, 1982.

At the time of application of the high loads on April 23, 1982, the high strain spars had completed 2784 environmental cycles, which is 0.48 of a lifetime.

The bay in which failure occurred was thus loaded in shear above design ultimate load eight times, four times to 119 percent and one time each to -116 and -117 percent over a little more than two weeks. Then two weeks later it withstood +120 percent before failing at -112 percent.

The conclusion is that failure occurred due to catastrophic growth of damage caused by repeated loading close to the ultimate strength.

A panel was cut from each of the two failed spars and sent to Lockheed-Georgia Company for test. Short beam shear and compression tests were performed on coupons cut from these panels. The results were then compared with the results of the original process control tests performed on coupons cut from the discs removed when the web access holes were machined. The results of the tests are shown in table 11. The results of the original tests performed on November 16, 1979 are lower than those from the new tests performed on July 28, 1982. These tests showed that no degradation in strength occurred.

5.3 Cover Test Results

The covers were loaded in fully reversed tension-compression load cycles so load was relatively constant along the length. Each specimen was loaded separately.

5.3.1 Durability testing of the covers.- The durability testing on the covers commenced on June 22, 1979 when Chamber 4 containing six-basic covers were brought on line. Chamber 3 containing four basic covers and two-high strain covers came on line on February 27, 1980. Figure 71 shows typical load-deflection data for two covers in Chamber 3. These deflections have been corrected to remove the fixture deflection. Deflection data did not exhibit the drop which occurred with the spars. Nothing of any significance occurred during the cover durability tests.

As with the spars, static strain-deflection surveys were performed periodically on the covers. During the last survey in April 1982, dial gages were attached to each component to measure the specimen deflection alone. The

TABLE 10. - STRAIN AND DEFLECTION SURVEY LOAD HISTORY FOR HIGH STRAIN SPARS

Date	% Design Ultimate Load Applied at VSS 97.19	% Design Ultimate Load Applied to Web Above VSS 121
February 20, 1981	0 +58	+70
	0 -57	-69
	0 +58	+70
	0 -57	-69
November 8, 1981	0 +85	+103
	0 -85	-103
January 6, 1982	0 +53	+64
	0 -49	-58
April 23, 1982	0 +77	+93*
	0 +81*	+97*
	0 +99*	+119*
	0 +99	+119
	0 -97	-116
May 6, 1982	0 +99	+119
	0 -97	-117
May 7, 1982	0 +99	+119

*System dumped due to oscillations in high-strain loading system.

TABLE 11. - HI-STRAIN SPARS - COUPON TESTS

Spar Number	Test Type	Compression (ksi)		Short Beam Shear (ksi)	
	Test Date	11-16-69	7-28-82	11-16-79	7-28-82
23		67.4	82.8	7.4	9.4
		67.4	74.6	6.1	8.5
		73.2	78.9	8.2	6.0
		72.3		7.1	
		65.9		7.4	
		73.6		7.3	
	AVG	70.0	78.8	7.25	8.0
24		73.6	79.3	7.3	9.1
		64.7	87.1	7.8	8.2
		68.3	80.0	8.0	8.9
		72.2		7.9	
		69.9		7.1	
		71.1		7.6	
	AVG	71.3	82.1	7.62	8.7

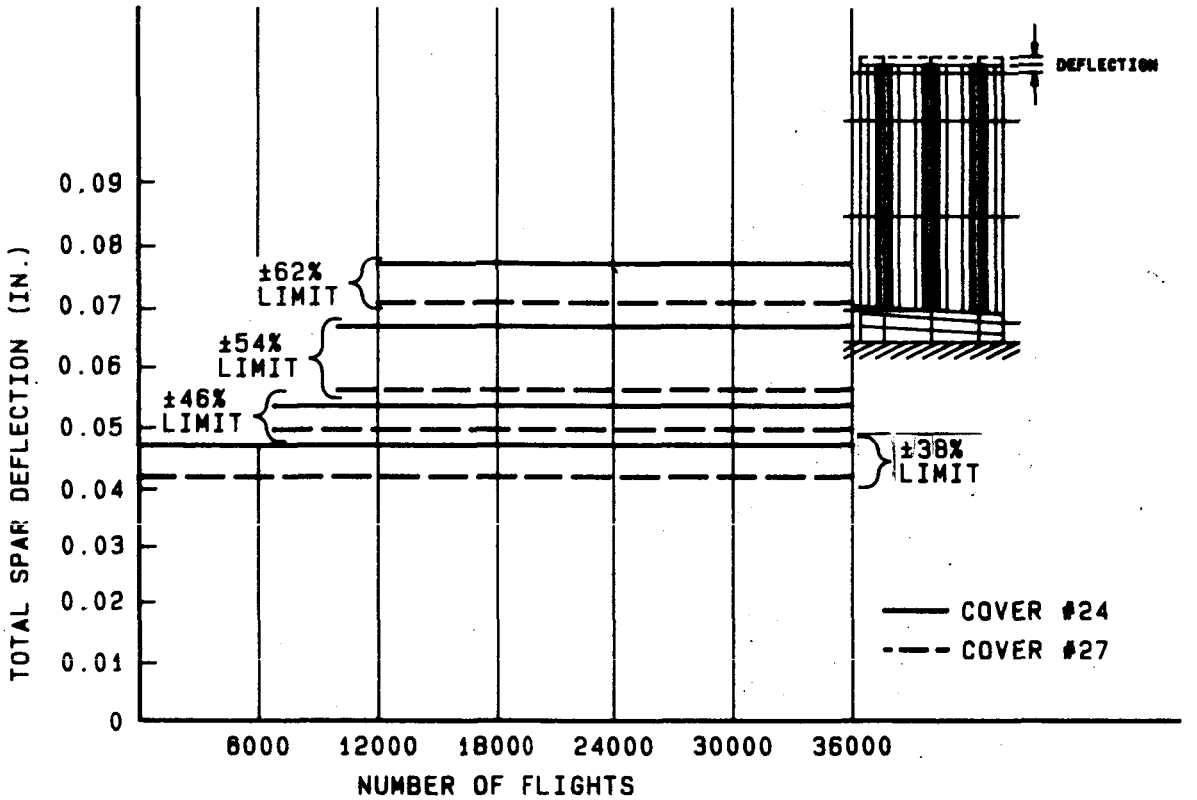

Figure 71. - Load-deflection data for Chamber 3 basic covers.

arrangement of these dial gages is shown in figure 72. The load-deflection behaviour of the covers alone as measured by the dial gages is compared for Chamber 3 in figure 73 and for Chamber 4 in figure 74. Some hysteresis is evident.

Total system deflection for Chamber 3 specimens is shown prior to testing in figure 75 and during survey 4 in figure 76. The same conditions for Chamber 4 specimens are shown in figures 77 and 78. There was no change in the response of any of the cover specimens.

The locations and identification of strain gages mounted on the cover specimens are shown in figure 46. The four axial gages (1 through 4) at VSS 109.5 were at the midpoint of the first bay outboard of the root attachment, and monitored column bowing and differential degradation, if it occurred. The set of gages at VSS 121.45 were directly under the rib centerline and provided information on uniformity of loading and on the amount of shear carried by the diagonal webs of the hat stiffeners. A full complement of seven axial gages and one rosette was installed on Cover 6. The high-strain cover specimens (Nos. 18 and 25) each carried gages 1, 2, 3, and 4. The remaining cover specimens carried the single gage at Station 2.

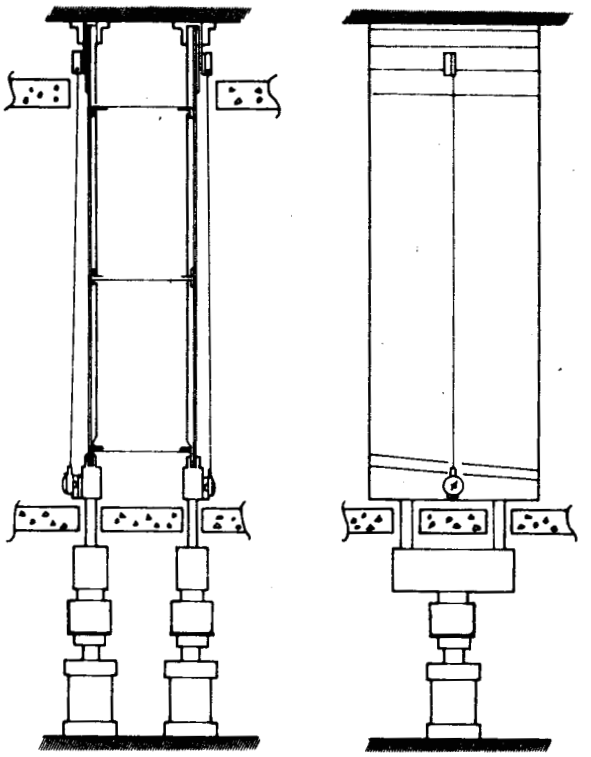

Figure 72. - Schematic of cover specimen assembly showing arrangement of dial gages for deflection measurement, April, 1982.

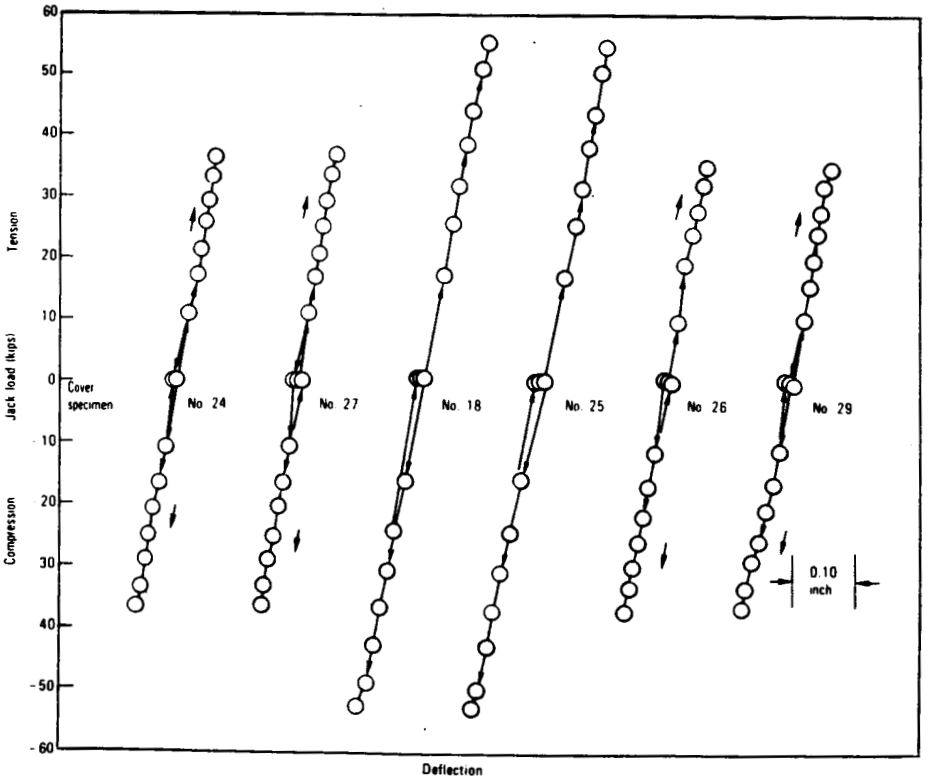

Figure 73. - Load vs specimen deflection cover specimens in Chamber 3 test conducted April 30, 1982.

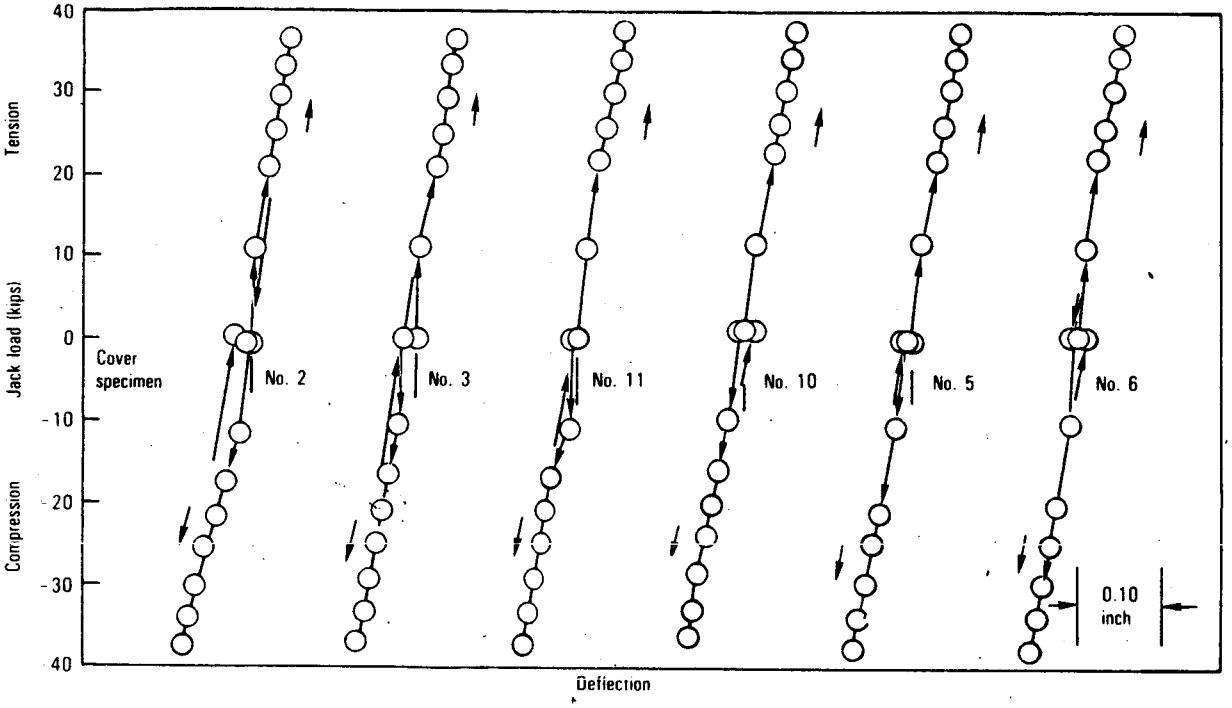

Figure 74. - Load vs specimen deflection cover specimens in Chamber 4 test conducted April 30, 1982.

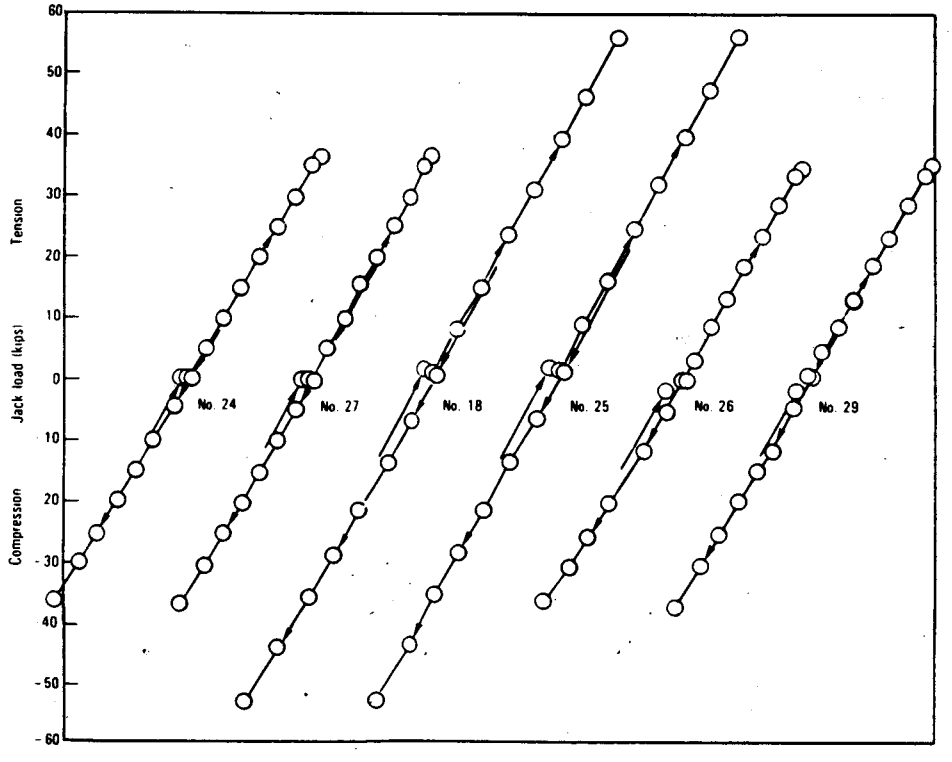

Figure 75. - Load vs system deflection, cover specimens in Chamber 3, prior to durability testing February 14, 1980.

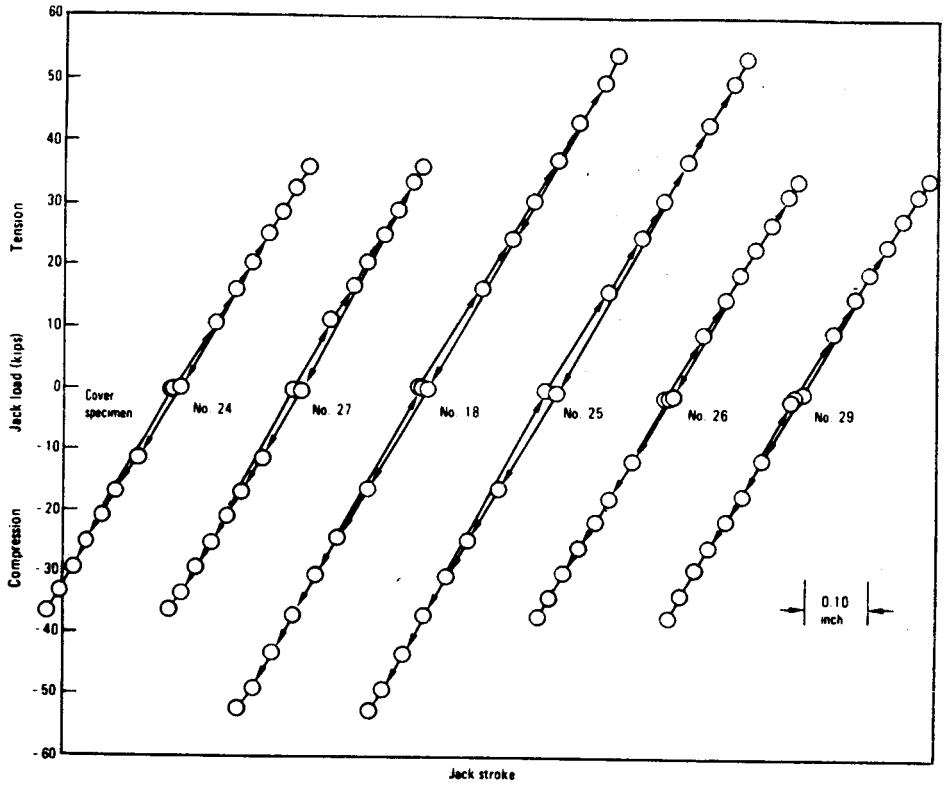

Figure 76. - Load vs system deflection cover specimens in Chamber 3, after durability testing April 30, 1982.

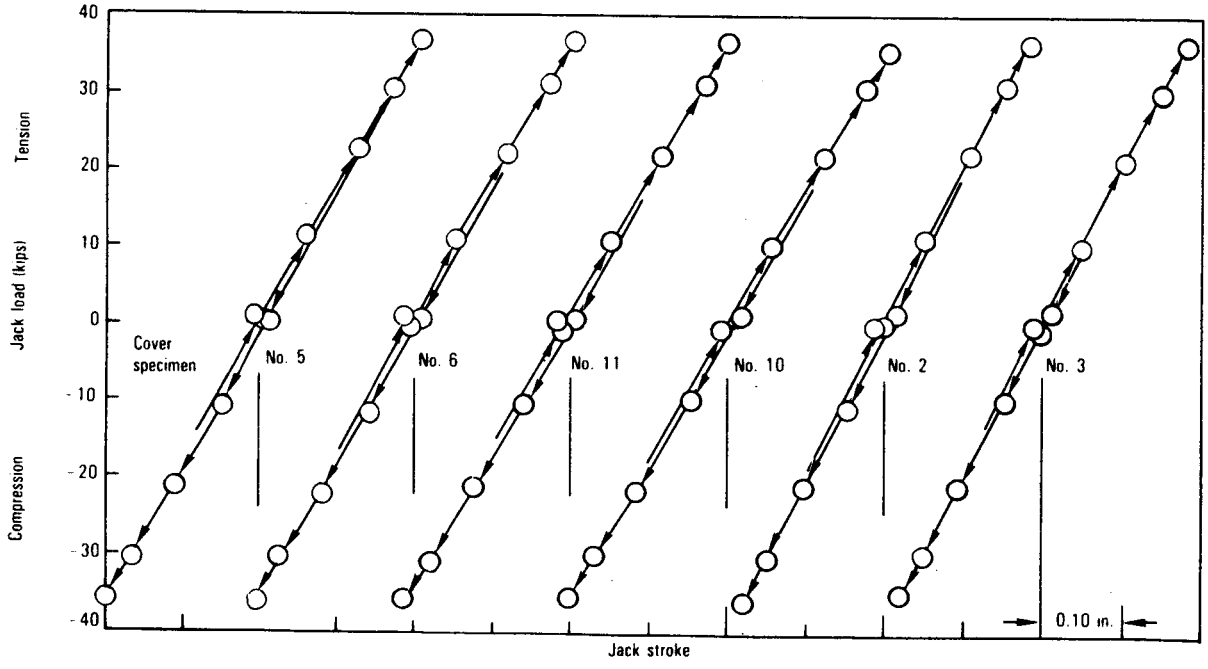

Figure 77. - Load vs system deflection, cover specimens Chamber 4, prior to durability testing June 15, 1979.

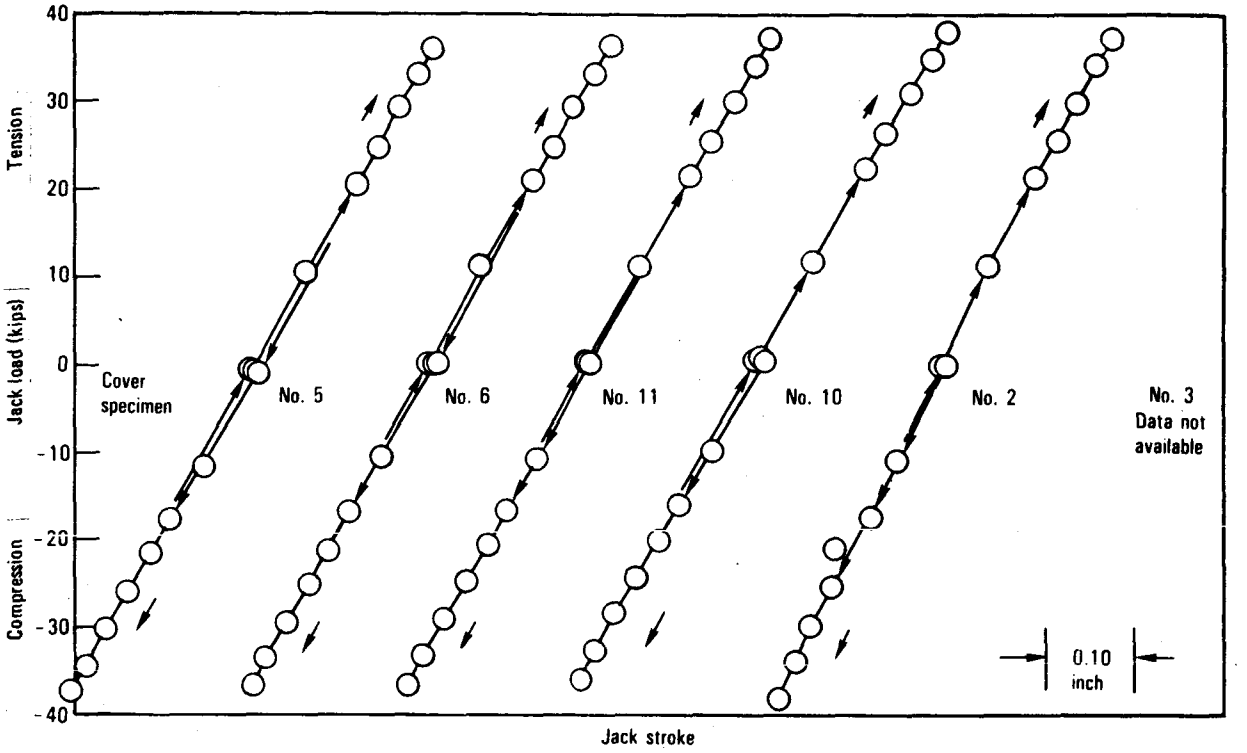

Figure 78. - Load vs system deflection, cover specimens Chamber 4, after durability testing April 27, 1982.

A comparison was made between some of the deflection and strain data recorded during the first three surveys. The data were corrected for hysteresis as necessary. Figure 79 and figure 80 show the overall load deflection comparison for a typical cover in each chamber. Comparison of the strains on the same covers is shown in figures 81 and 82. No change in response occurred.

5.4 Moisture Content

Moisture content in the spars and covers was tracked by installation of weight gain travelers in each chamber. A total of 50 travelers were used. In the spar chambers a tee section of cap and web material and a web section were cut from spar scraps so that the traveler had section properties the same as the spars. Likewise, cover hat and skin sections were fabricated.

These travelers were cut, weighed, and installed in the chambers prior to the test start-up, without any drying just as the spars and covers. Each one was indexed to a specific location in the chamber and after weighing returned to that spot. Weight gain measurements were made at intervals and are presented graphically in figures 85 and 86. Thickness ranges are also shown.

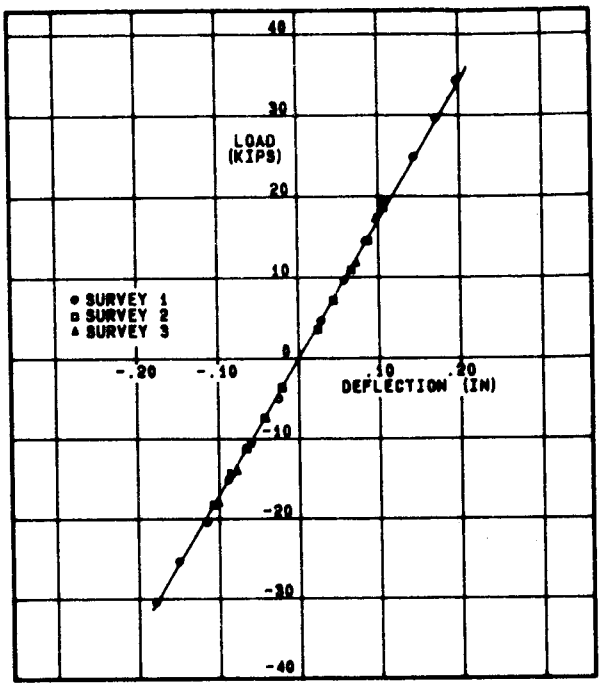

Figure 79. - Deflection comparison for cover 24 (Chamber 3).

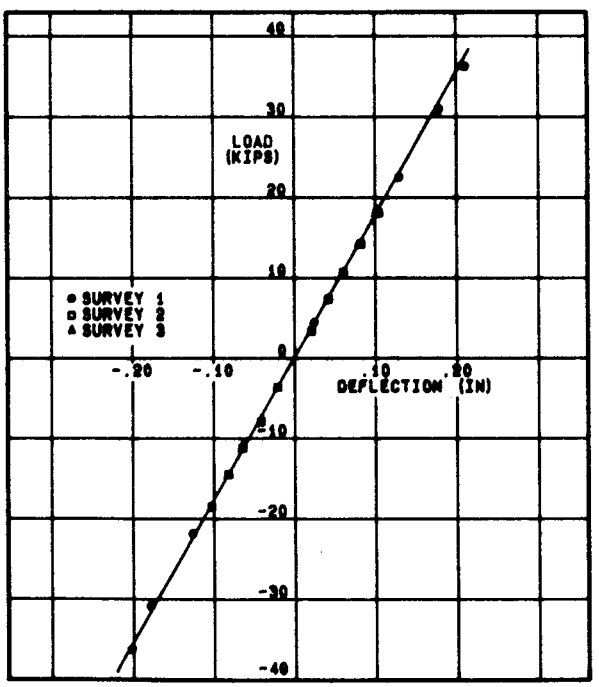

Figure 80. - Deflection comparison for cover 5 (Chamber 4).

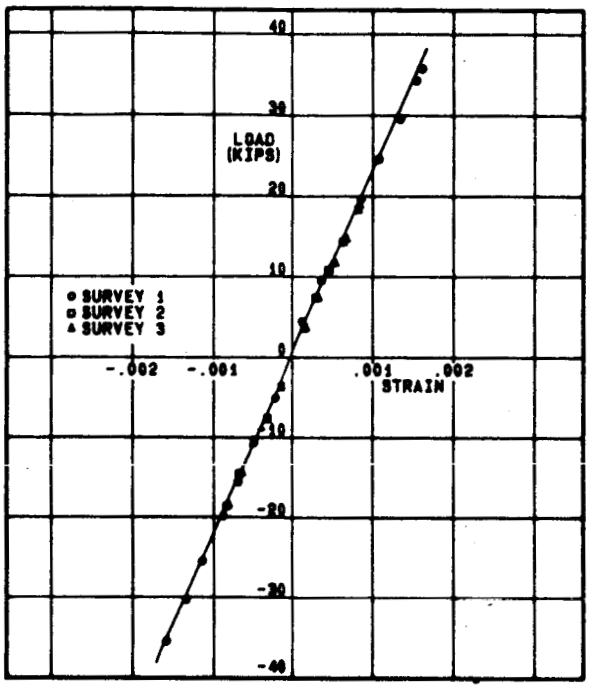

Figure 81. - Strain comparison for cover 26 (strain gage 2).

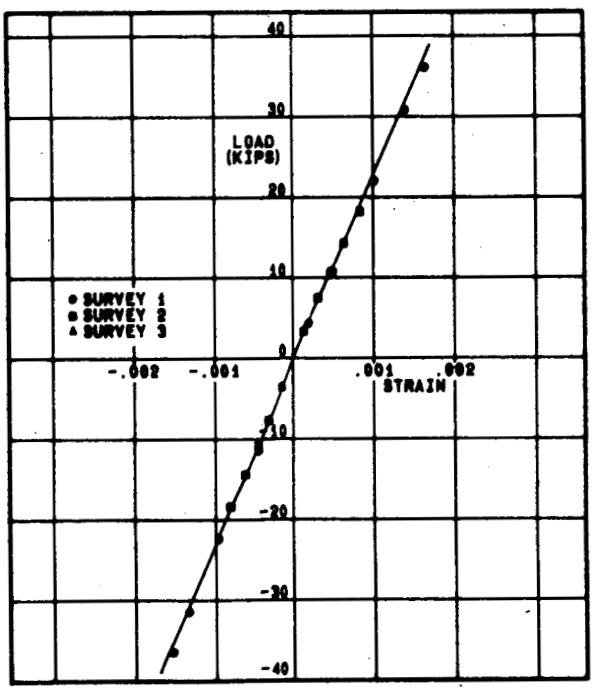

Figure 82. - Strain comparison for cover 5 (gage 2).

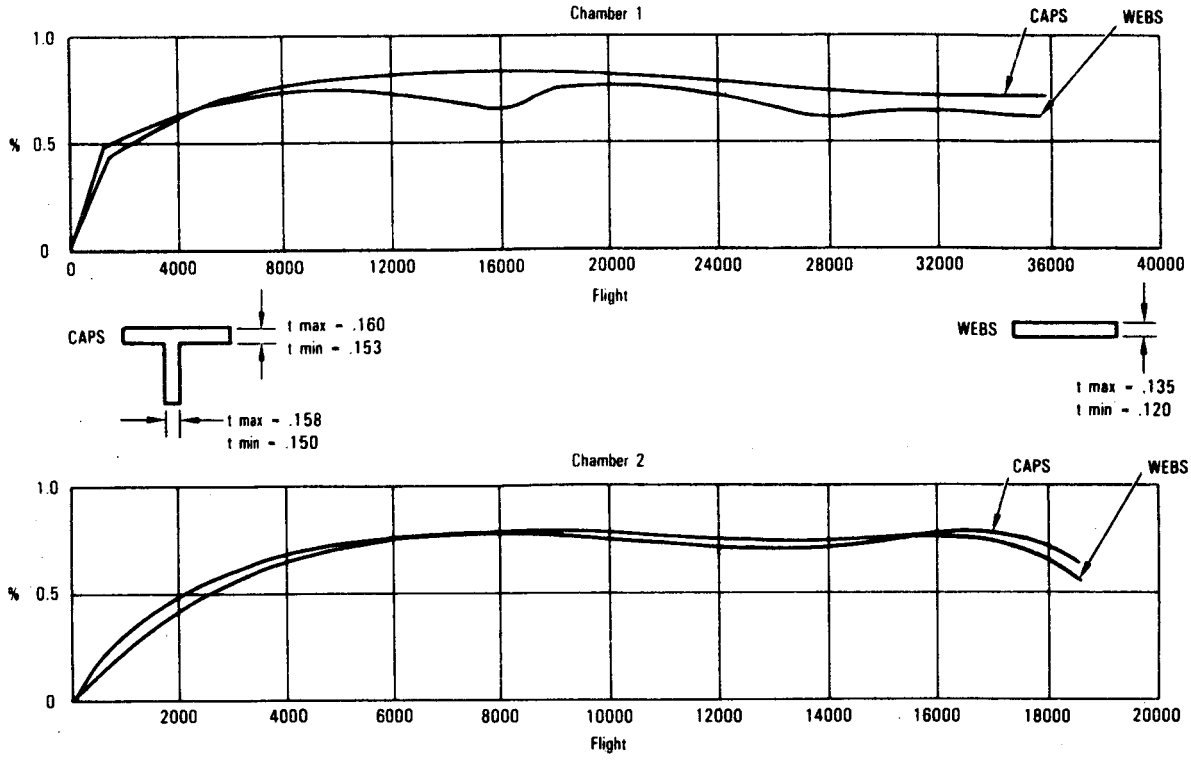

Figure 83. - Spar moisture weight gain/traveler coupons.

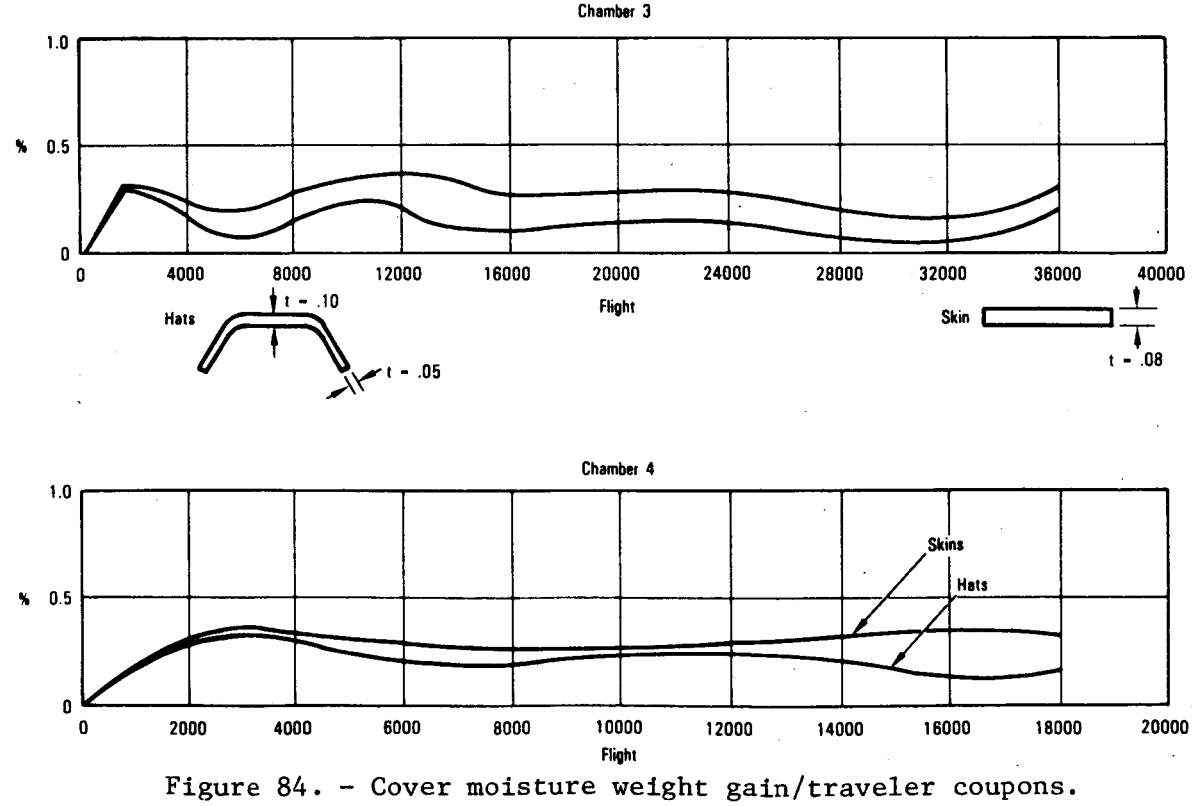

Figure 84. - Cover moisture weight gain/traveler coupons.

Approximate dimensions for the spar chamber cap tee sections were 1.5 inches wide by 3.0 inches long for the cap piece and 1.75 inches high for the web piece. For the web-only traveler, dimensions were 1.5 by 4.5 inches. Cover hat dimensions were 1.1 inches high by 1.7 inches wide. Cover skin dimensions were approximately 2 x 7 inches.

In April 1982, twenty-seven travelers were removed, some from each chamber and type, and dried in a vacuum at 150°F until weight loss stabilized. These data presented graphically in figures 85 and 86. Spar travelers from the webs in Chamber 1 seem to stabilize at approximately -1.0 percent and cap travelers at approximately -1.1 percent. The difference after drying is 0.23 percent for the web travelers and approximately 0.24 percent for the cap travelers as the initial moisture content in the parts at test start.

Due to oil contamination of the drying chamber, the drying operation was terminated after 6000 hours. The data trends however are quite clear and can be extrapolated to stabilization.

After the high-strain spars failed, four coupons were cut from the web areas and added to the drying chamber. These data are shown in figure 87 and track very closely with the traveler data, verifying the accuracy of the traveler data.

5.5 Thermal Cycles

At randomly selected points during the scheduled 5800 thermal cycles, which represented the full 20 years of service, 40 temperature excursions to 160°F and 10 to 180°F were to be applied. Since Chambers 2 and 4 did not complete the 5800 thermal cycles they received fewer high temperature cycles. Table 12 summarizes the number of cycles applied to the specimens in each chamber.

The application of these cycles was not programmed into the computer and had to be applied manually. Due to the longer heat-up time this application caused a sequencing delay in all other chambers. Manual application was desirable to minimize the sequencing delay and to carefully observe specimen temperatures from a safety standpoint.

5.6 Residual Strength Tests

At the completion of the durability testing the 10 surviving spars and the 12 covers were shipped to NASA Langley Research Center. Six of the covers and five of the spars were then residual strength tested to determine if any degradation had taken place.

A thorough inspection was made of each component. Spar 13 was found to have a delamination which started in the edge of an access hole and extended

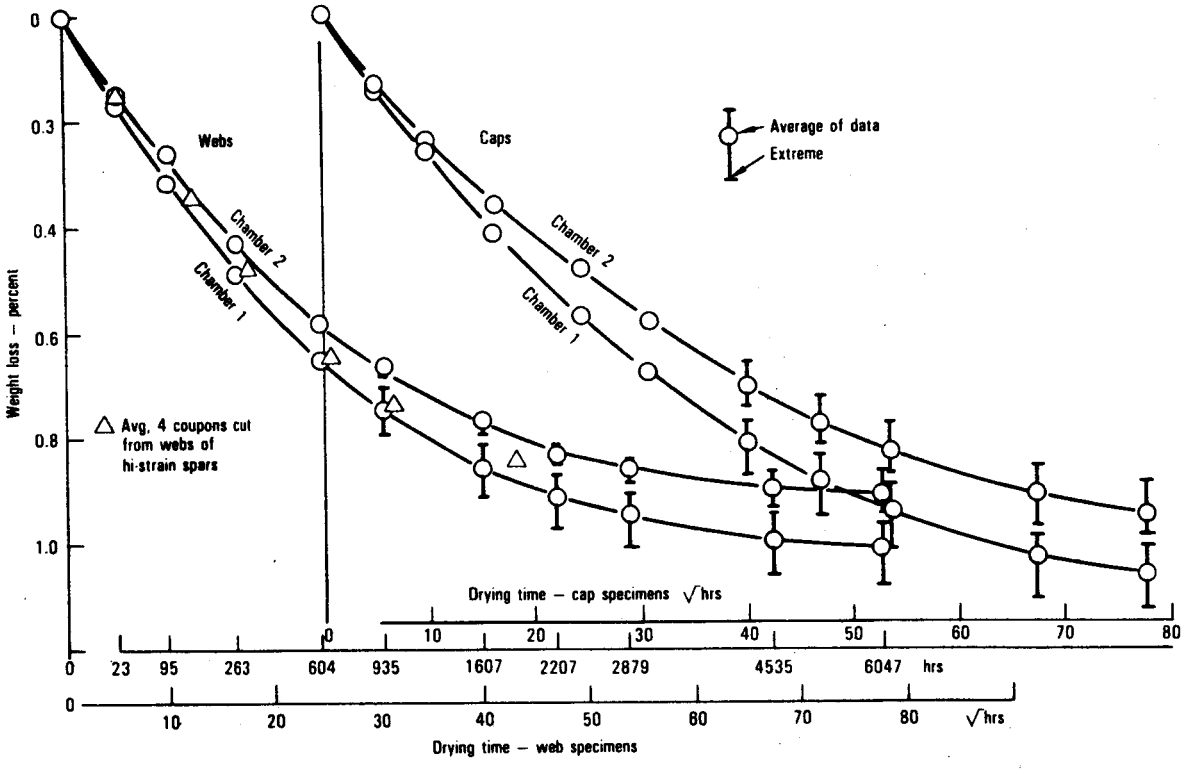

Figure 85. - Spar traveler coupon drying curves.

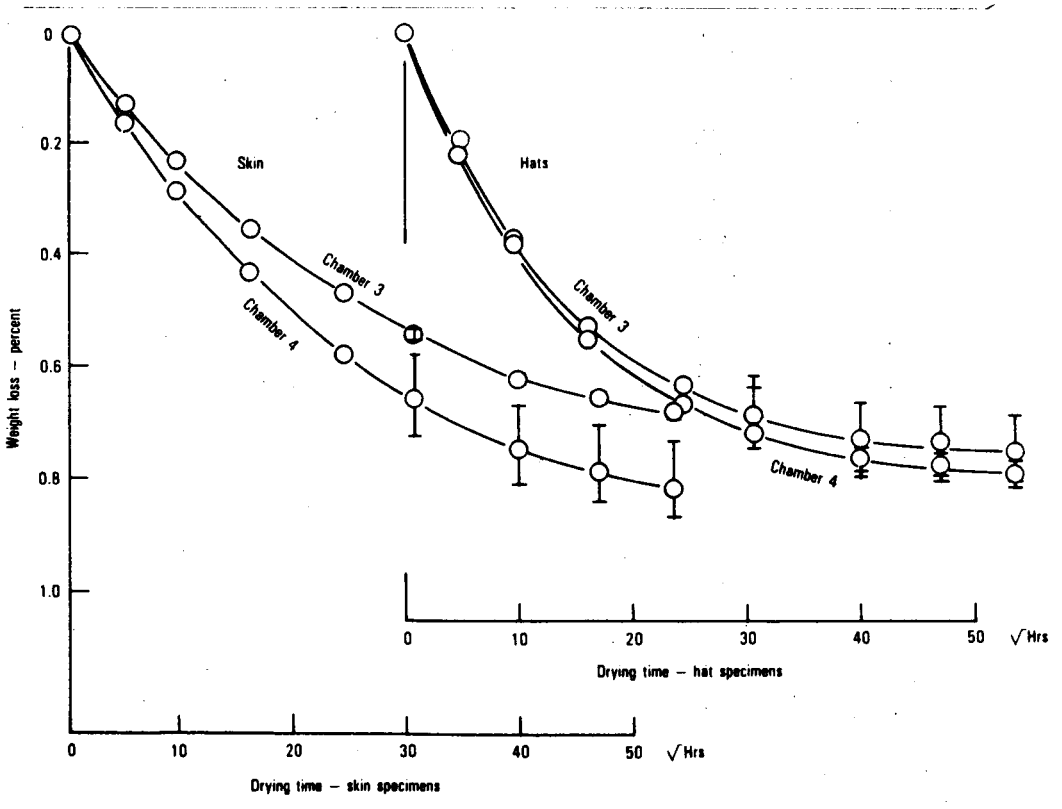

Figure 86. - Cover traveler coupon drying curves.

TABLE 12. - THERMAL CYCLE HISTORY

L-1011 design lifetime: 20 years of service
5800 thermal cycles

	Thermal cycles			
	140°F -30°F	160°F -30°F	180°F -30°F	Σ
Spars				
Chamber no. 1 (4 spars)	5750	40	10	5800
Chamber no. 1 (2 spars)*	2836	19	6	2861
Chamber no. 2 (6 spars)	2954	17	5	2976
Cover				
Chamber no. 3 (4 covers)	5750	40	10	5800
Chamber no. 3 (2 covers)*	5750	40	10	5800
Chamber no. 4 (6 covers)	2875	20	5	2900

*High strain specimens

up under a stiffener, which was loosened, and well into the next bay. A review of the inspection records showed that several access holes in this spar had been repaired due to delamination during machining. The hole, where the delamination was discovered after test, was not repaired after machining as no delamination had been found by NDI. It is surmised that some damage had occurred during machining and that this damage had propagated during durability testing.

The residual static tests exhibited generally higher strengths than the original static tests on virgin specimens. Even the damaged spar 13 was above average for the original ten specimens. The results of these tests are summarized in tables 13 and 14 and shown graphically in figures 87 and 88.

6. CONCLUSIONS

The three questions posed at the beginning of the program have now been answered.

The range of production qualities that can be expected for components manufactured under conditions similar to those expected in production has been established. The spars were produced using tooling which underwent only minor modifications during the run of 24 components, similar to a production run. The covers were fabricated using tooling that underwent various modifications during a run of 28 components. Thus extremes of the production environment were encountered.

TABLE 13. - COVER RESIDUAL STATIC STRENGTH TEST RESULTS

Cover No.	Flights	Equivalent Service Years	Failure Load lb	% DUL
5	18,472	10.26	-94,000	163.5
6	18,472	10.26	-97,600	169.7
26	36,000	20.00	-91,000	158.3
29	36,000	20.00	-89,500	155.7
18**	36,000	20.00	-95,000	165.2
25**	36,000	20.00	-92,000	160.0
		Average*	-93,183	162.1

*Average of original 10 static was -92,390 lb (160.7%)
**High strain covers

TABLE 14. - SPAR RESIDUAL STATIC STRENGTH TEST RESULTS

Spur No.	Flights	Equivalent Service Years	Upper Jackload at Failure lb	% DUL
6	18,000	10.00	32,000	154.5
11	18,000	10.00	31,600	152.5
13	36,000	20.00	30,500	147.2
16	36,000	20.00	33,000	159.3
18	36,000	20.00	32,500	156.8
		Average*	31,920	154.1

*Average of original 10 static was 27,940 lb (134.9%)

The quality control procedures used proved adequate in identifying discrepancies. In particular NDI techniques developed and refined during the program worked very well. The mechanical process control tests proved to be of varied effectiveness individually but when viewed on a combined basis for each component correlated well with NDI and physical tests.

The static test results showed excellent uniformity. The coefficients of variation (CV), 3.3 percent for the cover and 6.1 percent for the spars compare favorably with those of other common structural materials. The allowables used were derived from coupon data. The failure modes of the covers and spars are influenced primarily by stiffness. The specimens in all cases failed at loads higher than predicted. The allowables used for prediction were based on average coupon data whereas design allowables are statistically reduced below those levels. The allowable thus proved adequate to account for structure static strength variability.

The durability testing showed that the combined effects of long-term cyclic environment and cyclic loads below design limit load have no deleterious effects. The high strain components showed that cyclic loads up to design ultimate do not have a deleterious effect. The failure of the two high strain spars was due to load applications in the failure bay well in excess of design ultimate.

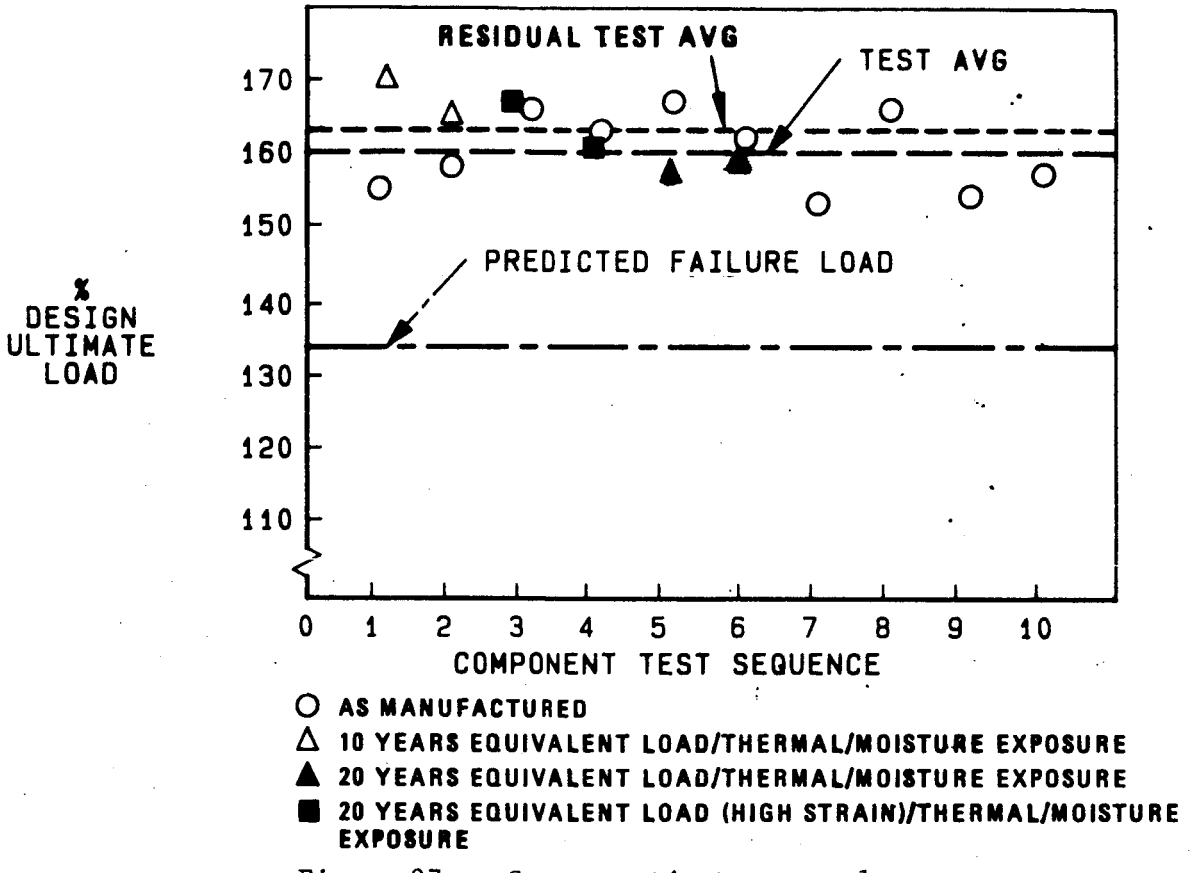

Figure 87. - Cover static test results.

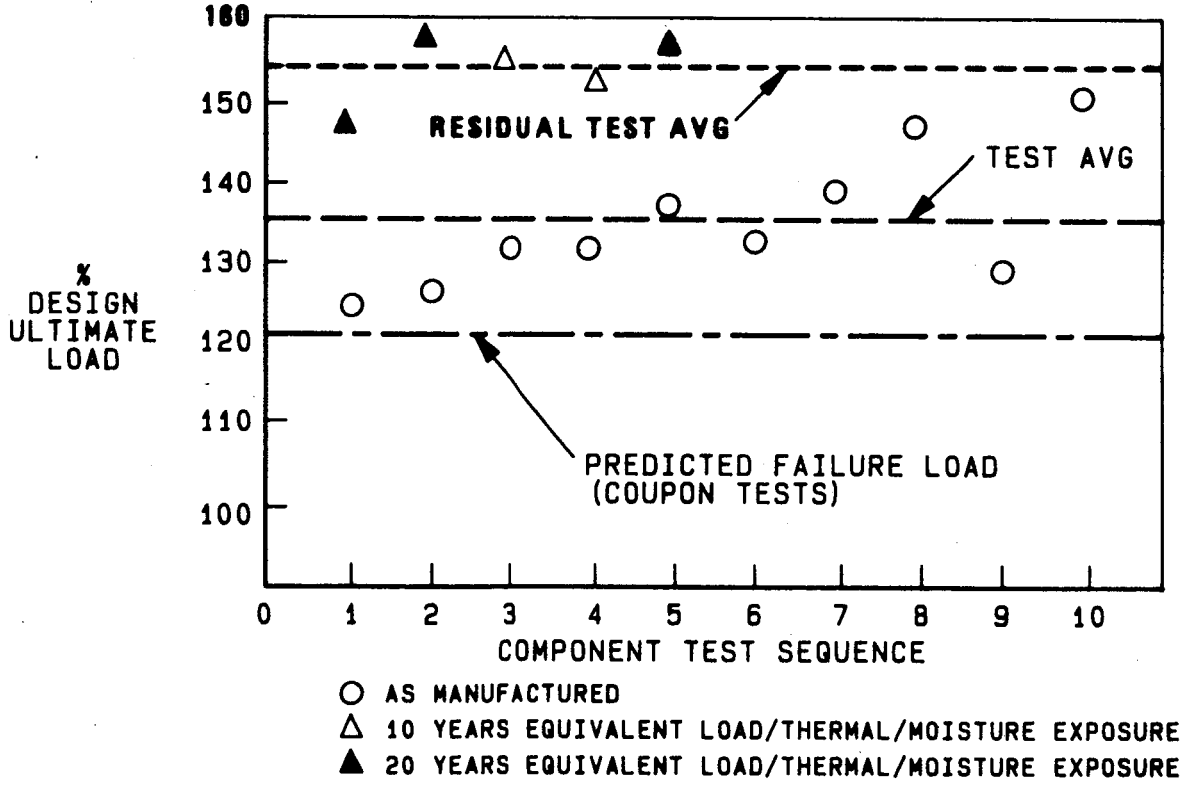

Figure 88. - Spar static test results.

REFERENCES

1. Ary, A., et al, Flight Service Evaluation of an Advanced Composite Empennage Component on Commercial Transport Aircraft, Phase I Final Report, Engineering Development, NASA CR-144986, May 1976.

2. Jackson, A. C., et al, Advanced Manufacturing Development of a Composite Empennage Component for L-1011 Aircraft, Phase II Final Report, Design and Analysis, NASA CR-165634, April 1981.

3. Alva, F., et al, Advanced Manufacturing Development of a Composite Empennage Component for L-1011 Aircraft, Phase IV Final Report, Manufacturing Development, NASA CR-165885, May 1982.

4. Jackson, A., Dorward, F., Advanced Manufacturing Development of a Composite Empennage Component for L-1011 Aircraft, Phase V Final Report, Full-Scale Ground Test, NASA CR-166015, December 1982.

APPENDIX A
UNUSUAL EFFECT OF MOISTURE SORPTION ON THE DEFLECTION OF A GRAPHITE/EPOXY JOINT

INTRODUCTION

The original test plan for the PRVT durability tests of spars and covers provided for detailed study of stress and deflection data only at infrequent intervals. Compilation of data from computer printouts in March, 1981 revealed some surprising effects which were not apparent from the day-to-day monitoring of performance: namely, an apparent increase in stiffness of all the spar specimens.

Studies were initiated to confirm the increase in stiffness as a result of the PRVT exposure. The stiffness variation of the spar specimens with PRVT equivalent flights and with load level, is presented in figure A1.

A possible explanation for the stiffness increase linked the apparent stiffness to a partial transfer of load in the spar-to-cap joint by friction, and an increase in friction to swelling of the graphite/epoxy laminate with moisture sorption. The tests described here were made primarily on Lockheed funding to check this hypothesis.

SPECIMEN

A specimen designed to investigate load transfer by friction in the ACVF spar flange to cover joint was constructed from salvaged pieces of the PRVT spar static test specimen no. 3. This tested article, consisting of graphite/epoxy web and flanges and 0.50 by 7.00 inch 7075-T76 aluminum alloy caps, had been sawn in two in a horizontal plane at about VSS 124. Some 18 inches of one of the flange-to-cap joints inboard of this station was modified as shown in figure A2, to obtain a specimen which could be loaded in tension to place shear on the joint. A photograph of the specimen is presented as figure A3.

An exact simulation of the PRVT flange-to-cap joint would have required that the shear load be introduced in distributed fashion at the web-flange junction. Instead, the total joint load was applied as tension at one end of the cap. This simplification limited the load to something less than what would be allowable in distributed shear; also, it caused differential straining of the cap. To ensure that slippage could occur in the attachment without local overload, all holes in the graphite/epoxy laminate were enlarged using a 7/32 inch diameter drill. The graphite/epoxy spar flange and the 0.50 by 7.00 inch aluminum alloy cap were then reassembled using close tolerance titanium alloy bolts, Hi-Lok collars, and sealant per Lockheed process bulletins, as were the original PRVT specimen assemblies. The HL97V-6 collars torque off at 25 to 35 in-lb., which limits initial fastener clamping force to the order of 1000 pounds.

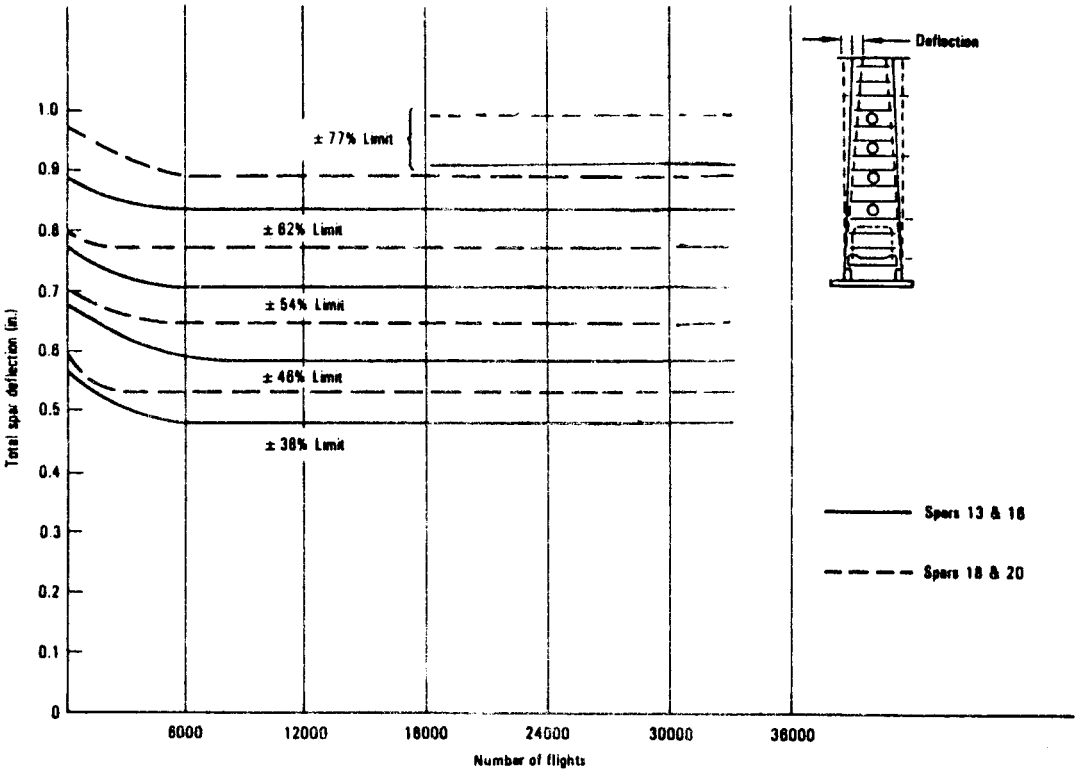

Figure A1. - Load-deflection data for Chamber 1 four basic spars.

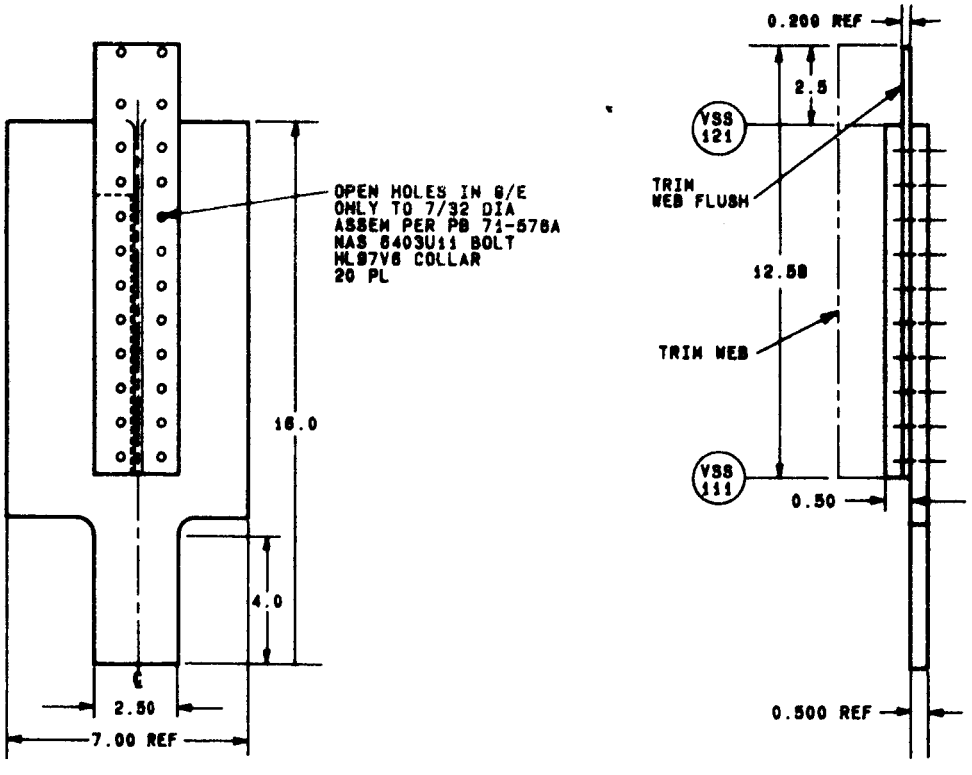

Figure A2. - Test specimen geometry.

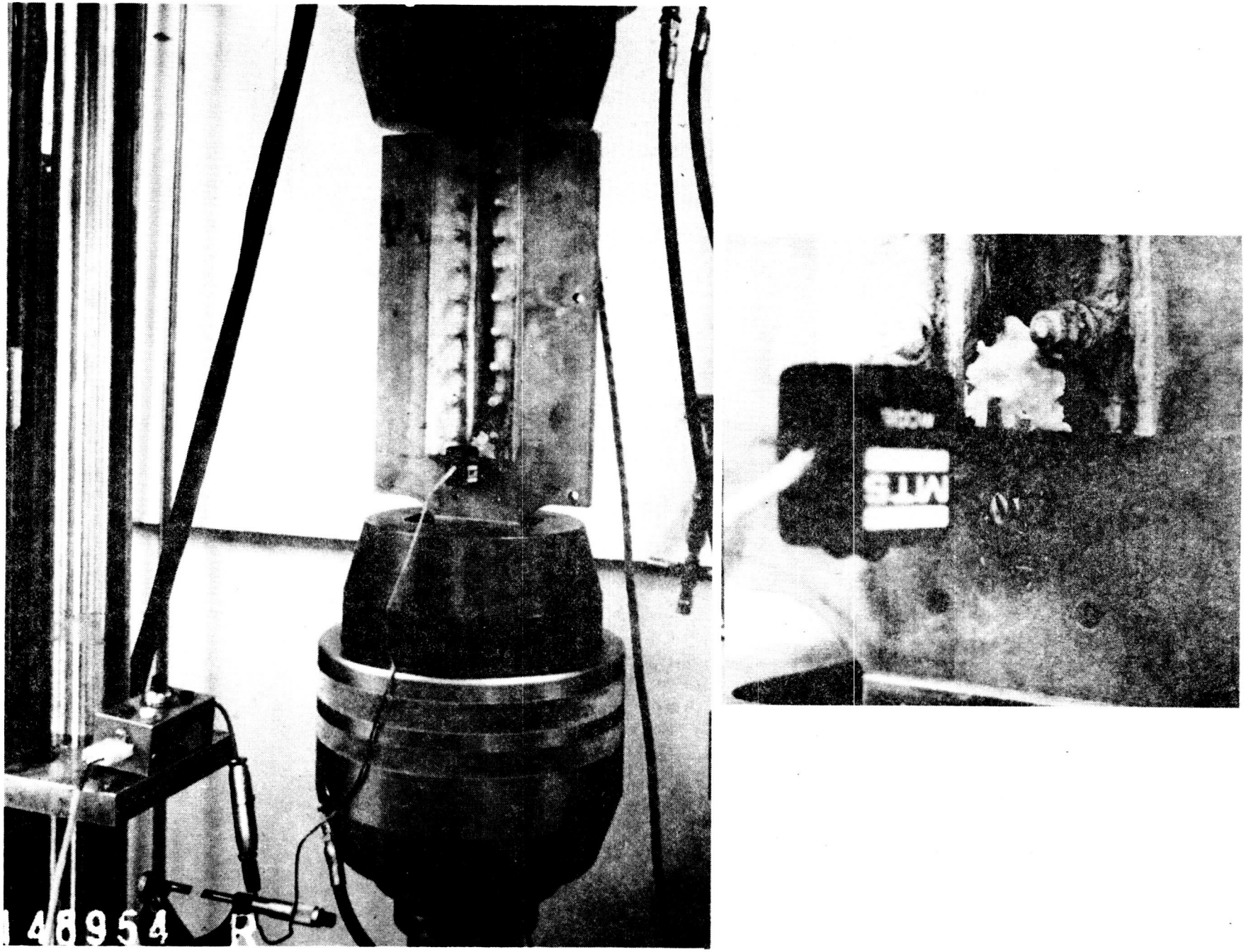

Figure A3. - Joint specimen mounted in MTS hydraulic grips with extensometer attached for deflection measurements.

TEST PROCEDURES AND RESULTS

Tests were conducted to determine the load-deflection characteristics of the specimen after the following exposures:

1. Immediately after fabrication.

2. After 5 weeks exposure to the PRVT environmental conditioning.

3. After 9 months immersion in water at 180°F.

4. After drying out for 16 months at 160°F.

Reversed load tests were conducted in an MTS 50-kip universal testing machine to obtain load-deflection hysteresis determinations under total loads of ±1000 pounds and ±2500 pounds. A clip gage (MTS 632.01) was mounted at the end of the graphite/epoxy spar flange, to measure displacement of this end point with respect to the heavy aluminum alloy cap as shown in figure A3. Load and slip gage displacement data were recorded, reduced, and plotted by the Rye Canyon central data acquisition system.

Additionally, thickness of the protruding end of the spar flange was measured with a micrometer at four locations, as a rough confirmation of the extent of moisture sorption.

Baseline Data

A group of three tests, to obtain baseline data on stiffness, was conducted within a few days after fabrication. The load versus time history for these tests and the corresponding load versus deflection data are presented in figures A4 through A9. Several tests were made at this time in order to confirm the data obtained and to make certain that the load-deflection characteristics were fully identified. Three unusual effects were noted:

1. Large hysteresis obvious in the first test (figures A4 and A5) was considerably reduced in tests conducted only three days later (figures A6 through A9). It is believed that the reduction in hysteresis can be attributed to the curing of the sealant material used in assembly.

2. The direction of prior large load establishes the reference position about which subsequent smaller cyclic loads establish their hysteresis loops. This is best seen in figure A9. Run 3, to ±1000 pounds, produced a hysteresis loop initiating at zero deflection; after the cyclic loading to ±2500 pounds in run 4, the repeat loading to ±1000 pounds in run 5 provided a hysteresis loop displacement by -0.0004 inch. A large "dead zone" is seen to exist within which the structure appears to behave in an engineering fashion, but wherein deflection under a given load is determined primarily by prior loading history.

C-2

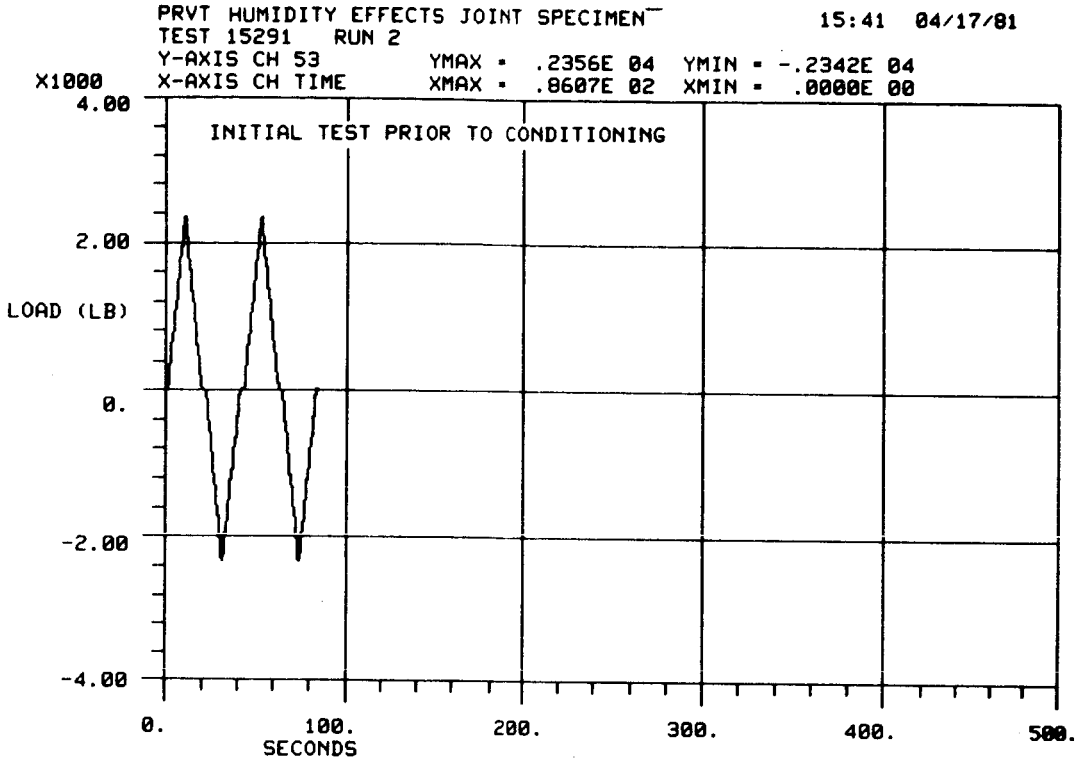

Figure A4. - Initial load cycles.

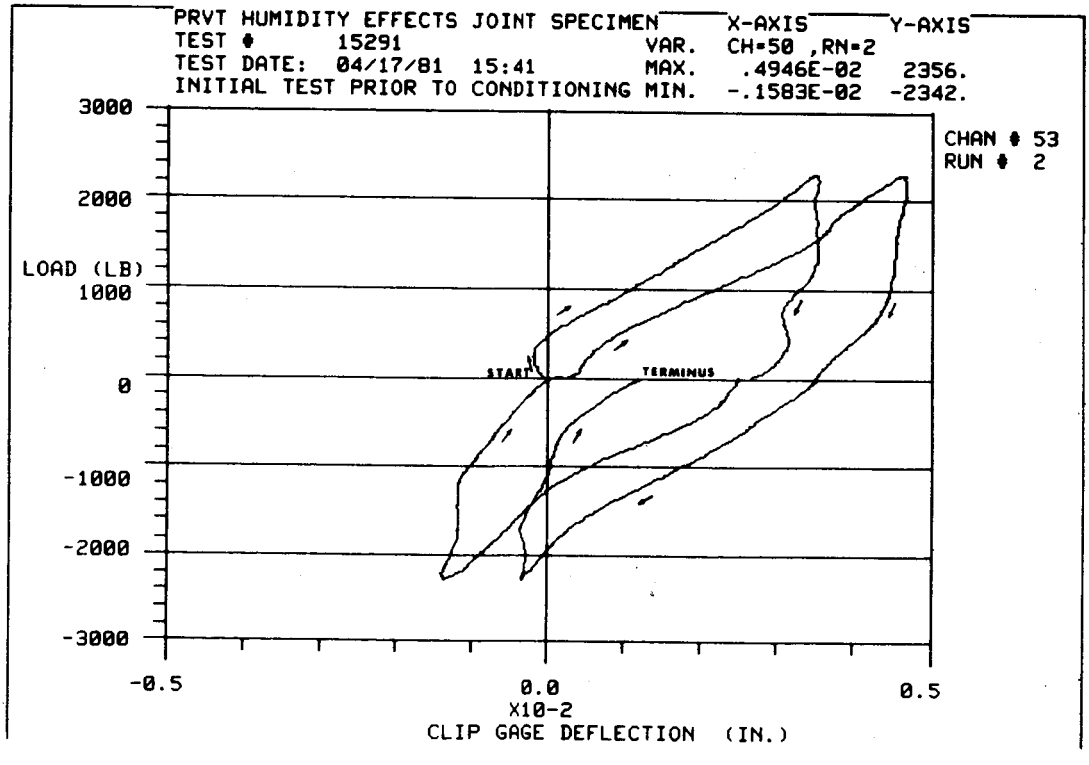

Figure A5. - Hysteresis effects during initial load cycles.

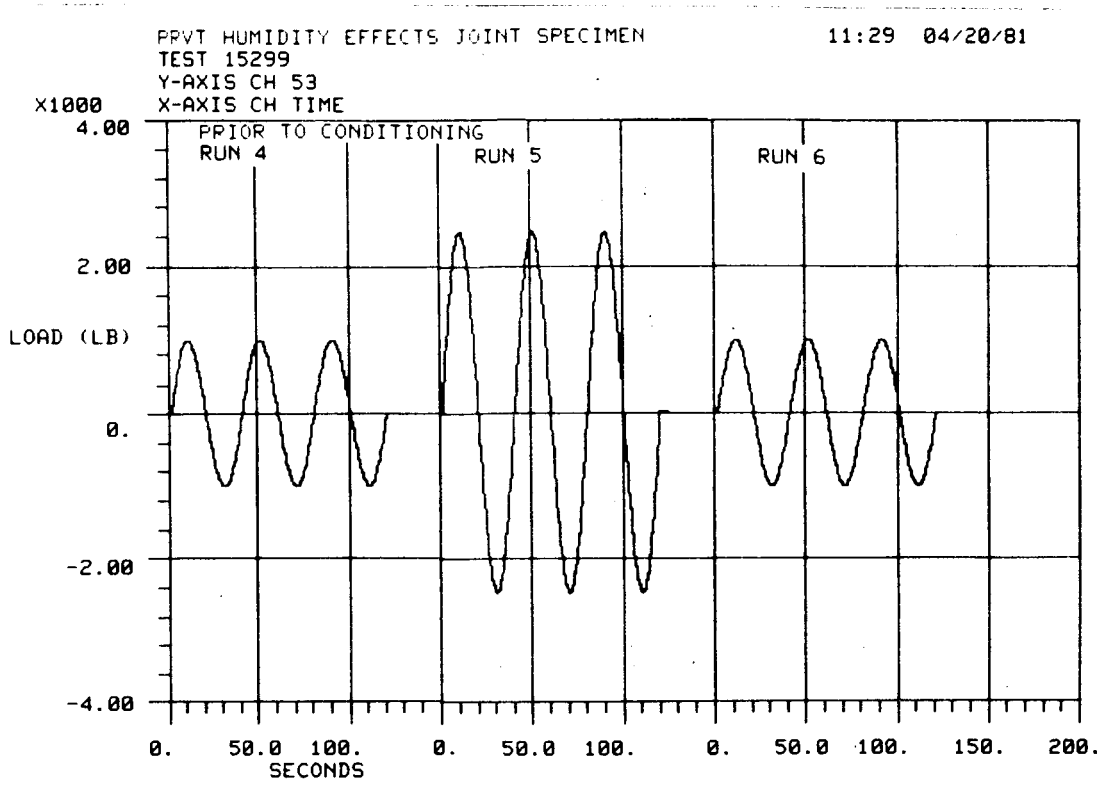

Figure A6. - Load cycles applied after 3 days conditioning.

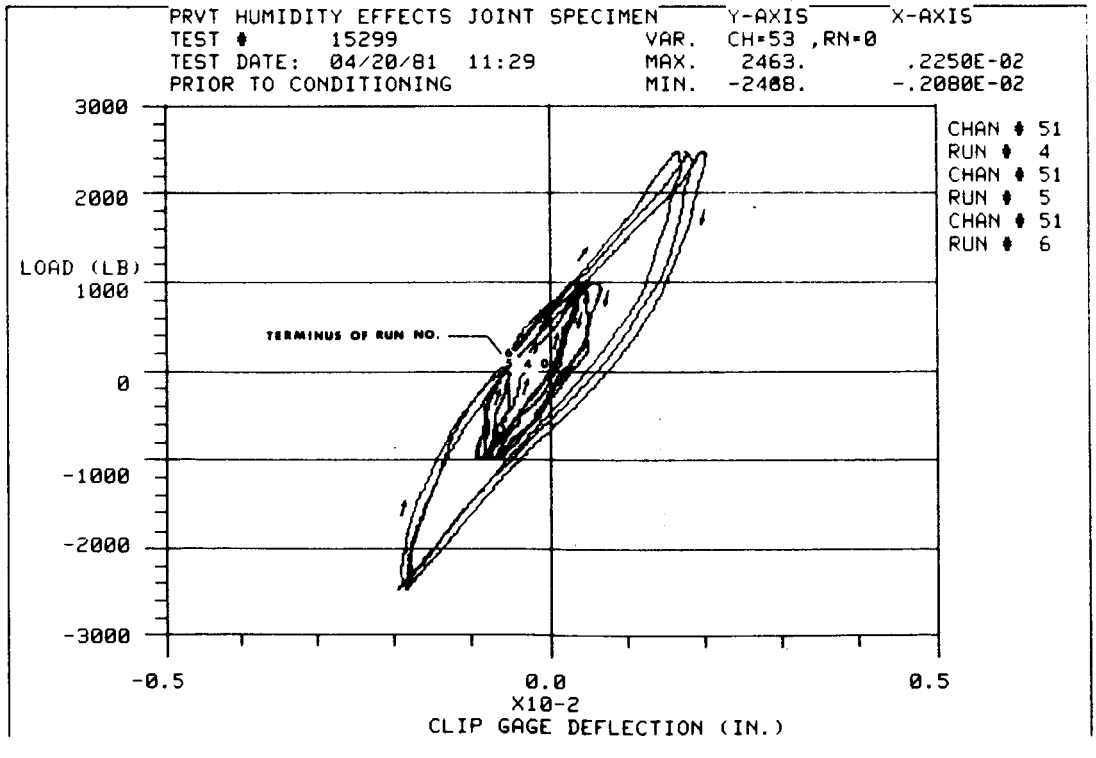

Figure A7. - Hysteresis after 3 days conditioning.

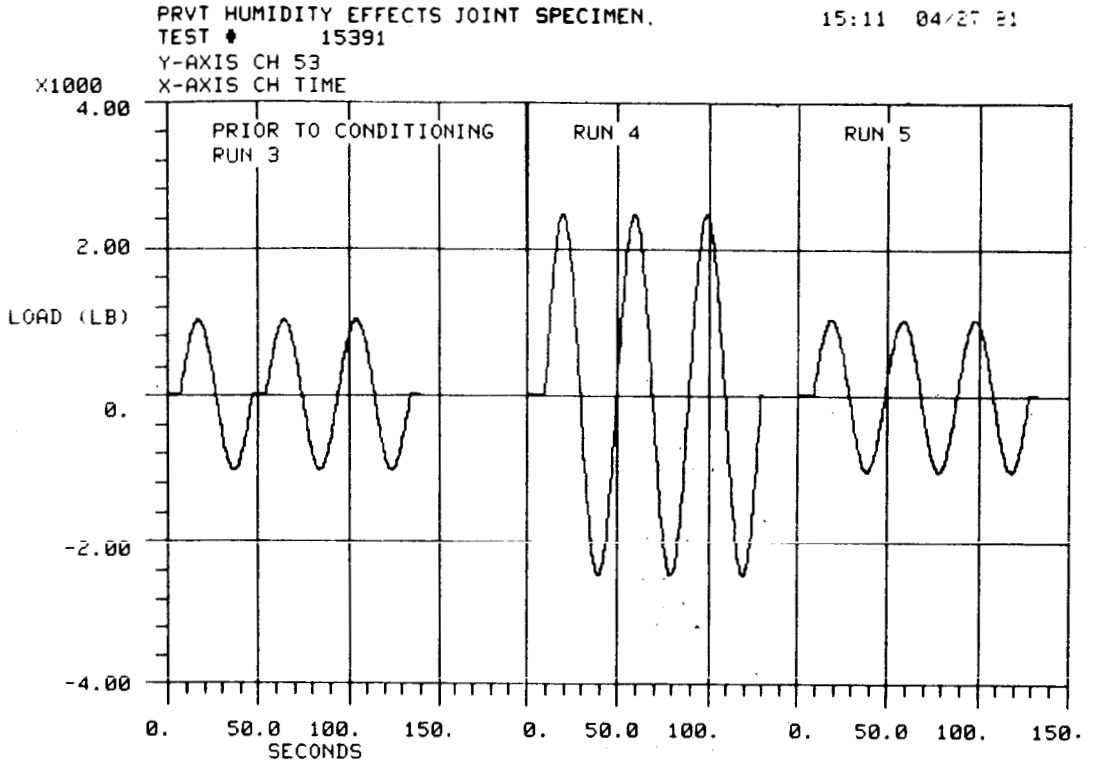

Figure A8. - Load cycles after 10 days conditioning.

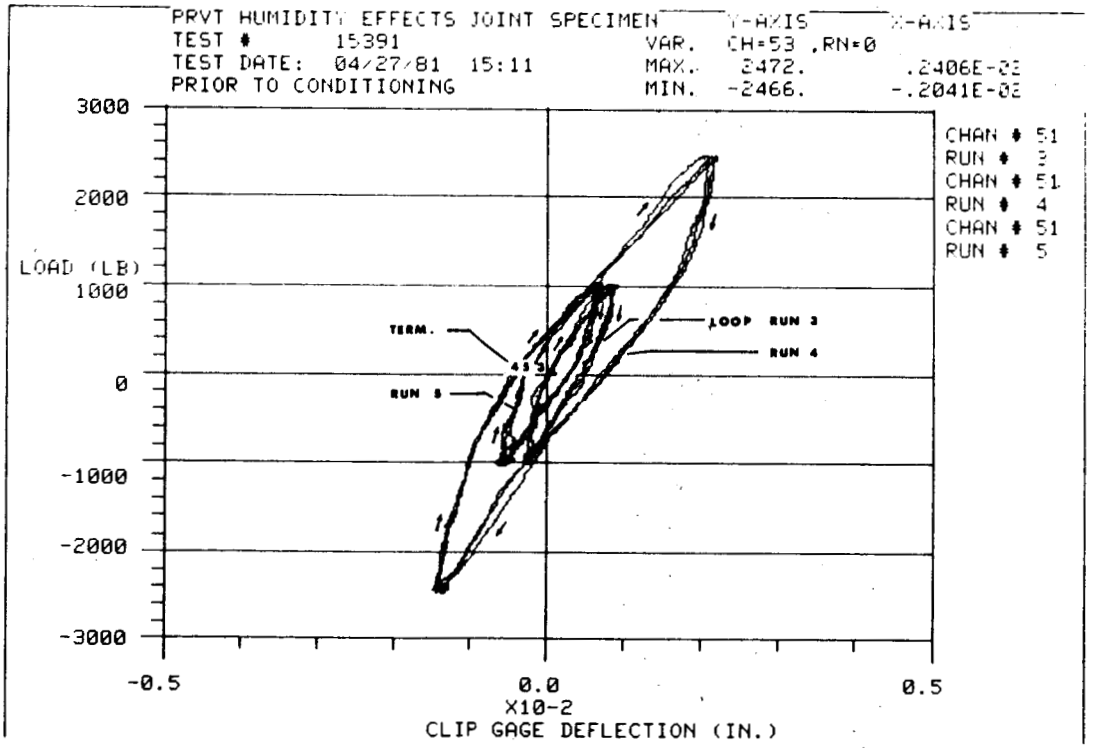

Figure A9. - Hysteresis after 10 days conditioning.

3. The apparent stiffness under low cyclic load is significantly higher than that at high load (as evidenced by peak-to-peak comparisons in figures A7 and A9).

Effect of PRVT Exposure

Results of the reversed load tests made after the specimen was exposed to PRVT environmental cycling for five months are presented in figure A10. The data indicate that:

- The nature of the hysteresis effects, together with the "dead zone" were similar to those previously observed.
- The apparent stiffness under ±2500 pound reversed load had decreased.
- The apparent stiffness under ±1000 pound load had not changed significantly.

It was suspected that these negative results might not be representative of the PRVT spars because of the much larger bolt clearances used in the small joint specimen. The additional long-time immersion at 180°F was therefore planned, in order that the effect of moisture sorption would be maximized.

Effect of Moisture Saturation

The behavior of the specimen after immersion for nine months at 180°F and presumably saturated is shown in figures A11 through A13. Because of a change in behavior with number of applications of high load, the reversed load program was repeated twice, with different directions of traverse about the hysteresis loop. Results are summarized as follows:

- Under ±1000 pounds loading, the hysteresis was reduced to a third or less of previous value. Joint slippage had been greatly reduced.
- At the same loading, the stiffness had been increased by a factor of two to three times.
- At ±2500 pounds loading, the slope of the initial loading curve, and of the load-removal curves, had also been increased. Repeated high load, however, appeared to have a loosening effect, resulting in increasing hysteresis for successive cycles to high load.
- Changing the direction of high loading (that is, from tension to compression) appears simply to reverse the direction of subsequent effects at low load. The apparent stiffness as low load can be quite large, yet the actual deflection with respect to an initial reference is governed by the prior history of high load application.

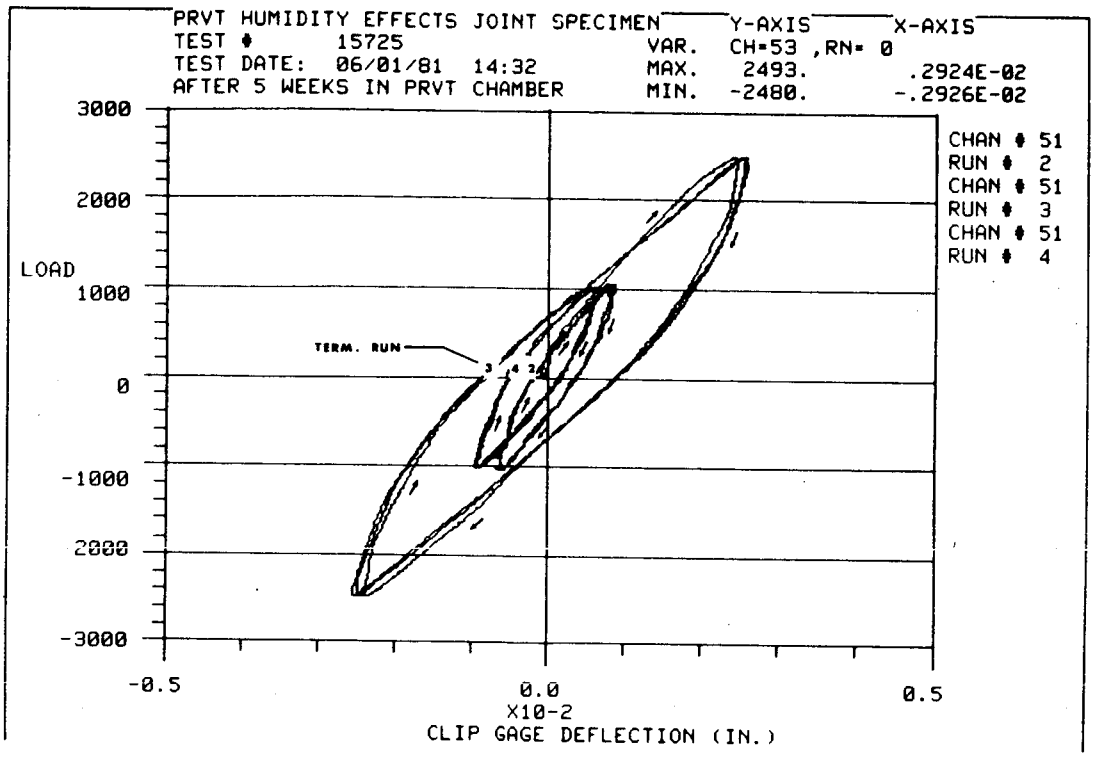

Figure A10. - Hysteresis after 5 months conditioning.

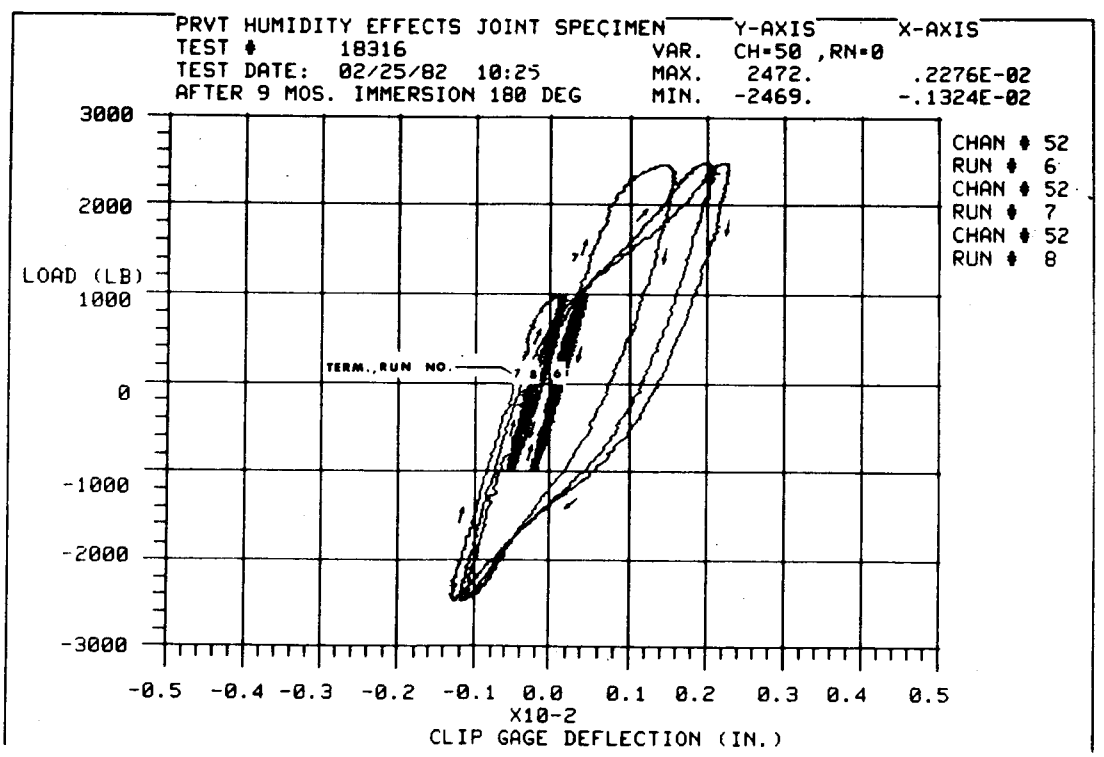

Figure A11. - Hysteresis after 9 months conditioning.

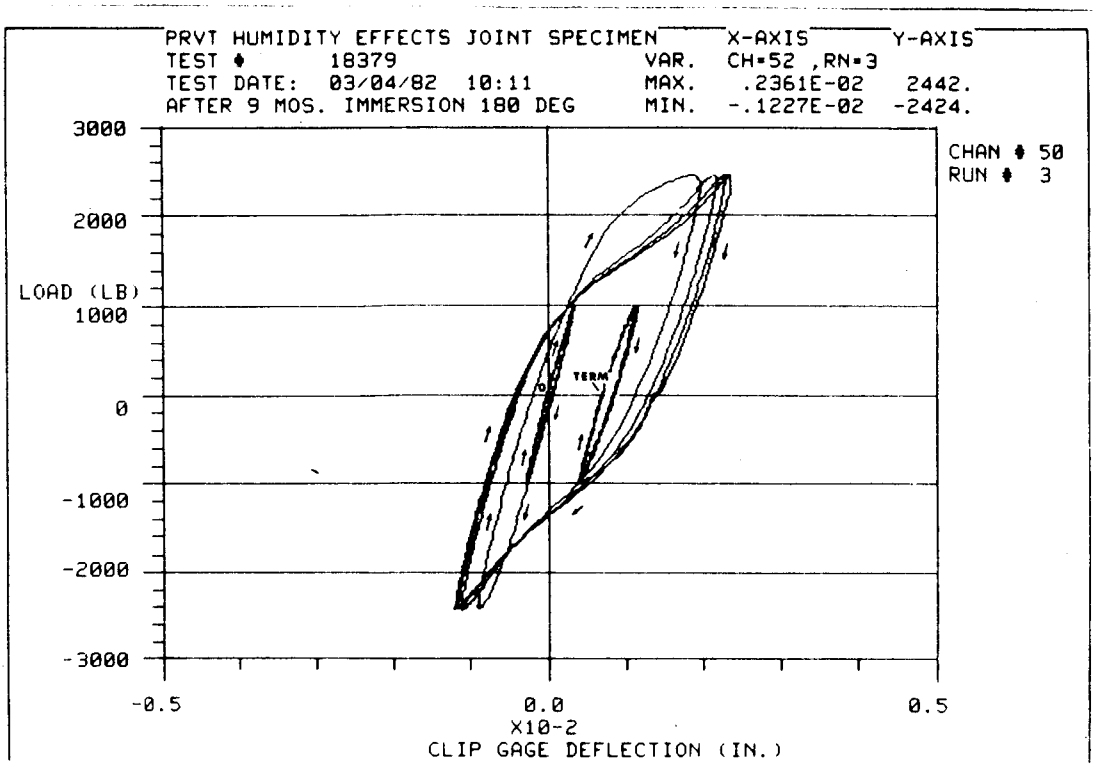

Figure A12. - Hysteresis after 9 months conditioning.

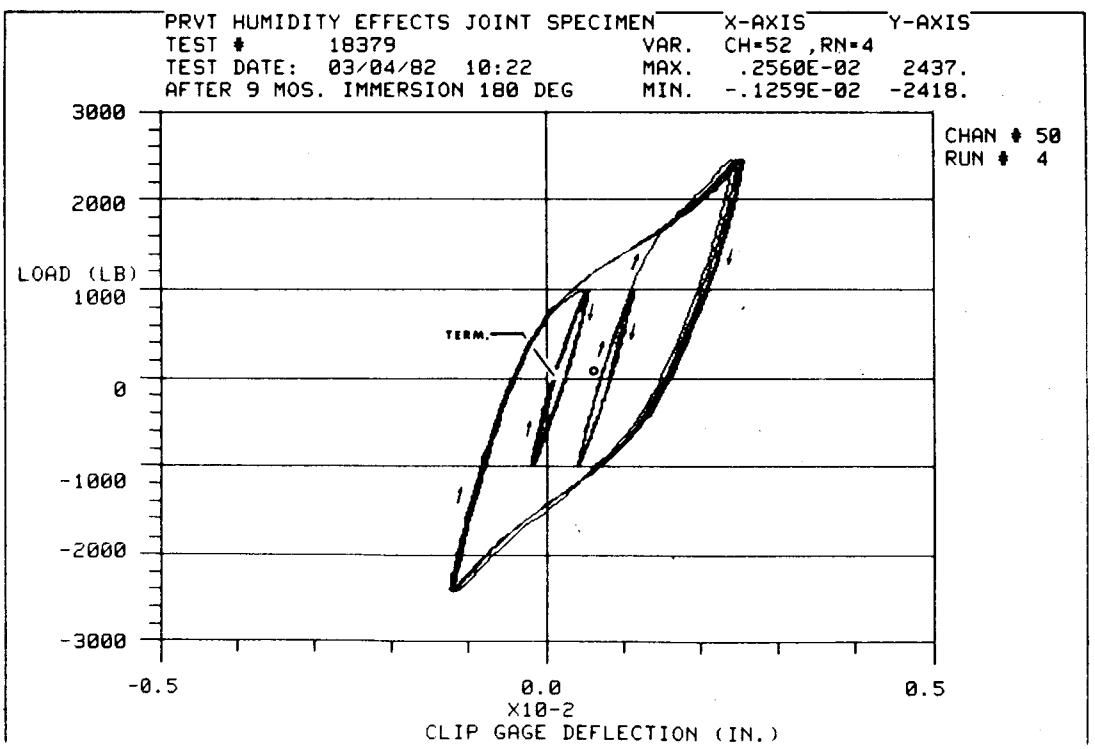

Figure A13. - Hysteresis after 9 months conditioning.

Effect of Drying Out

After some 16 months drying at 160°F, a concluding set of tests provided the data shown in figure A14, for compression applied first, and figuure A15 for tension applied first. In summary,

- Stiffnesses, when dry, were much lower than under any previous test condition.
- Hysteresis effects were much larger.

Stiffness measurements.- Table A1 presents apparent stiffness under the various test conditions as determined by peak-to-peak deflection data. The values support the qualitative observations made on the basis of examination of figures A4 through A15.

Thickness measurements.- Measurements of thickness are presented in Table A2 and plotted against time of observation in figure A16. The data indicate a variation entirely consistent with the sorption of moisture expected under the various exposure conditions.

CONCLUSIONS

A joint which transfers shear in graphite/epoxy laminate, made with shear pins having limited clamping tension placed in oversize holes, displays unusual load-deflection characteristics which can change dramatically with the change in moisture content of the laminate.

Specifically,

1. Substantial hysteresis may be evident, differing from the usual hysteresis associated with material yielding in that there is no proportional limit but a progressive increase in slip beginning at relatively low load.
2. Because of the nature of the slip, the load-increasing curve shows lower stiffness than load-decreasing. If stiffness is determined by measurements of deflection at peak loads, the stiffness will be less for larger values of load.
3. The apparent stiffness can be increased substantially with moisture sorption by the laminate, and decreased by drying out. The probable mechanism for this effect is the increase in laminate thickness with moisture pick-up resulting in greater clamping pressure between bolt fasteners of fixed length and consequent greater frictional effects.

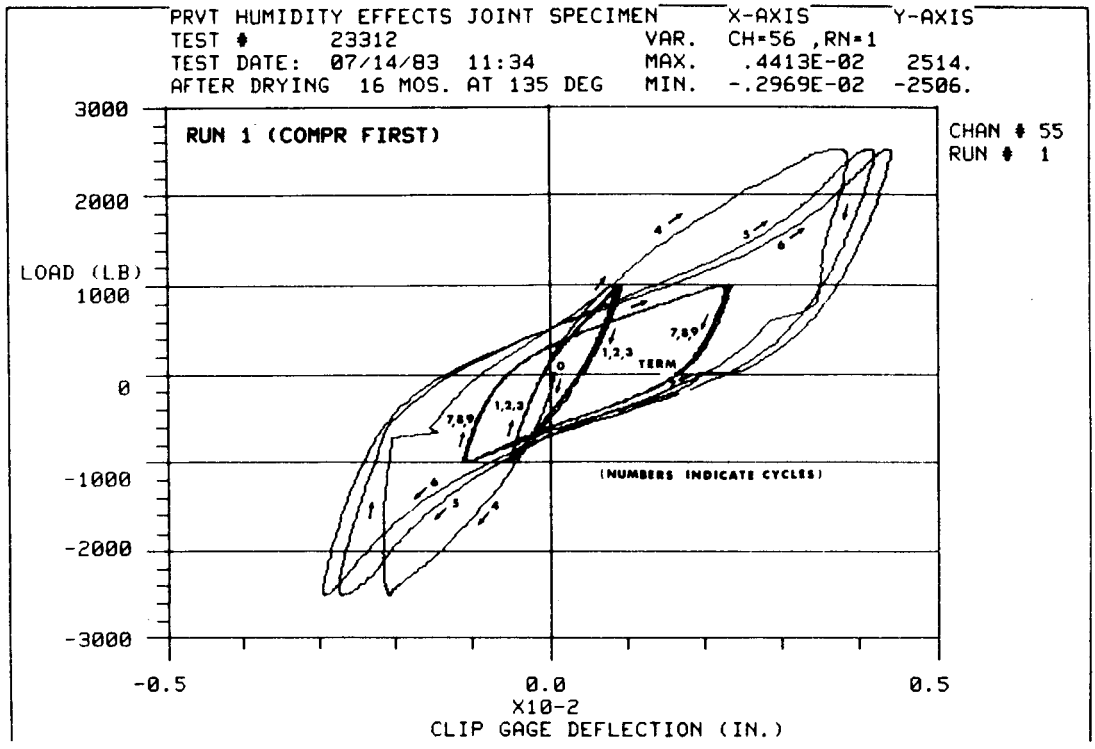

Figure A14. - Hysteresis effects after drying out.

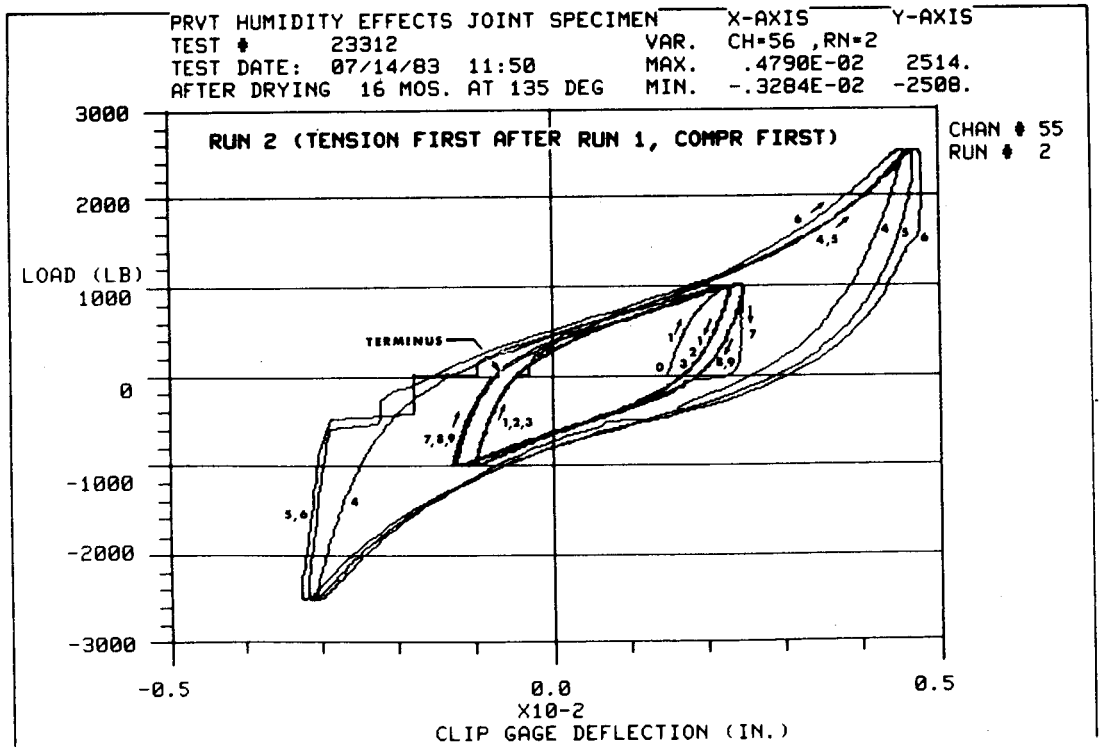

Figure A15. - Hysteresis effects after drying out.

TABLE A-1. - SUMMARY OF TESTS OF PRVT HUMIDITY EFFECTS ON JOINT SPECIMEN

Test No.	Condition	Loading	Apparent Stiffness* (10^6 lb/in)
15291	Prior to exposure	+2400,-2400; 2 cycles	0.9
15299	Prior to exposure	+1000,-1000; 3 cycles	1.6
		+2500,-2500; 3 cycles	1.3
		+1000,-1000; 3 cycles	1.6
		+2500,-2500; 1 cycle	1.3
		+1000,-1000; 10 cycles	1.6
		+1000,-1000; 1 cycles	1.8
15391	Prior to exposure	+1000,-1000; 3 cycles	1.8
		+2500,-2500; 3 cycles	1.4
		+1000,-1000; 3 cycles	1.7
		+2500,-2500; 1 cycles	1.4
		+1000,-1000; 11 cycles	1.6
15725	After 5 weeks in PRVT Chamber 1	+1000,-1000; 3 cycles	1.4
		+2500,-2500; 3 cycles	1.0
		+1000,-1000; 3 cycles	1.4
		+2500,-2500; 1 cycles	1.0
18316	After 9 months immersion 180°F	+1000,-1000; 3 cycles	3.2
		+2500,-2500; 3 cycles	1.5
		+1000,-1000; 3 cycles	3.0
		+2500,-2500; 1 cycles	1.3
		+1000,-1000; 11 cycles	2.8
18379	After 9 months immersion 180°F	-1000,+1000; 4 cycles	3.3
		-2500,+2500; 4 cycles	1.4
		-1000,+1000; 4 cycles	2.7
		+1000,-1000; 4 cycles	2.8
		+2500,-2500; 4 cycles	1.3
		+1000,-1000; 4 cycles	2.8
23312	After drying for 16 months at 130°F	-1000,+1000; 4 cycles	1.4
		-2500,+2500; 4 cycles	0.7
		-1000,+1000; 4 cycles	0.6
		+1000,-1000 4 cycles	0.6
		+2500,-2500; 4 cycles	0.6
		+1000,-1000; 4 cycles	0.6

*Ratio, peak load range to peak deflection range.

TABLE A-2. - THICKNESS MEASUREMENTS

Date	Measured, Inches				Increment, % of Original				
	A	B	C	D	A	B	C	D	Avg.
4/13/81	0.2030	0.2162	0.2177	0.2003	0	0	0	0	0
6/4/81	0.2033	0.2165	0.2175	0.2022	+0.15	+0.15	-0.09	+0.85	+0.27
2/25/82	0.2040	0.2205	0.2202	0.2030	+0.49	1.99	1.15	1.35	+1.25
7/29/83	0.2031	0.2165	0.2165	0.2012	+0.05	+0.15	-0.55	0.45	+0.10

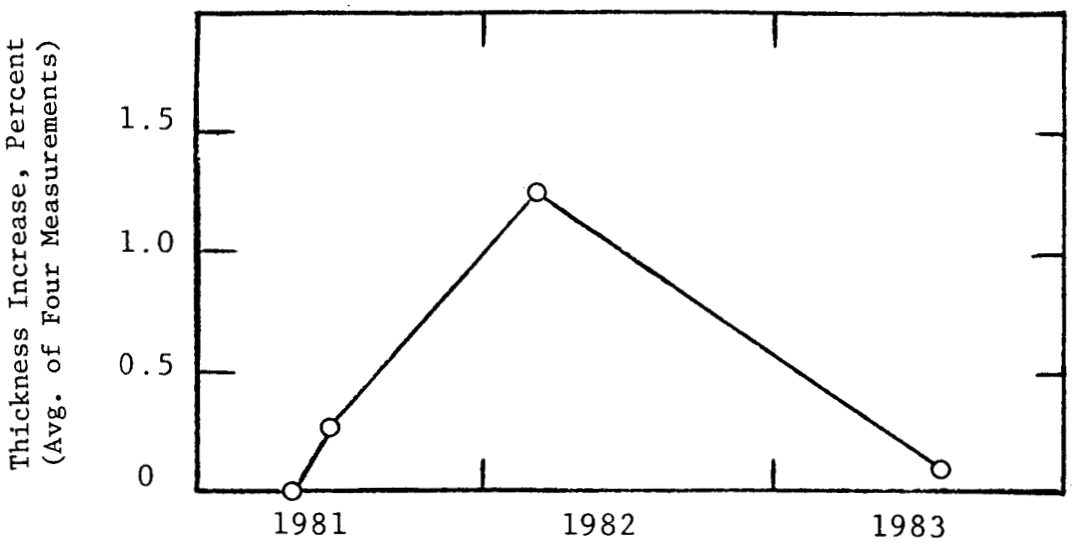

Figure A16. - Measured thickness changes in stub end of graphite/epoxy joint specimen.

1. Report No.	2. Government Accession No.	3. Recipient's Catalog No.
NASA CR 172383		

4. Title and Subtitle	5. Report Date
ADVANCED MANUFACTURING DEVELOPMENT OF A COMPOSITE EMPENNAGE COMPONENT FOR L-1011 AIRCRAFT PHASE III FINAL REPORT, PRODUCTION READINESS VERIFICATION TESTING	August 1984
	6. Performing Organization Code
7. Author(s) A. Jackson, J. Sandifer, P. Sandorff, and R. Van Cleave	8. Performing Organization Report No. LR 30760
	10. Work Unit No.
9. Performing Organization Name and Address Lockheed-California Company P.O. Box 551 Burbank, California 91520	11. Contract or Grant No. NAS1-14000
	13. Type of Report and Period Covered Contractor Report
12. Sponsoring Agency Name and Address National Aeronautics and Space Administration Washington, DC 20546	14. Sponsoring Agency Code

15. Supplementary Notes

Langley Technical Monitor: Marvin Dow

16. Abstract The Production Readiness Verification Tests (PRVT) were designed to provide information to answer the following questions:

- What is the range of production qualities that can be expected for components manufactured under conditions similar to those expected in production, and how realistic and effective are proposed quality levels and quality control procedures?
- What variability in static strength can be expected for production quality components, and are the margins sufficient to account for this variability?
- Will production quality components survive extended time laboratory fatigue tests involving both load and environment simulation of sufficient duration and severity to provide confidence in in-service durability?

To provide data, 22 components of each of two key structural elements of the ACVF were fabricated for test. One element represented the front spar/fuselage attachment area, and the other element represented the cover/fuselage joint area. Ten of each element were static strength tested. The remainder were durability tested for up to the equivalent of 20 years of service. Reproducibility was demonstrated and the quality control procedures verified.

Static strength variability has been demonstrated to be comparable to metallic structures. The range of production qualities has been established. The long-term durability of advanced composite components has been demonstrated.

17. Key Words (Suggested by Author(s))	18. Distribution Statement
Composites, Reproducibility, Strength Variability, Durability Environmental Effect, Transport Aircraft, Graphite Epoxy	[redacted] Subject Category 24

19. Security Classif. (of this report)	20. Security Classif. (of this page)	21. No. of Pages	22. Price
Unclassified	Unclassified	107	

Available: NASA's Industrial Applications Centers